



This is a repository copy of *Pattern, style and timing of British–Irish Ice Sheet retreat : Shetland and northern North Sea sector*.

White Rose Research Online URL for this paper:  
<https://eprints.whiterose.ac.uk/154011/>

Version: Published Version

---

**Article:**

Bradwell, T., Small, D., Fabel, D. et al. (14 more authors) (2021) Pattern, style and timing of British–Irish Ice Sheet retreat : Shetland and northern North Sea sector. *Journal of Quaternary Science*, 36 (5). pp. 681-722. ISSN 0267-8179

<https://doi.org/10.1002/jqs.3163>

---

**Reuse**

This article is distributed under the terms of the Creative Commons Attribution (CC BY) licence. This licence allows you to distribute, remix, tweak, and build upon the work, even commercially, as long as you credit the authors for the original work. More information and the full terms of the licence here:  
<https://creativecommons.org/licenses/>

**Takedown**

If you consider content in White Rose Research Online to be in breach of UK law, please notify us by emailing [eprints@whiterose.ac.uk](mailto:eprints@whiterose.ac.uk) including the URL of the record and the reason for the withdrawal request.



[eprints@whiterose.ac.uk](mailto:eprints@whiterose.ac.uk)  
<https://eprints.whiterose.ac.uk/>

## Pattern, style and timing of British–Irish Ice Sheet retreat: Shetland and northern North Sea sector

TOM BRADWELL,<sup>1,2\*</sup> DAVID SMALL,<sup>3</sup> DEREK FABEL,<sup>4</sup> CHRIS D. CLARK,<sup>5</sup> RICHARD C. CHIVERRELL,<sup>6</sup> MARGOT H. SAHER,<sup>7</sup> DAYTON DOVE,<sup>2</sup> S. LOUISE CALLARD,<sup>8</sup> MATTHEW J. BURKE,<sup>6</sup> STEVEN G. MORETON,<sup>9</sup> ALICIA MEDIALDEA,<sup>10</sup> MARK D. BATEMAN,<sup>5</sup> DAVID H. ROBERTS,<sup>3</sup> NICHOLAS R. GOLLEDGE,<sup>11</sup> ANDREW FINLAYSON,<sup>2</sup> SALLY MORGAN<sup>12</sup> and COLM Ó COFAIGH<sup>3</sup>

<sup>1</sup>University of Stirling, UK

<sup>2</sup>British Geological Survey, Edinburgh, UK

<sup>3</sup>Durham University, UK

<sup>4</sup>University of Glasgow, Scottish Universities Environmental Research Centre (SUERC), UK

<sup>5</sup>University of Sheffield, UK

<sup>6</sup>University of Liverpool, UK

<sup>7</sup>University of Bangor, UK

<sup>8</sup>Newcastle University, UK

<sup>9</sup>NERC Radiocarbon Laboratory, East Kilbride, UK

<sup>10</sup>University of Cologne, Germany

<sup>11</sup>Victoria University of Wellington, New Zealand

<sup>12</sup>University of Leicester, UK

Received 8 June 2018; Revised 23 September 2019; Accepted 7 October 2019

**ABSTRACT:** The offshore sector around Shetland remains one of the least well-studied parts of the former British–Irish Ice Sheet with several long-standing scientific issues unresolved. These key issues include (i) the dominance of a locally sourced ‘Shetland ice cap’ vs an invasive Fennoscandian Ice Sheet; (ii) the flow configuration and style of glaciation at the Last Glacial Maximum (i.e. terrestrial vs marine glaciation); (iii) the nature of confluence between the British–Irish and Fennoscandian Ice Sheets; (iv) the cause, style and rate of ice sheet separation; and (v) the wider implications of ice sheet uncoupling on the tempo of subsequent deglaciation. As part of the Britice-Chrono project, we present new geological (seabed cores), geomorphological, marine geophysical and geochronological data from the northernmost sector of the last British–Irish Ice Sheet (north of 59.5°N) to address these questions. The study area covers ca. 95 000 km<sup>2</sup>, an area approximately the size of Ireland, and includes the islands of Shetland and the surrounding continental shelf, some of the continental slope, and the western margin of the Norwegian Channel. We collect and analyse data from onshore in Shetland and along key transects offshore, to establish the most coherent picture, so far, of former ice-sheet deglaciation in this important sector. Alongside new seabed mapping and Quaternary sediment analysis, we use a multi-proxy suite of new isotopic age assessments, including 32 cosmogenic-nuclide exposure ages from glacially transported boulders and 35 radiocarbon dates from deglacial marine sediments, to develop a synoptic sector-wide reconstruction combining strong onshore and offshore geological evidence with Bayesian chronosequence modelling. The results show widespread and significant spatial fluctuations in size, shape and flow configuration of an ice sheet/ice cap centred on, or to the east of, the Orkney–Shetland Platform, between ~30 and ~15 ka BP. At its maximum extent ca. 26–25 ka BP, this ice sheet was coalescent with the Fennoscandian Ice Sheet to the east. Between ~25 and 23 ka BP the ice sheet in this sector underwent a significant size reduction from ca. 85 000 to <50 000 km<sup>2</sup>, accompanied by several ice-margin oscillations. Soon after, connection was lost with the Fennoscandian Ice Sheet and a marine corridor opened to the east of Shetland. This triggered initial (and unstable) re-growth of a glaciologically independent Shetland Ice Cap ca. 21–20 ka BP with a strong east–west asymmetry with respect to topography. Ice mass growth was followed by rapid collapse, from an area of ca. 45 000 km<sup>2</sup> to ca. 15 000 km<sup>2</sup> between 19 and 18 ka BP, stabilizing at ca. 2000 km<sup>2</sup> by ~17 ka BP. Final deglaciation of Shetland occurred ca. 17–15 ka BP, and may have involved one or more subsidiary ice centres on now-submerged parts of the continental shelf. We suggest that the unusually dynamic behaviour of the northernmost sector of the British–Irish Ice Sheet between 21 and 18 ka BP – characterized by numerous extensive ice sheet/ice mass readvances, rapid loss and flow redistributions – was driven by significant changes in ice mass geometry, ice divide location and calving flux as the glaciologically independent ice cap adjusted to new boundary conditions. We propose that this dynamism was forced to a large degree by internal (glaciological) factors specific to the strongly marine-influenced Shetland Ice Cap. Copyright © 2019 The Authors. Journal of Quaternary Science Published by John Wiley & Sons Ltd.

**KEYWORDS:** continental shelf; deglaciation; geochronology; ice sheet; Pleistocene

\*Correspondence: Tom Bradwell, as above.

E-mail: tom.bradwell@stir.ac.uk

## Introduction

The last British–Irish Ice Sheet (BIIS) is thought to have covered ~850 000 km<sup>2</sup> at its maximum extent, around 24 000–27 000 years ago, and contained enough ice to raise global sea levels by around 2.5 m when it melted (Clark *et al.*, 2012). The zone of interaction between the BIIS and the larger Fennoscandian Ice Sheet (FIS) remains the largest uncertainty in spatial and chronological reconstructions of the last BIIS. In fact, in their recent, comprehensive, palaeoglaciological synthesis of the whole Eurasian ice sheet complex, which includes the BIIS and FIS, Hughes *et al.* (2016) highlighted the North Sea Basin as one of two areas of major uncertainty, along with the eastern Barents Sea, where progress has been surprisingly limited over the past 50 years. Although evidence for BIIS and FIS confluence in the North Sea Basin during the last glacial cycle is strong and the concept is now generally accepted (e.g. Sejrup *et al.*, 1994, 2005, 2009; Carr *et al.*, 2006; Bradwell *et al.*, 2008; Graham *et al.*, 2009, 2011; Clark *et al.*, 2012; Svendsen *et al.*, 2015; Merritt *et al.*, 2017; Becker *et al.*, 2018; Hjelstuen *et al.*, 2018), key questions remain unresolved (see reconstructions by Clark *et al.*, 2012 and Hughes *et al.*, 2016). The most important of these questions relate to the nature and timing of BIIS–FIS interactions in the northern North Sea, east of Shetland: specifically, to the flow configuration in this sector at maximum stage; the style of deglaciation (whether predominantly marine or terrestrial); the cause and mechanism of ice-sheet separation; and consequently the

implications of this separation on the glaciological response and flow geometry of both ice sheets in this strongly marine-influenced sector.

Although pattern information regarding ice-sheet deglaciation in the northern North Sea Basin (north of 58°N) and around Shetland has greatly improved over the last 10 years (Bradwell *et al.*, 2008; Clark *et al.*, 2012; Bradwell and Stoker, 2015; Sejrup *et al.*, 2016), chronological constraint is currently lacking throughout much of this area, with one or two notable exceptions (Graham *et al.*, 2007, 2009; Sejrup *et al.*, 2015). In short, the paucity of Late Pleistocene dating evidence across the vast majority of the North Sea Basin means that the timing of key events relating to the northernmost sector of the BIIS, including the growth and decay of a ‘Shetland ice cap’, FIS–BIIS ice-sheet interaction and separation, and subsequent ice-mass deglaciation, are only weakly constrained or still uncertain. In this paper we seek to address this long-standing knowledge gap by providing new dating constraints for the glaciation of the northern North Sea Basin, the West Shetland Shelf and the Shetland Islands using a multi-proxy approach on glacial deposits both onshore and offshore [e.g. accelerator mass spectrometry (AMS) radiocarbon, optically stimulated luminescence (OSL) and cosmogenic-nuclide analyses]. The ultimate aim is to decipher the pattern and timing of ice-sheet decay in this key sector of the BIIS, part of the former Eurasian Ice Sheet complex. This work forms part of a larger targeted 5-year project, called Britice-Chrono, seeking to greatly improve the existing

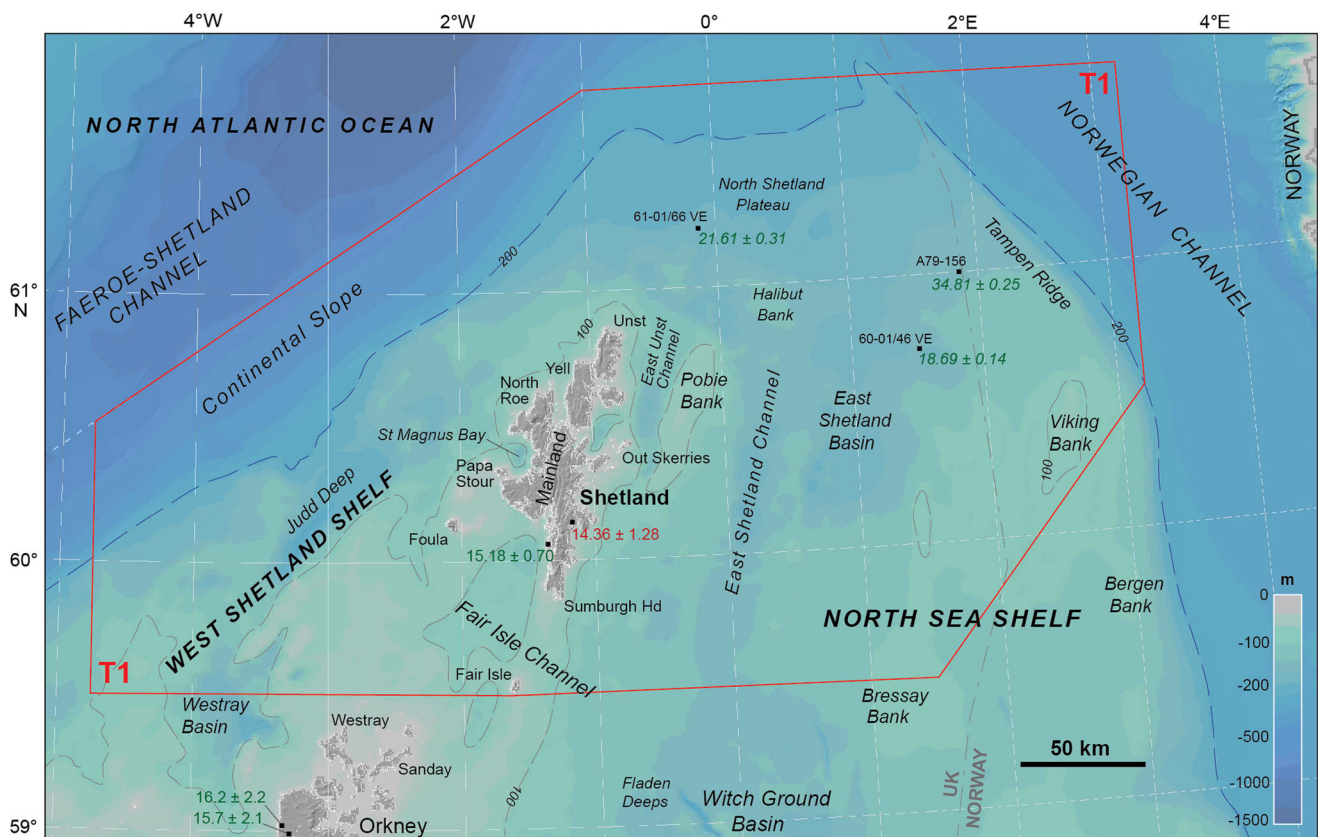


**Figure 1.** Merged topographic-bathymetric elevation map showing location of Shetland and the surrounding bathymetry of the NW European Atlantic margin. Red line defines study area, referred to hereafter as Transect 1 (T1). The 200-m isobath, approximating to the continental shelf break, is also shown. Bathymetry data from British Geological Survey and GEMCO sources. Places referred to in text are labelled; hydrographic names in *italic* font; terrestrial locations in roman font. Key pre-existing age assessments (onshore and offshore) with colour coding also shown (green = reliable and/or robust; red = unreliable and/or poor context; after Small *et al.*, 2017). See Table 1 for details. Surface exposure ages from Orkney re-calculated from Phillips *et al.* (2008). All ages are in calendar years (cal ka) before present (BP). [Color figure can be viewed at [wileyonlinelibrary.com](http://wileyonlinelibrary.com)].



glacial tunnel valleys (Bradwell *et al.*, 2008; Graham *et al.*, 2009; Sejrup *et al.*, 2016). The whole study area, defined by the thin red line in Fig. 1, covering ~95 000 km<sup>2</sup>, is hereby referred to as Transect 1 (T1) of the Britice-Chrono Project.

## Previous work and existing models

The glacial history of Shetland and the surrounding continental shelf to the east and west is controversial and currently unresolved. Despite numerous studies, stretching back over 150 years, highlighting the islands' geographical importance (e.g. Croll, 1870; Peach and Horne, 1879; Home, 1881), attempts to decipher the pattern and timing of glacial events in Shetland have yielded many different, seemingly incompatible, reconstructions. From these chiefly land-based reconstructions, backed by credible geological and geomorphological field evidence, two opposing views have developed:

1. That Shetland hosted its own ice cap throughout the last glacial cycle and was not overwhelmed by the Fennoscandian (or any other) ice sheet
2. That, during times of maximal glaciation, Shetland was dominated by ice-sheet glaciation from Fennoscandia, but may have hosted its own ice cap during build-up and/or deglaciation.

These two opposing models have existed for more than 100 years and have coloured, albeit inadvertently, most of the research undertaken on this topic since (e.g. Flinn, 1967, 1973, 1994; Hoppe, 1974; Mykura, 1976; Sutherland, 1984; Carr *et al.*, 2006; Bradwell *et al.*, 2008; Gollidge *et al.*, 2008; Carr and Hiemstra, 2013). Indeed, at the start of this 5-year project, Hall (2014, p. 229) summarized that 'the question of whether or not ice cap or ice sheet glaciation dominated on Shetland ... remains open'.

Since the 1980s the offshore record of glaciation around Shetland has become the focus of more detailed and systematic study. The number of papers published in total, and since the year 2000, is still small, as can be seen from the first and second Britice map-database compilations (Clark *et al.*, 2004a, 2018). However, research emphasis has now clearly shifted from a solely terrestrial to a combined onshore-offshore approach or an exclusively marine approach (e.g. Carr *et al.*, 2006; Bradwell *et al.*, 2008; Clark *et al.*, 2012; Sejrup *et al.*, 2015, 2016). Much pioneering work relating to the stratigraphy of Pleistocene glacial deposits in the northern North Sea Basin and West Shetland Shelf was carried out by the British Geological Survey (BGS) during the UK Continental Shelf mapping programme (1970–1990). Although this information sets out a broad stratigraphic framework of Late Quaternary events it is underpinned by very few absolute ages. Rather than review this stratigraphic and Quaternary geological framework – most of which is published within three BGS Offshore Regional Reports (Johnson *et al.*, 1993; Stoker *et al.*, 1993; Ritchie *et al.*, 2011), and supplemented by a number of comprehensive reviews (e.g. Carr *et al.*, 2006; Graham *et al.*, 2011; Merritt *et al.*, 2017) – we briefly summarize the existing Late Pleistocene reference dates within the northernmost sector (T1) of the former BIIS.

## Existing geochronology

Geochronological control around Shetland is currently based on a small number of radiocarbon dates on marine shells from cored sediments offshore and basal radiocarbon dates from Lateglacial–postglacial sediment sequences onshore. All

dating constraints relating to the last BIIS were compiled and collated in a geographical information system (GIS) before the start of the Britice-Chrono project (Hughes *et al.*, 2011). This database was updated in 2014 and all dates were quality-checked using a semi-quantitative 'traffic light' system (Small *et al.*, 2017), where green denotes reliable, robust ages and red denotes unreliable or poor context dates. The key existing deglacial age assessments are shown in Fig. 1 and presented in Table 1. It is notable that only one dated deglacial site within the entire offshore T1 sector passed the 'green' quality-control filter undertaken by Small *et al.* (2017): namely BGS 60-01/46 VE (Peacock, 1995). We have upgraded one further site to 'green': BGS 61-01/66 VE (Ross, 1996). A third 'green' site relates to the timing of glaciation onset: core A79-156 (Rise and Rokoengen, 1984).

Onshore, perhaps surprisingly, no published terrestrial cosmogenic-nuclide (TCN) exposure ages currently exist from Shetland (Small *et al.*, 2017; and as of May 2018). Several Lateglacial sites provide radiocarbon ages for the timing of organic sediment deposition (13–16 ka BP), and hence are thought to indicate *minimum* ages for ice-free conditions. The most robust of these, herein coded 'green' based on the criteria of Small *et al.* (2017), constrains the timing of final deglaciation at Clettnadal in SW Shetland to before  $15.18 \pm 0.70$  ka BP (Whittington *et al.*, 2003) (Fig. 1). It is worth noting that some <sup>14</sup>C assays from Shetland were undertaken before the routine use of AMS analyses, while others are affected by geological problems such as hard-water effects and/or the likely introduction of old carbon (e.g. Hoppe, 1974; Birnie and Harkness, 1993). These chronological uncertainties have resulted in 'red' quality-control grading for all but one of the previously dated sites from Shetland (Fig. 1). This extremely small number of well-dated sites, onshore and offshore, particularly west of Shetland, makes this currently the least well-chronologically constrained sector of the BIIS.

## Research aims and methodological strategy

To test the hypothesis of 'local ice cap' vs 'invasive ice sheet' glaciation we devised an onshore spatial sampling strategy that incorporated the maximum land area of Shetland and its outlying islands – targeting the geographical extremities where possible. It was hypothesized that invasion of the islands, and subsequent deglaciation, by the FIS to the east would result in a deglaciation chronology that gets progressively younger (i.e. decreases in exposure-age) from west to east. Conversely, a local Shetland ice cap would result in no preferred younging from west to east; rather, the distribution of ages would take on a concentric trend – older at the periphery and demonstrably younger in the centre of the island group.

Given the resources and funds available (maximum of ~30 TCN analyses and 10 OSL analyses) it was decided to constrain the onshore pattern and timing of deglaciation accurately and robustly at a modest number ( $n < 10$ ) of carefully selected good-context sites along three approximately NNE–SSW transects. Our objective was to generate internally consistent, robust exposure-ages (= 'green' status; Small *et al.*, 2017) across a wide temporal range of deglaciated sites – with the minimum number of samples per site ( $n = 3$ ), at sites covering the maximum geographical area (Fig. 2).

The offshore sampling strategy widened the geographical focus considerably in order to explore the pattern and timing of ice sheet (or ice cap) deglaciation across the northern North Sea and West Shetland continental shelves (north of 59.5°N). Four marine transects were planned (Fig. 2) to investigate the

**Table 1.** Existing, previously published, good-context basal radiocarbon dates within the study area (T1). These four sites (three marine and one terrestrial) yield age assessments which pass the ‘green’ (robustly dated) quality-control criteria, as defined by Small *et al.* (2017).

Marine											
Core	Sample ID (Lab code)	Reference	Latitude (°N)	Longitude (°E)	Water depth (m)	Sample depth (cm)	Sample type (species)	Conventional radiocarbon age ( <sup>14</sup> C a BP)	+/- 1σ	Calibrated age* (cal a BP)	+/- 2σ
61-01/66 VE	AA-16906	Ross (1996)	61.244	-0.109	161	290 (approx.)	<i>Trochanta elliptica</i>	18 230	280	21 605	310
60-01/46 VE	OxA-4139	Peacock (1995)	60.727764	1.504589	143	165	<i>Musculus discors</i>	15 860	180	18 694	138
A79-156	T-3827	Rise and Rokoengen (1984)	61.00	1.8333	130	?	<i>Macoma calcarea</i>	30 190	360	34 814	245
Terrestrial Site	Sample ID (Lab code)	Reference	Latitude (°N)	Longitude (°E)	Elevation (m asl)	Profile depth (cm)	Sample material	Conventional radiocarbon age ( <sup>14</sup> C a BP)	+/- 1σ	Calibrated age† (cal a BP)	+/- 2σ
Clettnadal (Burra)	AA-33284	Whittington <i>et al.</i> (2003)	60.0552	-1.3585	20	310	Bulked sediment (blue-grey micaceous silt; ~5% organic)	12 780	90	15 180	700

\*Radiocarbon dates from marine carbonate (shells) converted from conventional radiocarbon years using OxCal 4.3 (Bronk Ramsey, 2013) and Marine13 (Reimer *et al.*, 2013). Calibrated ages are presented in years BP (i.e. before 1950 CE) as mean of two-sigma uncertainty; local marine-reservoir correction ( $\Delta R$ ) = 0.

†Radiocarbon dates from terrestrial organic material converted using OxCal 4.3 (Bronk Ramsey, 2013) and IntCal09 (Reimer *et al.*, 2013). Calibrated ages are presented in calendar years BP (i.e. before 1950 CE) as mean of two-sigma uncertainty.

following key areas, each of which addressed a separate avenue of specific scientific interest:

1. Deglaciation of the shelf NE of Shetland, including the complex nested moraine sequence NE of Unst
2. Deglaciation of the outer West Shetland shelf, including Otter Bank Formation moraines
3. Deglaciation of the inner West Shetland shelf, including St Magnus Bay
4. Deglaciation of the shelf east of Shetland, including the area thought to include the 'unzipping zone' between the BISS and FIS (Bradwell *et al.*, 2008; Sejrup *et al.*, 2016).

Again, given the time and resources available (maximum of 10 days' ship time) it was decided to collect continuous marine geophysical data (multibeam echo sounder and sub-bottom profiler) along these four 50–200-km-long transects, taking between eight and 12 carefully selected Quaternary sediment cores per transect. Our offshore objective was to establish a substantial number ( $n \approx 20$ ) of robustly dated, good-context deglacial sites along these four transects to greatly improve the density of geochronological reference data and to answer pertinent questions about the timing of ice-sheet deglaciation east and west of Shetland.

## Methods

Onshore and offshore data for this study were collected in two complementary field campaigns. The first, onshore in May 2014, involved an intensive fieldwork campaign in Shetland; the second, offshore in July 2015, constituted one-third of the 30-day scientific cruise (JC123) onboard the *RRS James Cook*. Legacy data analysis and revised glacial landform mapping

was undertaken before the onshore fieldwork and offshore cruise. The data were supplemented, interpreted and revisited during and after the respective data-collection campaigns (Figs. 2–4). The numerous methods and datasets used in this research are described below.

### *Terrestrial cosmogenic-nuclide exposure-age dating*

Potential sampling sites on Shetland were identified based on their strategic importance to test the competing glaciological reconstructions and optimally constrain the wider deglaciation pattern. As well as identifying specific glacial landforms (e.g. recessional moraines), we also targeted clear and unambiguous glacially transported boulders in geographically important localities (e.g. Foula, Out Skerries) (Figs. 2 and 4). In the field, glacially transported boulders were chosen based on their specific lithological suitability (quartz-bearing), morphological setting (to avoid local shielding) and large size (to avoid potential disturbance). Samples were collected from the top surface of boulders using a hammer and chisel. Boulders exhibiting unusual surface weathering or potential signs of pre-glacial exposure were avoided. GNSS geolocations, detailed site-specific descriptions and topographic shielding were all recorded for each sample (Table 2). At least three separate samples were collected from each site, where possible. We assumed that samples at each site or on each landform, typically collected within a 500-m radius, would share a common deglaciation history and therefore common exposure age (Applegate *et al.*, 2012; Small *et al.*, 2017).

All samples were prepared and processed at the University of Glasgow (School of Geographical and Earth Sciences). Following crushing, washing and sieving, quartz was

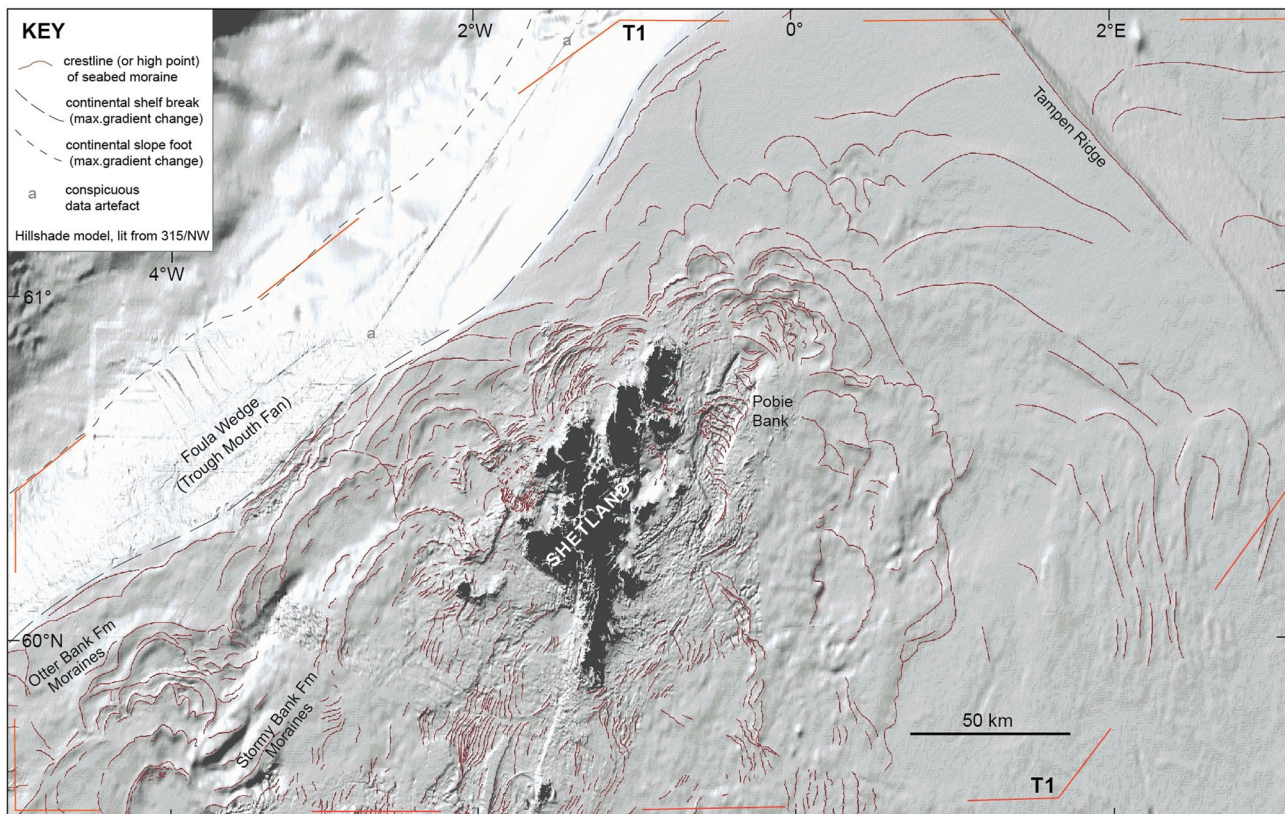


**Figure 3.** Best available shelf-wide (EMODnet) bathymetric surface model, greyscale with hillshade from NW (315°). All seabed moraines, mapped in ArcGIS, shown as crestlines only (brown lines). Note that geomorphological mapping was undertaken at various scales using different bathymetric models (not only EMODnet data). This new geomorphological mapping supersedes, refines and/or extends previously published compilations of the same area (e.g. Bradwell *et al.*, 2008; Clark *et al.*, 2012; Sejrup *et al.*, 2016). [Color figure can be viewed at [wileyonlinelibrary.com](http://wileyonlinelibrary.com)].

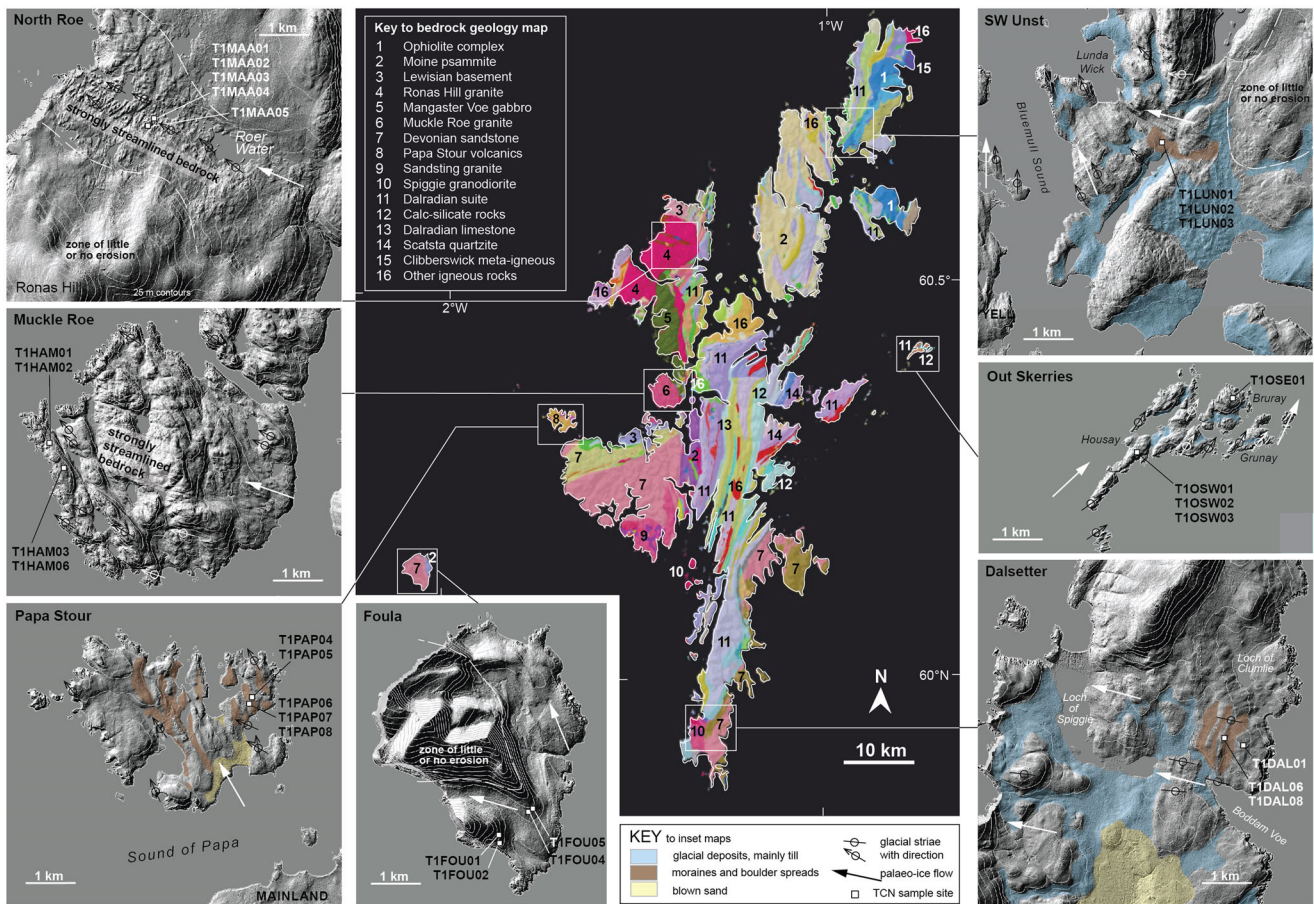


**Figure 4.** Simplified bedrock geology map of Shetland (modified from BGS, 2018) (central panel). Surrounding panels show more detailed maps of seven of the field sites specifically chosen for TCN sample collection, all at similar scale and same grid orientation. White arrows show direction of former ice flow based on geomorphological and geological evidence (e.g. glacial streamlining, striae and erratic carry). Hill-shaded surface models are overlain with Quaternary geology, where appropriate (see key), based on field mapping and existing data (BGS, 1971, 1978, 1982, 2018). Topographic contours at 25-m vertical intervals. TCN sample data are presented in Table 2. Hill-shaded surface models contain elevation data from NEXTMap GB (Intermap Technologies). [Color figure can be viewed at [wileyonlinelibrary.com](http://wileyonlinelibrary.com)].

separated from the 250–500- $\mu\text{m}$  fraction using standard mineral separation techniques (Kohl and Nishiizumi, 1992) and purified by ultrasonification in 2% HF/HNO<sub>3</sub> to remove remaining contaminants, mainly feldspars and meteoric <sup>10</sup>Be. The purity of the leached samples was assessed by aluminium content using flame atomic absorption spectrometry with bulk Al content considered a proxy for the presence of feldspars. Be extraction was carried out at two independent laboratories housed at the Scottish Universities Environmental Research Centre (SUERC): the NERC Cosmogenic Isotope Analysis Facility and the SUERC Cosmogenic Nuclide Laboratory, using established procedures (Child *et al.*, 2000). The <sup>10</sup>Be/<sup>9</sup>Be ratios of all samples were measured on the 5-MV accelerator mass spectrometer at SUERC (Xu *et al.*, 2010). NIST27900 [<sup>10</sup>Be/<sup>9</sup>Be = 2.79 × 10<sup>-11</sup>] standardization was used in the AMS measurements. Measured ratios were converted to concentrations of <sup>10</sup>Be in quartz (atoms g<sup>-1</sup>). Blank corrections ranged from 1.2 to 10.3% and were propagated in quadrature with attendant AMS analytical uncertainties (Table 3).

We calculate <sup>10</sup>Be exposure ages using the CRONUS-Earth calculator (Developmental version; Wrapper script 2.3, Main calculator 2.1, constants 2.2.1, muons 1.1; [http://hess.ess.washington.edu/math/al\\_be\\_v22/al\\_be\\_calibrate\\_v22.php](http://hess.ess.washington.edu/math/al_be_v22/al_be_calibrate_v22.php); accessed 18/7/2016; Balco *et al.*, 2008) and the CRONUScalc calculator ([web1.itcc.ku.edu:8888/2.0/html](http://web1.itcc.ku.edu:8888/2.0/html); accessed 02/06/2016; Marrero *et al.*, 2016). Ages calculated in the CRONUS-Earth calculator (Balco *et al.*, 2008) were calibrated using a local production rate to reduce scaling uncertainties and to improve agreement with other geochronological techniques

(e.g. Balco *et al.*, 2009; Putnam *et al.*, 2010; Kaplan *et al.*, 2011; Young *et al.*, 2013; Phillips *et al.*, 2016). Two independently calibrated local production rates are available from the British Isles, the Loch Lomond (LLPR) and the Glen Roy production rate (GRPR) (Small and Fabel, 2015). These production rates agree within uncertainties. We adopt the most securely calibrated local <sup>10</sup>Be production rate (LLPR; Fabel *et al.*, 2012) in all calculations (4.02 ± 0.18 atoms g<sup>-1</sup>), noting that this is almost identical to the global mean <sup>10</sup>Be production rate calculated from the CRONUS-Earth primary dataset (Borchers *et al.*, 2016). For a discussion of the LLPR with respect to other production rates see Small and Fabel (2016). All TCN ages in this study are presented rounded to the nearest 0.1 ka with full external uncertainties at ±1 sigma, unless otherwise stated (Table 4).

Exposure-age distributions for each sample were plotted as probability density functions and visually compared, to identify any obvious outliers, before statistical treatments were applied. We calculated the uncertainty-weighted mean and associated uncertainties for exposure ages at each site. A two-tailed generalized extreme Studentized deviate test (gESD) – a tool within the iceTEA online interface (Jones *et al.*, 2019) – was used to check for and remove outliers. To test for clustering and goodness of fit in multiple samples from the same feature (or in close proximity) we used the reduced Chi-squared test ( $\chi^2$ ), as done by others (e.g. Balco *et al.*, 2008; Heyman *et al.*, 2016; Small *et al.*, 2017). A reduced- $\chi^2$ -value ≈ 1 (typically < 2) indicates that the scatter can be explained solely by measurement uncertainty, and a value » 1 indicates

**Table 2.** TCN sample locations and physical properties. Note: a density of 2.6 g cm<sup>-3</sup> was used for all samples.

Sample	Location	Latitude (°N)	Longitude (°W)	Elevation (m OD)	Sample lithology	Sample thickness (mm)	Shielding correction
T1DAL01	Dalsetter	59.92799	1.27866	50	Conglomeratic sandstone	8	1.0000
T1DAL06	Dalsetter	59.92950	1.28494	61	Conglomerate	18	1.0000
T1DAL08	Dalsetter	59.92964	1.28494	65	Conglomeratic sandstone	18	1.0000
T1FOU01	Foula	60.12014	2.07151	89	Granite	22	0.9984
T1FOU02	Foula	60.11866	2.07165	73	Granite	8	0.9982
T1FOU04	Foula	60.12434	2.06065	72	Conglomeratic sandstone	11	0.9986
T1FOU05	Foula	60.12487	2.05984	77	Granite	10	0.9988
T1HAM01	Muckle Roe	60.36609	1.46268	94	Granite	10	1.0000
T1HAM02	Muckle Roe	60.36609	1.46268	94	Granite	28	1.0000
T1HAM03	Muckle Roe	60.36227	1.46016	86	Granite	10	1.0000
T1HAM06	Muckle Roe	60.36215	1.45906	84	White granite	20	1.0000
T1LUN01	SW Unst	60.70791	0.93968	27	Gneiss/psammite	10	0.9999
T1LUN02	SW Unst	60.70772	0.93843	27	Quartz vein in psammite	15	1.0000
T1LUN03	SW Unst	60.70745	0.93939	22	Quartz vein in psammite	10	0.9999
T1MAA01	North Roe	60.56319	1.41646	150	Granite	10	1.0000
T1MAA02	North Roe	60.56390	1.41467	133	Granite	30	1.0000
T1MAA03	North Roe	60.56390	1.41467	133	Granite	20	1.0000
T1MAA04	North Roe	60.56390	1.41467	133	Granite	25	0.9995
T1MAA05	North Roe	60.56390	1.41467	133	Granite	30	0.9995
T1OSE01	Out Skerries	60.42831	0.74678	46	Pegmatite	27	0.9999
T1OSW01	Out Skerries	60.41977	0.78120	28	Schist	8	1.0000
T1OSW03	Out Skerries	60.41937	0.78076	26	Granite	15	1.0000
T1OSW04	Out Skerries	60.41939	0.78011	24	Granite	8	1.0000
T1PAP04	Papa Stour	60.33484	1.67399	23	Psammite	10	1.0000
T1PAP05	Papa Stour	60.33501	1.67248	23	Psammite	20	1.0000
T1PAP06	Papa Stour	60.33362	1.67361	26	Gneiss	20	1.0000
T1PAP07	Papa Stour	60.33373	1.67334	28	Psammite	16	1.0000
T1PAP08	Papa Stour	60.33419	1.67388	26	Psammite	18	1.0000
BGS_BR1	Skella Dale	60.3883	1.3265	42	Quartz vein in psammite	50	0.9993
BGS_BR2	Skella Dale	60.3900	1.3311	38	Quartz vein in psammite	50	0.9993
BGS_WH1	Norwick, NE Unst	60.8051	0.8294	26	Quartz vein	50	0.9994
BGS_WH2	Norwick, NE Unst	60.8051	0.8294	25	Quartz vein in psammite	50	0.9996

an additional source of variance in the dataset (Balco *et al.*, 2008; Jones *et al.*, 2019). These tests were performed iteratively to ensure optimal data reduction at each site. To build the final geochronology we used a uniform-phase Bayesian sequence model using OxCal 4.3 (Bronk Ramsey, 2013), which was run in outlier mode to assess for outliers in time (Bronk Ramsey, 2009a) (described fully in the Interpretation section).

### Optically stimulated luminescence dating

To support the TCN chronology we also sought material for OSL dating. Only two suitable sites, hosting glaciofluvially deposited sand-grade material, were found and sampled for OSL dating using opaque 30-mm-diameter plastic tubes hammered into the sediment facies. Two separate samples were collected at each site. Samples were capped and labelled and kept in dark conditions at all times during analysis to prevent exposure to sunlight. For each OSL sample, the external gamma dose-rates were determined using *in situ* gamma spectrometry, with external beta dose-rates calculated from U, Th and K concentrations determined using inductively coupled plasma mass spectrometry (ICP-MS). Appropriate conversion and attenuation factors were used to calculate the final total dose rate, applying an assumed moisture of 23% for partially saturated samples (Sel Ayre) and 27% for saturated samples (Gon Firth) (Table 5).

OSL samples were measured using the 212–250- $\mu$ m quartz grain fraction mounted on small multi-grain aliquots each with approximately 20 grains. These were stimulated using a blue (470  $\pm$  30 nm) light-emitting diode array providing a

stimulation power of  $\sim$ 80 mW cm<sup>-2</sup> at the sample position. Luminescence signal was detected through a 735-nm Hoya U-340 filter. Equivalent doses ( $D_e$ ) were measured using the single aliquot regeneration procedure with a pre-heat of 220 °C for 10 s.

Although between 1700 and 8000 single-grain measurements were made on samples, these failed to measure sufficient  $D_e$  values to meet the acceptance criteria for age reporting. For the small aliquot measurements,  $D_e$  distributions were found to be highly scattered and overdispersed (OD >70%). Whilst a minimum-age approach would normally have been adopted in such instances (e.g. Bateman *et al.*, 2018), it was noted that all samples had a low  $D_e$  component yielding ages too young to be considered coherent with the site geology. This component was isolated and removed using the Finite Mixture Model (FMM; Galbraith and Green, 1990) before the internal-external uncertainty model (IEU) was used to provide the final  $D_e$  for age calculation purposes (see Supporting Information).

### Bathymetric data compilation and geomorphological mapping

The entire seabed within the T1 study area is covered by digital bathymetry data (Fig. 2). However, the datasets are of different resolution, different areal coverage and are from different sources. The datasets have been compiled to form a seamless elevation model of the submarine landscape around Scotland and are available via the European Marine Observation and Data Network (EMODnet) Digital Terrain Model ([www.emodnet-bathymetry.eu/data-products](http://www.emodnet-bathymetry.eu/data-products)). We use this bathymetry data re-gridded at  $\sim$ 100  $\times$  200 m cell size. In addition to the

**Table 3.** TCN beryllium isotope analytical data for all samples from T1. AMS  $^{10}\text{Be}$  analyses were conducted at SUERC AMS Laboratory, East Kilbride. Errors include laboratory procedural uncertainties and individual AMS measurement errors.

Sample ID	Blank ID	Sample and carrier masses				AMS data					
		Be spike ( $\mu\text{g}$ )	Uncert.	Total Quartz (g)	Be cathode	$^{10}\text{Be}/^9\text{Be}$	Uncert.	$^{10}\text{Be}/\text{Be}$ process blank	Uncert.	$^{10}\text{Be}$ (g)	$\delta^{10}\text{Be}$ (g)
T1DAL01	CFG1411	258.56	1.81	26	b8580	1.24E-13	3.49E-15	5.33E-15	1.16E-15	78 632	2507
T1DAL06	CFG1411	258.72	1.81	26.994	b8581	1.27E-13	3.74E-15	5.33E-15	1.16E-15	77 931	2568
T1DAL08	CFG1411	258.72	1.81	31.529	b8583	1.58E-13	4.05E-15	5.33E-15	1.16E-15	83 550	2384
T1FOU01	CFG1419	240.67	1.68	15.157	b9683	4.99E-14	2.20E-15	3.63E-15	7.00E-16	49 158	2478
T1FOU02	CFG1411	259.54	1.82	23.036	b8584	9.88E-14	3.32E-15	5.33E-15	1.16E-15	70 408	2695
T1FOU04	CFG1411	257.57	1.80	35.415	b8585	9.60E-14	3.12E-15	5.33E-15	1.16E-15	44 074	1651
T1FOU05	CFG1411	256.75	1.80	31.382	b8586	1.41E-13	4.21E-15	5.33E-15	1.16E-15	74 434	2449
T1HAM01	CB211015	220.23	3.69	20.0898	b10138	1.13E-13	3.10E-15	6.05E-15	8.40E-16	78 388	2728
T1HAM02	CFG1603	228.38	3.23	11.346	b10501	6.31E-14	1.87E-15	2.44E-15	6.31E-16	81 551	2916
T1HAM03	CB211015	222.18	3.72	20.0898	b10135	1.13E-13	5.30E-15	6.05E-15	8.40E-16	78 916	4203
T1HAM06	CB220116	250.62	2.51	21.3644	b10289	8.59E-14	2.70E-15	2.37E-15	4.13E-16	65 510	2247
T1LUN01	CFG1602	225.49	3.19	21.912	b10381	1.07E-13	2.66E-15	3.40E-15	7.25E-16	70 869	2167
T1LUN02	CFG1411	255.60	1.79	43.74	b8592	1.34E-13	3.79E-15	5.33E-15	1.16E-15	50 432	1593
T1LUN03	CFG1602	226.34	3.20	15.813	b10382	6.28E-14	2.27E-15	3.40E-15	7.25E-16	56 688	2442
T1MAA01	CB120116	255.21	3.61	19.7432	b10275	9.04E-14	2.23E-15	4.85E-15	6.11E-16	73 955	2284
T1MAA02	CB220116	248.25	2.48	18.4217	b10290	8.98E-14	3.12E-15	2.37E-15	4.13E-16	78 751	2952
T1MAA03	CB220116	249.86	2.50	21.7421	b10291	8.98E-14	3.82E-15	2.37E-15	4.13E-16	67 169	3032
T1MAA04	CFG1603	228.55	3.23	8.363	b10502	4.77E-14	1.66E-15	2.44E-15	6.31E-16	82 703	3470
T1MAA05	CFG1603	229.06	3.24	17.462	b10504	8.98E-14	2.69E-15	2.44E-15	6.31E-16	76 630	2666
T1OSE01	CFG1419	240.99	1.69	18.319	b9684	7.59E-14	2.43E-15	3.63E-15	7.00E-16	63 542	2268
T1OSW01	CFG1411	258.56	1.81	35.558	b8589	1.62E-13	4.30E-15	5.33E-15	1.16E-15	75 933	2230
T1OSW03	CFG1411	260.69	1.82	33.605	b8590	1.50E-13	4.38E-15	5.33E-15	1.16E-15	74 812	2408
T1OSW04	CFG1411	259.05	1.81	41.682	b8591	1.72E-13	4.88E-15	5.33E-15	1.16E-15	69 191	2142
T1PAP04	CB120116	252.07	3.56	13.8918	b10276	6.05E-14	1.81E-15	4.85E-15	6.11E-16	67 544	2536
T1PAP05	CB120116	254.11	3.59	19.5972	b10278	8.93E-14	2.56E-15	4.85E-15	6.11E-16	73 199	2527
T1PAP06	CB120116	254.53	3.60	21.8559	b10279	9.37E-14	2.76E-15	4.85E-15	6.11E-16	69 224	2426
T1PAP07	CFG1603	228.64	3.23	21.095	b10505	1.02E-13	2.68E-15	2.44E-15	6.31E-16	72 000	2247
T1PAP08	CFG1603	228.89	3.24	19.876	b10506	9.29E-14	2.79E-15	2.44E-15	6.31E-16	69 633	2421
BGS_BR1	CFG0706	254.04	5.06	16.216	b1406	7.76E-14	4.99E-15	3.18E-15	1.07E-15	77 959	5580
BGS_BR2	CFG0706	253.61	5.06	12.087	b1407	5.50E-14	4.94E-15	3.18E-15	1.07E-15	72 722	7240
BGS_WH1	CFG0703	252.45	5.03	20.859	b1418	1.18E-13	5.86E-15	3.40E-15	8.26E-16	92 670	5151
BGS_WH2	CFG0704	253.43	5.05	19.567	b1419	1.10E-13	4.44E-15	6.98E-15	1.27E-15	89 116	4422

EMODnet data, shelf-wide single-beam echo-sounder bathymetric datasets (Olex), available via the BGS data licence, and high-resolution multibeam echo-sounder (MBES) data collected by the UK Maritime and Coastguard Agency's Civil Hydrography Programme were used – available through the UKHO data portal: <https://data.admiralty.co.uk/portal/apps/sites/#/marine-data-portal>. These datasets were supplemented by continuous MBES data collected on scientific cruise JC123 using a Kongsberg EM710 system operating at 70–100 kHz. Data were imported into CARIS for processing and cleaning before being exported for 3-D visualization purposes. Submarine glacial landforms were digitized on screen in ArcGIS 10.4 at 1: 10 000 scale from all the available bathymetry data. As this research focuses on the deglaciation record, particular attention was paid to ice-marginal features (moraines) within the study area (Fig. 3). To avoid mapping errors caused by azimuth bias (Clark and Meehan, 2001; Smith *et al.*, 2006) several hillshade angles and 2D cross-sectional profiling techniques were employed (in ArcGIS), alongside the first- and second-order derivatives of the digital (bathymetric) elevation model.

### Sub-seabed acoustic stratigraphy

Continuous high-resolution acoustic sub-bottom profile data were collected during scientific cruise JC123. The SBP120 system used a sweep frequency of 2.5–6.5 kHz at a ping interval of 500 ms. The data are of good quality and were

automatically processed using a match filter and time-varying gain. Data were continuously logged in .seg and .raw form and visualized on a digital echogram. These digital acoustic profile data, in addition to existing lower-frequency (sparker, airgun) analogue lines acquired by the BGS between 1970 and 1995, were used to interpret the shallow sub-seabed stratigraphy and determine geological core sites.

### Marine geology and sedimentology

To prove the Quaternary stratigraphy at key locations and recover material for dating purposes, 41 seabed cores were taken within the study area (T1) during scientific cruise JC123: 38 vibrocores (VC) and three piston cores (PC) from four sub-transects (Fig. 2). Seabed cores were taken using the BGS vibrocorer (6-m barrel) and National Oceanography Centre (NERC Marine Facilities) piston corer (9- and 12-m barrel), depending on the nature of the seabed and sub-seabed sediment. Cores were numbered sequentially followed by either the suffix VC or PC to denote the type of corer used (i.e. JC123-002VC, JC123-003PC, etc.). All cores were cut into 1-m-long sections onboard, labelled and geophysically scanned at 2-cm downcore resolution using a Geotek multi-sensor core logger (MSCL-S). The physical sediment properties measured included magnetic susceptibility, bulk density, P-wave velocity and electrical resistivity. Each core section was then split lengthways and the sediments were logged with information on sediment colour, grain size, sorting, structures, bedding contacts and macrofaunal content recorded.

**Table 4.** TCN  $^{10}\text{Be}$  exposure ages for all samples from T1. Derived using CRONUS-Earth calculator (Developmental version; Wrapper script 2.3, Main calculator 2.1, constants 2.2.1, muons 1.1; Balco *et al.*, 2008). Internal uncertainties ( $\pm 1\sigma$ ) reflect analytical uncertainties on  $^{10}\text{Be}$  measurements only. External uncertainties ( $\pm 1\sigma$ ) incorporate additional uncertainties in the calibration and scaling procedure. UWM = uncertainty-weighted mean (per location). Erosion rate of  $1 \text{ mm ka}^{-1}$  assumed. Adoption of different erosion rates ( $\leq 3 \text{ mm ka}^{-1}$ ) has very little effect on mean ages of samples ( $<1.5\%$  difference). Ages in bold are those used to calculate UWM ages. Ages in italics denote outliers (see text for details). Underlining in final column relates to quality-control scheme used throughout [underline = green = robustly dated; no underline = amber = acceptable, but not robust; n/a = not applicable].

Sample data		Surface exposure age						UWM (ka)
		CRONUS 2.3 with LLPR LM (ka)	Internal uncert. (ka)	External uncert. (ka)	CRONUScalc v2.0 LM(ka)	Internal uncert. (ka)	External uncert. (ka)	
T1DAL01	Dalsetter	<b>18.2</b>	0.6	<b>1.0</b>	18.2	0.6	1.6	
T1DAL06	Dalsetter	<b>17.9</b>	0.6	<b>1.0</b>	18.0	0.6	1.5	<b><u>18.5 ± 1.0</u></b>
T1DAL08	Dalsetter	<b>19.2</b>	0.6	<b>1.0</b>	19.2	0.6	1.6	
T1FOU01	Foula	<i>10.9</i>	0.6	<i>0.7</i>	11.0	0.6	1.0	
T1FOU02	Foula	<b>15.8</b>	0.6	<b>0.9</b>	15.9	0.6	1.4	<b><u>16.3 ± 0.8</u></b>
T1FOU04	Foula	<i>9.9</i>	0.4	<i>0.6</i>	9.9	0.4	0.9	
T1FOU05	Foula	<b>16.7</b>	0.6	<b>0.9</b>	16.7	0.6	1.4	
T1HAM01	Muckle Roe	<b>17.3</b>	0.6	<b>1.0</b>	17.3	0.6	1.5	
T1HAM02	Muckle Roe	<b>18.2</b>	0.7	<b>1.0</b>	18.3	0.7	1.6	<b><u>17.6 ± 1.0</u></b>
T1HAM03	Muckle Roe	<b>17.4</b>	0.9	<b>1.2</b>	17.4	0.9	1.7	
T1HAM06	Muckle Roe	<i>14.7</i>	0.5	<i>0.8</i>	14.7	0.5	1.3	
T1LUN01	SW Unst	<b>16.8</b>	0.5	<b>0.9</b>	16.9	0.5	1.4	
T1LUN02	SW Unst	<i>11.9</i>	0.4	<i>0.6</i>	12.0	0.4	1.0	n/a
T1LUN03	SW Unst	<i>13.4</i>	0.6	<i>0.8</i>	13.4	0.6	1.2	
T1MAA01	North Roe	<b>15.3</b>	0.5	<b>0.8</b>	15.3	0.5	1.3	
T1MAA02	North Roe	<b>16.9</b>	0.6	<b>1.0</b>	16.9	0.6	1.5	
T1MAA03	North Roe	<i>14.3</i>	0.7	<i>0.9</i>	14.3	0.7	1.3	<b><u>16.4 ± 0.8</u></b>
T1MAA04	North Roe	<b>17.7</b>	0.8	<b>1.1</b>	17.7	0.8	1.6	
T1MAA05	North Roe	<b>16.4</b>	0.6	<b>0.9</b>	16.5	0.6	1.4	
T1OSE01	Out Skerries	<i>14.9</i>	0.5	<i>0.9</i>	14.9	0.5	1.3	
T1OSW01	Out Skerries	<b>17.9</b>	0.5	<b>1.0</b>	18.0	0.5	1.5	<b><u>17.3 ± 0.9</u></b>
T1OSW03	Out Skerries	<b>17.8</b>	0.6	<b>1.0</b>	17.8	0.6	1.5	
T1OSW04	Out Skerries	<b>16.4</b>	0.5	<b>0.9</b>	16.4	0.5	1.4	
T1PAP04	Papa Stour	<b>15.9</b>	0.6	<b>0.9</b>	15.9	0.6	1.4	
T1PAP05	Papa Stour	<b>17.5</b>	0.6	<b>1.0</b>	17.5	0.6	1.5	
T1PAP06	Papa Stour	<b>16.5</b>	0.6	<b>0.9</b>	16.5	0.6	1.4	<b><u>16.8 ± 0.8</u></b>
T1PAP07	Papa Stour	<b>17.1</b>	0.5	<b>0.9</b>	17.1	0.5	1.5	
T1PAP08	Papa Stour	<b>16.6</b>	0.6	<b>0.9</b>	16.6	0.6	1.4	
BGS_BR1	Skella Dale	<b>19.1</b>	1.4	<b>1.6</b>	19.4	1.4	2.1	
BGS_BR2	Skella Dale	<b>17.8</b>	1.8	<b>2.0</b>	18.4	1.9	2.4	<b><u>18.6 ± 1.4</u></b>
BGS_WH1	Norwick, NE Unst	<b>22.4</b>	1.3	<b>1.6</b>	23.8	1.4	2.5	
BGS_WH2	Norwick, NE Unst	<b>21.6</b>	1.1	<b>1.5</b>	23.3	1.3	2.4	<b><u>21.9 ± 1.3</u></b>

Undrained shear strength of sediment in kilopascals was recorded using a hand-operated Torvane. Selected cores were X-rayed using a Geotek XCT X-radiography core scanner (in Daventry, UK). X-radiographs were captured at 100- $\mu\text{m}$  resolution and output as 16-bit greyscale images.

### Radiocarbon dating

Marine shells (articulated, single or broken valves) at key stratigraphic horizons within cores were identified from X-radiography images or from visual inspection and subsequently sampled. Where no macrofossil shells could be identified, cold-water carbonate microfossils (foraminifera) were sampled from mud- (silt/clay) grade material. Radiocarbon analyses were performed on shells and foraminifera at NERC Radiocarbon Laboratory in East Kilbride, Scotland. The outer 20% by weight of the shells was removed by controlled hydrolysis with dilute HCl, but foraminifera samples were not etched. All samples were then rinsed in deionized water, dried and homogenized. A known weight of the pretreated sample was hydrolysed to  $\text{CO}_2$  using 85% orthophosphoric acid at

room temperature. The  $\text{CO}_2$  was converted to graphite by Fe/Zn reduction. AMS analyses were conducted at SUERC, East Kilbride. Very small samples ( $<5 \mu\text{g}$ ) were measured at Keck C Cycle AMS Lab, University of California (UCIAMS).

Radiocarbon dates from marine cores have been calculated and converted from conventional radiocarbon years using OxCal 4.3 (Bronk Ramsey, 2013) and Marine13 (Reimer *et al.*, 2013). Calibrated ages are presented in calendar years BP (i.e. before 1950 CE) as the mean of the two-sigma uncertainty (Table 6). Owing to uncertainties surrounding the magnitude, timing and duration of fluctuations in the marine reservoir effect around the NE Atlantic (Stern and Lisiecki, 2013, and references therein), we prefer not to assume a local  $\Delta R$  marine-reservoir correction when calibrating the  $^{14}\text{C}$  ages (i.e.  $\Delta R = 0$ ). (See Results and Table 7 for further discussion of  $\Delta R$ ).

### Results

In the following we present a valuable new chronological database of 71 age assessments from Shetland and the

**Table 5.** Summary of OSL age estimates and associated information for Con Firth and Sel Ayre sites. Sample depth, water content and calculated contribution to total dose rates are summarized. The table also includes information on total number of aliquots measured with OSL (those which passed acceptance criteria in parentheses), palaeodose and overdispersion of  $D_e$  replicates. (Also see Supporting Information.).

Site	Lab code	Depth (m)	W* (%)	$\beta$ dose rate (Gy ka <sup>-1</sup> )	$\gamma$ dose rate (Gy ka <sup>-1</sup> )	Cosmic dose rate (Gy ka <sup>-1</sup> )	Total dose rate (Gy ka <sup>-1</sup> )	Aliquots measured (accepted)	OD <sup>†</sup> (%)	Dose <sup>‡</sup> ( $D_0$ ) (Gy)	Age (ka)
Con Firth	Shfd14140	2.0	27	1.09 ± 0.09	0.70 ± 0.05	0.16 ± 0.01	1.98 ± 0.10	144 (53)	100	27.3 ± 2.2	13.8 ± 1.3
	Shfd14141	2.0	27	1.09 ± 0.08	0.68 ± 0.05	0.16 ± 0.01	1.87 ± 0.96	140 (40)	83	30.8 ± 3.0	16.4 ± 1.8
Sel Ayre	Shfd14142	7.5	23	1.45 ± 0.12	0.72 ± 0.05	0.08 ± 0.00	2.28 ± 0.13	158 (50)	100	29.6 ± 2.7	13.0 ± 1.4
	Shfd14143	8.0	23	1.40 ± 0.12	0.83 ± 0.05	0.08 ± 0.00	2.34 ± 0.13	96 (41)	71	53.0 ± 3.8	22.7 ± 2.1

\*Palaeomoiesture content assumed to be at, or near, saturation for burial period.

†Overdispersion value from Central Age Model, indicating poor exposure of sediment to sunlight before burial.

‡Dose or equivalent dose; dose accumulated while sediment buried.

surrounding continental shelf to the east and west of the islands. We also present a new geomorphological map of seafloor moraines around Shetland, covering a total area of ca. 85 000 km<sup>2</sup> (Fig. 3). Our new chronological dataset exceeds the total number of previously published deglacial ages for this important sector of the BIIS–FIS (according to Hughes *et al.*, 2016; Small *et al.*, 2017). The new age assessments break down as follows: 32 TCN exposure ages and four OSL ages from 11 terrestrial deglacial sites in Shetland; and 35 AMS radiocarbon dates from 23 marine cores recording deglaciation offshore (Tables 2–6). Many show good statistical agreement, while others are more problematic. In the following sections we report all of these results, provide site-specific information, and provide geological/stratigraphic and geomorphological context. Terrestrial sites (TCN then OSL) are presented first (clockwise from N), followed by marine sites (clockwise from N by sub-transect).

### TCN geochronology

#### Unst

Unst is the northernmost and third largest island in the Shetland group. Its landscape is hilly in the north and west, rising to 340 m along its northern headland, but relatively low relief in the south and east. The bedrock geology of the island is unusual and complex – even by Scottish Highlands standards (Fig. 4). The eastern half of the island is dominated by a distinctive suite of mafic and ultramafic igneous rocks that formed within a thick section of oceanic crust – the Unst Ophiolite. This was subsequently thrust up during the Caledonian orogeny ca. 350 million years ago onto older continental rocks which now form the metamorphic suite of lithologies in the western half of the island. The island's unique geology has been the subject of considerable research and as such a comprehensive and detailed knowledge of the bedrock geology exists (Mykura, 1976; BGS, 2002; Flinn, 2014). However, the unusual rock types and geologically controlled landscape elements present problems for palaeoglaciological research. Although there is fragmentary sedimentological and weak geomorphological evidence of former glaciation in Unst (Flinn, 1994, 2014; Hall, 2014), the hallmarks of glaciation are subtle, especially in northern and eastern Unst. Hydrolysis weathering rates of mafic igneous and meta-igneous rocks are high, which aids mechanical breakdown – for instance on the olivine-rich metaharzburgite of Hill of Clibberswick (Fig. 4). Walkover field surveys of this hill covering ~1.0 km<sup>2</sup> found no definitive evidence of glacial erosion or glacially transported erratic boulders and only a sparse scattering of possible glacially transported (non-erratic) debris, in line with previous research (Flinn, 1994; BGS, 2002; Hall, 2014). None of this material was deemed viable for TCN analysis based on lithological and/or geomorphological grounds.

Perhaps the best glacio-geomorphological evidence on Unst is preserved in the broad valley around the Burn of Norwick (Figs. 2 and 5). Here, Colledge *et al.* (2008) mapped an assemblage of large sediment mounds and broad-crested ridges interspersed with several wide dry channels and subtle terraces, some of which show laminated fine sediments. Collectively, these features, which we call the 'North Unst moraine complex', relate to a significant pause of a former ice-margin crossing the island in a SW–NE direction at around 20–50 m asl. The uppermost surfaces of two quartz-rich schistose boulders were sampled from a prominent ridge within the moraine complex, 1 km west of Norwick, during an

**Table 6.** Locations, sample data and all radiocarbon dates from marine cores in T1 study area.

Core JC-123-	Sample ID	Latitude (°N)	Longitude (°E) [-ve is °W]	Water depth (m)	Sample depth (cm)*	Sample type and identification (and/or condition) [mass indicated for small samples]	Conventional radiocarbon age ( <sup>14</sup> C a BP)	+/- 1σ	Calibrated age <sup>†</sup> (cal a BP)	+/- 2σ
052VC	T1-052VC-180	60.19053	-4.59912	480	180	Cold water benthic foraminifera [0.0128 g]	20 158	52	23 785	218
052VC	T1-052VC-315	60.1905	-4.5991	480	315–321	Cold water foraminifera	27 702	104	31 197	178
053VC	T1-053VC-shoe	60.06398333	-4.356833	157	260 (shoe)	Shell and barnacle fragments	45 382	775	Out of range	
054VC	T1-054VC-174	60.04045	-4.31145	156	174–180	Single valve; <i>Mya truncata</i>	11 036	37	12 588	82
054VC	T1-054VC-228	60.04045	-4.31145	156	228	Single valve; species not identified	11 060	38	12 604	80
054VC	T1-054VC-234	60.04045	-4.31145	156	234	Single valve; <i>Mya truncata</i>	11 086	38	12 620	80
054VC	T1-054VC-297	60.04045	-4.31145	156	297	Shell fragment	Background			
056VC	T1-056VC-248	60.01728333	-4.267433	158	248	Single valve; species not identified	19 471	50	22 964	225
056VC	T1-056VC-256	60.01728	-4.267433	158	256	Cold water benthic foraminifera [0.0131 g]	21 005	55	24 802	314
056VC	T1-056VC-389	60.01728333	-4.267433	158	451–453	Shell ( <i>Macoma</i> species?)	Background			
059VC	T1-059VC-shoe	59.8738	-4.062266	124	410 (shoe)	Shell (? <i>Hiatella arctica</i> )	14 815	40	17 564	169
061VC	T1-061VC-shoe	59.67123333	-3.932466	123	450 (shoe)	Shell fragment	31 318	145	34 820	308
064PC	T1-064PC-502	60.3975	-1.58251	160	502	Single valve (articulated when found); species not identified	12 925	37	14 794	321
064PC	T1-064PC-564	60.3975	-1.58251	160	564–573	Cold water foraminifera	12 850	45	14 573	359
067VC	T1-067VC-shoe	60.41043333	-1.7966	104	80 (shoe)	Shell fragment	Background			
069VC	T1-069VC-331	60.4301	-1.8561	100	165	Single valve (articulated when found); species not identified	13 330	38	15 442	202
072VC	T1-072VC-202	60.59158333	-1.97466	139	202	Shell fragment	13 896	38	16 240	174
073VC	T1-073VC-315	60.6486	-2.0652	139	315–325	Cold water foraminifera	20 160	120	23 785	316
074VC	T1-074VC-300	61.47888333	0.064966	190	300	Shell; species not identified	26 022	83	29 756	368
075VC	T1-075VC-shoe	61.3261	-0.04268	168	335 (shoe)	Shell fragment	24 669	73	28 309	274
076VC	T1-076VC-214	61.10797	-0.19452	175	214	Shell fragment	Background			
078VC	T1-078VC-411	60.9647	-0.2937	146	411–414	Cold water foraminifera	Background			
079VC	T1-079VC- catcher	60.9211	-0.32332	157	310 (catcher)	Shell fragment	Background			
083PC	T1-083PC-674	60.96868333	2.658633	200	674	Shell; intact valve	11 118	38	12 637	82
083PC	T1-083PC-762	60.96868333	2.658633	200	762	Shell; fragile, intact when sampled	11 356	36	12 811	123
086VC	T1-086VC-205	60.70496667	2.1657	127	205–211	Cold water foraminifera	Background			
086VC	T1-086VC-shoe	60.70496667	2.1657	127	220 (shoe)	Shell; intact valve	51 951	1609	Out of range	
088VC	T1-088VC-140	60.55733333	0.07375	123	140	Shell (? <i>Hiatella arctica</i> )	13 706	38	15 994	176
089VC	T1-089VC-092	60.50055	0.43235	147	92–95	Cold water benthic foraminifera [0.0100 g]	13 944	40	16 311	186
089VC	T1-089VC-096	60.50055	0.43235	147	96	Single valve (articulated when found); <i>Astarte</i> species	13 662	38	15 936	172
090VC	T1-090VC-441	60.38898333	0.802833	162	440–442	Barnacles and shells	12 154	37	13 601	143
092VC	T1-092VC-150	60.39548333	1.1275833	152	150	Single valve (articulated when found); species not identified	10 839	37	12 345	210

(Continued)

Table 6. (Continued)

Core JC-123-	Sample ID	Latitude (°N)	Longitude (°E) [-ve is °W]	Water depth (m)	Sample depth (cm)*	Sample type and identification (and/or condition) [mass indicated for small samples]	Conventional radiocarbon age ( <sup>14</sup> C a BP)	+/- 1σ	Calibrated age <sup>†</sup> (cal a BP)	+/- 2σ
092VC	T1-092VC-258	60.39548333	1.1275833	152	258-264	Cold water foraminifera	15 209	41	18 005	155
092VC	T1-092VC-550	60.39548333	1.1275833	152	550	Shell fragment	Background			
093VC	T1-093VC-135	60.33503333	1.4648166	130	135	Shell fragment	57 472	3213	Out of range	

\*Sample depth = depth in core (cm), assuming that zero is seabed. 'Shoe' refers to the geological sample (<10 cm long) recovered from foot of vibrocorer, not included in the core barrel; 'catcher' refers to the geological sample recovered by core catcher mechanism at base of vibrocore core barrel. Depths for shoe and core-catcher samples are approximate.

<sup>†</sup>Radiocarbon dates from marine carbonate (shells) converted from conventional radiocarbon years using OxCal 4.3.2 (Bronk Ramsey, 2013) and Marine13 (Reimer *et al.*, 2013). Where appropriate (i.e. finite ages), calibrated ages are presented in calendar years BP (i.e. before 1950 CE) as mean of two-sigma uncertainty; local marine-reservoir correction ( $\Delta R$ ) = 0.

earlier field campaign in 2006 (Fig. 5). The two Norwick (NE Unst) samples yield apparent exposure ages of  $22.4 \pm 1.6$  and  $21.6 \pm 1.5$  ka, with relatively large but overlapping (full) uncertainties (Table 4; Figs. 5 and 6). Taken at face value these ages have an uncertainty-weighted mean of  $21.9 \pm 1.3$  ka, and *could* constrain ice-mass retreat from the continental shelf to the northern tip of Shetland and therefore the timing of deglaciation in northern Unst. However, given the light glacial modification, the general absence of unequivocally glacially transported material in the vicinity, and the lack of supporting age constraints, the accuracy of these two ages is uncertain. (See Interpretation for further discussion).

The geology and landscape of southern Unst is different to the northern half of the island (Fig. 4). Golledge *et al.* (2008) mapped 'pervasive streamlining' in bedrock in a NW–NNW direction across much of SW Unst and NE Yell – geomorphological evidence of an erosive, relatively fast-flowing, ice-sheet corridor adjacent to Bluemull Sound (Fig. 4). Evidence for glacial streamlining in SE Unst is much more subtle and less convincing, with west-directed and east-directed ice flow both possible (Golledge *et al.*, 2008; Hall, 2014). Three samples collected from southern Unst, 1.5 km SE of Bay of Lund (T1LUN01, T1LUN02, T1LUN03), potentially record the timing of ice-mass wastage across low ground in northern Shetland. The samples are from three of the largest glacially transported boulders (each >2 m<sup>3</sup>) within a low-density spread of sub-rounded glacial cobble and boulder debris, strewn across ~1 km<sup>2</sup> of otherwise featureless low-lying ground. All three boulders are the same lithology as the underlying schistose psammitic or semi-pelitic bedrock (i.e. pseudo-erratics, not true erratics) indicating limited transport distances of <1 km. Two samples were taken from projecting quartz veins on the upper boulder surfaces, showing little or no post-depositional weathering. Some old stone walls and possible archaeological features were noted in the vicinity but not at the sample sites.

The Lund (SW Unst) samples yield apparent exposure ages of  $16.8 \pm 0.9$ ,  $13.4 \pm 0.8$  and  $11.9 \pm 0.6$  ka (Table 4; Figs. 5 and 6). These three ages have a reduced Chi-squared value ( $\chi^2$ ) of 11.70 indicating that they are not from a single event or age population. Although two of the samples (T1LUN02 and T1LUN03) agree more closely in age (Table 3), their analytical uncertainties do not overlap and their full (external) uncertainties only marginally overlap, making it hard to group them on statistical grounds. Two possible scenarios concerning these three new exposure ages are presented here. First, if we assume the oldest apparent age (T1LUN01) suffers from pre-existing nuclide inheritance, it is tempting to place emphasis on the youngest two ages – which fall within or at the transition to Greenland Stadial 1 (= Younger Dryas Stadial: 11.55–12.70 ka BP; Lowe *et al.*, 2008). At this point, it is pertinent to note that Younger Dryas glaciation has not yet been confidently identified on Shetland but has been tentatively proposed for several sites on the main island based solely on glacial geomorphological grounds (Mykura, 1976; Gordon and Sutherland, 1993; Ross, 1996; Golledge *et al.*, 2008). Second, and alternatively, if we assume that the two 'young' ages have been significantly affected by post-depositional disturbance – either natural, in the form of cryoturbation/solifluction, or anthropogenic, by human disturbance or overturning – emphasis is then placed on the oldest plausible age, as per the methodology of Putkonen and Swanson (2003). This would put the more accurate timing of deglaciation in southern Unst around 17 ka BP. Based on an assumption of post-depositional disturbance at this site, we could also infer possible human movement of these large stones around 3500–5000 years BP (i.e. 16.9 ka minus 13.4 or 11.9 ka). That notwithstanding, the

**Table 7.** Radiocarbon ages from marine cores in this study presented with a range of  $\Delta R$  marine reservoir-effect corrections. Blank cells are where no calibration could be performed. For sample-specific metadata see Table 6.

Sample ID	Conventional radiocarbon age ( $^{14}\text{C}$ a BP)		Calibrated age (cal a BP) $\Delta R = 0$		Calibrated age (cal a BP) $\Delta R = 300$		Calibrated age (cal a BP) $\Delta R = 700$	
		+/- $1\sigma$	years	+/- $2\sigma$	years	+/- $2\sigma$	years	+/- $2\sigma$
T1-052VC-180	20 158	52	23 785	218	23 424	249	22 946	227
T1-052VC-315	27 702	104	31 197	178	31 050	180	30 848	200
T1-053VC-shoe	45 382	775	Out of range		Out of range		Out of range	
T1-054VC-174	11 036	37	12 588	82	12 173	216	11 361	210
T1-054VC-228	11 060	38	12 604	80	12 216	218	11 410	235
T1-054VC-234	11 086	38	12 620	80	12 258	220	11 460	247
T1-054VC-297	Background							
T1-056VC-248	19 471	50	22 964	225	22 617	192	22 244	208
T1-056VC-256	21 005	55	24 802	314	24 372	208	23 950	210
T1-056VC-389	Background							
T1-059VC-shoe	14 815	40	17 564	169	17 173	202	16 548	229
T1-061VC-shoe	31 318	145	34 820	308	34 555	321	34 242	323
T1-064PC-502	12 925	37	14 794	321	14 112	137	13 680	147
T1-064PC-564	12 850	45	14 573	359	14 031	139	13 598	151
T1-067VC-shoe	Background							
T1-069VC-331	13 330	38	15 442	202	15 000	212	14 119	141
T1-072VC-202	13 896	38	16 240	174	15 857	171	15 240	147
T1-073VC-315	20 160	120	23 785	316	23 423	363	22 953	367
T1-074VC-300	26 022	83	29 756	368	29 375	282	28 941	269
T1-075VC-shoe	24 669	73	28 309	274	27 987	233	27 695	157
T1-076VC-214	Background							
T1-078VC-411	Background							
T1-079VC-catcher	Background							
T1-083PC-674	11 118	38	12 637	82	12 310	218	11 516	251
T1-083PC-762	11 356	36	12 811	123	12 601	80	12 004	182
T1-086VC-205	Background							
T1-086VC-shoe	51 951	1609	Out of range		Out of range		Out of range	
T1-088VC-140	13 706	38	15 994	176	15 551	218	14 961	223
T1-089VC-092	13 944	40	16 311	186	15 914	172	15 311	184
T1-089VC-096	13 662	38	15 936	172	15 486	208	14 883	265
T1-090VC-441	12 154	37	13 601	143	13 322	100	12 914	149
T1-092VC-150	10 839	37	12 345	210	11 777	247	11 142	92
T1-092VC-258	15 209	41	18 005	155	17 685	182	17 164	204
T1-092VC-550	Background							
T1-093VC-135	57 472	3213	Out of range		Out of range		Out of range	



**Figure 5.** Field photographs and  $^{10}\text{Be}$  TCN exposure ages of samples from Shetland, from north to south (top to bottom of page). Note: all samples are described in the text and presented in Tables 2,3 and 4. This figure shows only a selection of those samples analysed from each site. Apparent exposure ages are in ka cal BP. [Color figure can be viewed at [wileyonlinelibrary.com](http://wileyonlinelibrary.com)].

three TCN exposure ages are equivocal and cannot be used, on their own, to accurately and robustly date the deglaciation of southern Unst (Figs. 5 and 6).

#### *Out Skerries*

Out Skerries (known simply as ‘Skerries’) lie 10 km east of Mainland Shetland and are the easternmost extremity of the Shetland Islands, 298 km due west of the Norwegian coast

(Fig. 1). The islands are small (total area = 2.2 km<sup>2</sup>), low lying (maximum elevation = 53 m asl) and rocky, with ice-abraded outcrops and perched glacially transported boulders common on all three main islands. The bedrock is Dalradian schistose meta-sediment with occasional limestone bands (Fig. 4). Small exposures of till directly overlying bedrock are seen backing several bays and coves.

Three samples collected from Housay, the western island (T1OSW01, T1OSW03, T1OSW04), constrain the timing of

deglaciation of the last ice mass to cover these islands. The samples are from three glacially transported boulders (each  $>1 \text{ m}^3$ ) perched directly on ice-worn bedrock outcrops (Fig. 5). Stoss-lee forms, rare striae and incomplete plucking along the western promontory all indicate ice movement from SW to NE. Two of the boulders sampled are granitic in composition (T1OSW03 & 04), a rock type not found on the Skerries, suggesting that they were sourced on the Shetland Mainland (Fig. 4). The third boulder is the same lithology as the local bedrock. No disturbance of the boulders is likely since deposition.

The Skerries samples have exposure ages of  $17.9 \pm 1.0$ ,  $17.8 \pm 1.0$  and  $16.4 \pm 0.9$  ka, with overlapping analytical uncertainties (Table 4; Figs. 5 and 6). These three ages have a reduced  $\chi^2$  of 2.48 indicating that they are probably from a single population. We consider the uncertainty-weighted mean age of  $17.3 \pm 0.9$  ka to be a good robust representation of the true exposure age. (For comparison the arithmetic mean age is  $17.4 \pm 1.0$  ka.) These ages therefore constrain the timing of ice-mass retreat from the surrounding continental shelf to easternmost Shetland by  $\sim 17.3$  ka BP.

One small ( $0.6 \text{ m}^3$ ) glacially transported boulder (T1OSE01) from 46 m asl on Bruray, 1.2 km east of the other three samples, yielded an apparent exposure age of  $14.9 \pm 0.9$  ka. We consider this single age to be anomalously young possibly owing to disturbance since deposition. Storm-wave action cannot be ruled out in this particular setting.

#### Dalsetter

The Mainland of Shetland extends south to Sumburgh Head as a long 5-km-wide promontory known as Dunrossness, with the Atlantic Ocean on one side and North Sea on the other. Around 8 km north of Sumburgh Head close to the east coast between Boddam Voe and Loch of Clumlie is a conspicuous spread of glacially transported rock debris forming a 100–500-m-wide boulder belt trending broadly north–south (Fig. 4). In places the boulders are quite large (exceeding  $\sim 3 \text{ m}^3$ ) and sporadically distributed (1 per  $50 \text{ m}^2$ ) (Fig. 5); in other places the mean boulder volume is smaller ( $<1 \text{ m}^3$ ) but their density distribution is greater ( $>1$  per  $4 \text{ m}^2$ ). Most of the boulders are quartz-arenite sandstone or conglomerate, with rare exotic boulders. Many are sub-rounded and typically show some evidence of post-depositional surface loss, with occasional quartz clasts protruding 10–20 mm from the present-day boulder surface. Bedrock exposures are rarely seen. It was in this locality that a  $0.8\text{-m}^3$  glacially transported boulder of Norwegian tonsbergite was found (Finlay, 1932; Le Bas, 1992). The ‘Dalsetter Stone’ now forms part of a field boundary, adjacent to the road; however, there is evidence, in the form of verbal accounts (Finlay, 1932; Flinn, 1992), that it was originally *in situ* – extracted from till in an adjacent field ca. AD 1930. Despite extensive searches, the ‘Dalsetter Stone’ erratic remains the only definitive boulder of Scandinavian origin found on Shetland.

Three samples from the boulder-belt moraine at Dalsetter constrain the timing of glacial retreat in southernmost Shetland (T1DAL01, T1DAL06, T1DAL08). All three samples are from large, glacially transported, conglomeratic quartz-arenite boulders ( $>1 \text{ m}^3$  in size) identified as Devonian ‘Old Red’ Sandstone – the same lithology as the local bedrock. No disturbance of the boulders is likely since deposition.

The Dalsetter samples have exposure ages of  $18.2 \pm 1.0$ ,  $17.9 \pm 1.0$  and  $19.2 \pm 1.0$  ka, with overlapping analytical uncertainties (Table 4; Figs. 5 and 6). These three ages have an uncertainty-weighted mean age of  $18.5 \pm 1.0$  ka and reduced  $\chi^2 = 1.23$ , indicating that they are from a single population

(with two degrees of freedom) and are an accurate robust representation of the true exposure age. These ages therefore constrain the retreat of an ice-mass margin from the surrounding continental shelf to Dunrossness by  $\sim 18.5$  ka (Fig. 6). The significance of this geographically important site for understanding the timing of ice-sheet retreat across the wider area, including the Fair Isle Channel, is discussed further in the Interpretation section.

#### Foula

Foula lies 30 km WSW of Mainland Shetland and is the westernmost of the Shetland Islands, 80 km due east of the continental shelf break (Figs. 1 and 2). The island is relatively small (area =  $12.7 \text{ km}^2$ ) but high relief, reaching 418 m asl at its highest point, with sheer cliffs along its west coast. The bedrock geology of Foula is relatively simple with the upland part of the island being formed of Devonian ‘Old Red’ quartz-arenite sandstones, conglomerates and shales; while the NE portion of the island comprises a Precambrian metamorphic complex similar to that seen in the Walls district of Mainland Shetland (Figs. 1 and 4). The glacial history of Foula was studied in detail by Flinn (1978) who presented convincing evidence for a thick erosive ice mass overwhelming the island from the ESE probably during the last glacial cycle [i.e. Marine Isotope Stage (MIS) 2–3/Late Weichselian]. Ice-abraded outcrops and glacio-erosional bedforms are common especially close to the coastline, although glacial deposits are relatively rare. Clear examples of glacially transported boulders are uncommon across much of the north of the island; by contrast, abundant granite and granodiorite erratics are found in the south of the island on the gently sloping hillsides above the community of Hametoun (Figs. 4 and 5).

Four samples from the boulder-strewn erratic-field NW of Hametoun were taken to constrain the timing of glacial retreat on Foula (T1FOU01, T1FOU02, T1FOU04, T1FOU05). All four samples are from large upstanding boulders ( $2\text{--}3 \text{ m}^3$  in size) within an area of  $\sim 1 \text{ km}^2$  located 75–90 m asl (Figs. 4 and 5). One is composed of local Devonian conglomeratic sandstone. Three are granitic/granodioritic in composition indicating an ice-transport path from the SE quadrant. Flinn (1978) presumed these erratic boulders were sourced from the Spiggie granite pluton on southern Shetland, although the exact source is undetermined as Spiggie granite outcrops also exist in Scalloway Bay above and below sea level, 20–30 km north of the main intrusion near Loch of Spiggie in Dunrossness (Fig. 4).

The Foula samples yield apparent exposure ages of  $10.9 \pm 0.7$ ,  $15.8 \pm 0.9$ ,  $9.9 \pm 0.6$  and  $16.7 \pm 0.9$  ka (Table 4; Figs. 5 and 6). The bi-modal distribution of these four ages is difficult to interpret as the samples are all from the same area and morphostratigraphic setting. Common statistical approaches for detecting outliers, such as Peirce’s criterion (e.g. Blomdin *et al.*, 2016) or a gESD test (e.g. Jones *et al.*, 2019), cannot be applied. Although neither show obvious signs of post-depositional disturbance, it is possible that the two ‘young’ boulders have been subjected to gelifluction/solifluction processes resulting in ploughing, tilting and/or overturning. Examination of high-resolution colour aerial photos shows numerous, well-developed, overlapping solifluction lobes with boulder rows immediately upslope of the erratic-boulder-strewn ground. Presently inactive in Foula’s mild maritime climate, these relict periglacial phenomena probably formed, or were re-activated, during Greenland Stadial 1 (= Younger Dryas) ca. 11.55–12.70 ka BP. Pronounced periglacial activity on Scotland’s Northern and Western Isles has been attributed, although not firmly dated, to this very cold interval

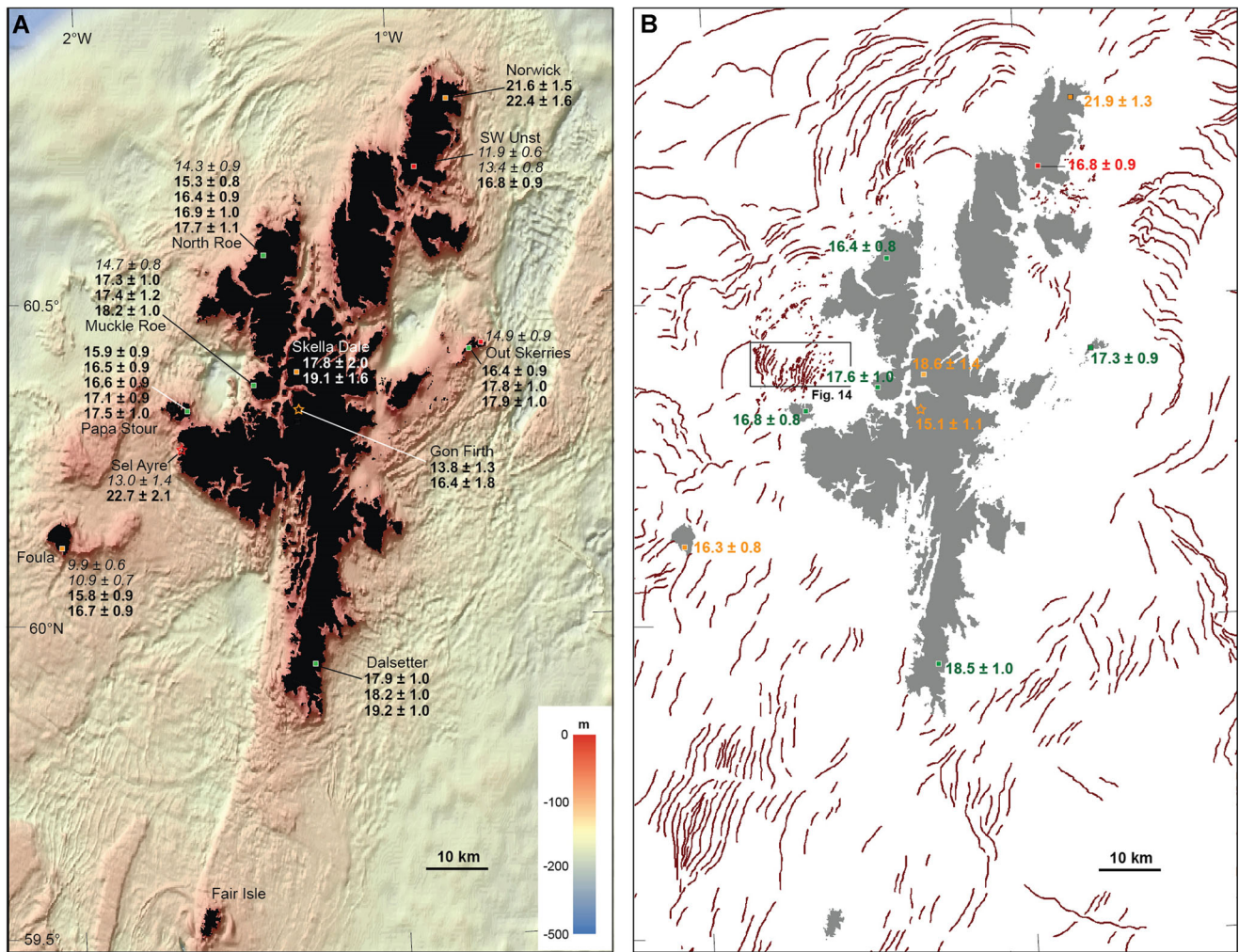


**Figure 6.** A. Map of Shetland showing location of all 32 TCN exposure ages with external (full) uncertainties, and four OSL ages with associated uncertainties. All ages are in ka cal BP. TCN sites – filled squares; OSL sites – stars. Italic font denotes anomalously young outliers (from reduced  $\chi^2$  tests and Bayesian modelling). Bathymetric basemap is extract of EMODnet hill-shaded surface elevation model. B. Mapped moraines (crestlines) on the continental shelf around Shetland. Uncertainty-weighted mean exposure ages with full uncertainties are shown for each named (onshore) site using the quality-control colour coding (after Small *et al.*, 2017) [green = robustly dated; amber = acceptable, but not robust; red = unreliable, possibly erroneous]. Box in St Magnus Bay shows location of Fig. 14. [Color figure can be viewed at [wileyonlinelibrary.com](http://wileyonlinelibrary.com)].

(Ballantyne *et al.*, 1998, 2017). The older two exposure ages from Foula have overlapping analytical uncertainties with an uncertainty-weighted mean age of  $16.3 \pm 0.6$  ka, but could also have been affected to some degree by periglacial processes. These problems aside, these are the first absolute age-constraints for the deglaciation of Foula – although we fully accept that their accuracy and robustness may have been compromised by post-depositional processes and/or other unknown geological factors.

#### Papa Stour

Papa Stour lies just 2 km off the west coast of Mainland Shetland separated from it by the Sound of Papa (Figs. 1 and 4). It is the westernmost island in the Shetland group, excluding Foula 35 km to the SW. Papa Stour is 8.3 km<sup>2</sup> in area and is relatively low relief, lacking hills but reaching a maximum elevation of 87 m asl in the west. The island is almost completely surrounded by 10–50-m-high cliffs and has a rugged highly eroded coastline. The island is composed almost entirely of Devonian rhyolitic tuff and lava with some basaltic lavas in the north (Fig. 4). The volcanic tuff bedrock is weak and highly susceptible to physical and chemical weathering processes, and hence glacial abrasion features are rare. However, excellent cross-cutting striae are found on basalt

exposures along the shoreline where glacial sediment has been recently removed by storm waves (Fig. 4). Notable boulder concentrations forming belts up to 250 m wide, some associated with small but conspicuous moraine mounds (2–5 m high), occur across the middle of the island. We map a series of discrete low-relief moraine belts trending NNW–SSE across the island (Fig. 4). Numerous glacially transported boulders occur, mostly associated with these moraines. Small exposures of till (1–3 m thick) directly overlying striated or disaggregated glaciotectionized bedrock are seen backing bays and coves in the east of the island.

Five boulders from the Papa Stour moraines were sampled to constrain the timing of ice-mass retreat from the continental shelf across the outer part of St Magnus Bay in westernmost Shetland (T1PAP04–08). All samples are from erratic boulders with lithologies exotic to the island; four schistose psammite boulders from the Dalradian complex, and one quartz-rich gneiss (T1PAP06) probably from the Precambrian complex in western Mainland Shetland (Fig. 4). Some of the sampled boulders were partly buried within the surrounding glaciogenic (morainic) diamict and, consequently, projected only 0.2–0.5 m above the land surface. No disturbance of the boulders is likely since deposition.

The five Papa Stour samples have exposure ages of  $15.9 \pm 0.9$ ,  $17.5 \pm 1.0$ ,  $16.5 \pm 0.9$ ,  $17.1 \pm 0.9$  and  $16.6 \pm 0.9$

ka, and yield a reduced- $\chi^2$  of 1.08 indicating that they are from a single population (with four degrees of freedom). We therefore consider the uncertainty-weighted mean age of  $16.8 \pm 0.8$  ka to be an accurate robust representation of the true exposure age, which closely constrains the timing of deglaciation of westernmost Shetland (Figs. 5 and 6).

### Muckle Roe

Muckle Roe is an almost circular island, 18 km<sup>2</sup> in area, at the head of St Magnus Bay, 12 km west of Papa Stour and just 30 m from Mainland Shetland (Figs. 2 and 4). The island is rugged and rocky with little Quaternary sediment cover and only a thin patchy soil. Muckle Roe is composed almost entirely of Devonian granite (the Muckle Roe intrusion), best exposed in the high cliffs that fringe the island's west coast (Fig. 4). The highest point on the island is 175 m asl. The landscape is typical of cnoc-and-lochan terrain (Mykura, 1976; Hall, 2014) with glacially eroded bedrock outcrops on a range of scales, including elongate streamlined hills, stoss-lee forms (roches moutonnées) and wholly abraded forms (whalebacks), interspersed with deeply carved linear valleys and rock basins, hosting an abundance of glacially transported boulders. The streamlined bedrock landscape on Muckle Roe, particularly at lower elevations (<80 m asl), indicates erosion by warm (wet)-based glaciers flowing in a NW–NNW direction (Fig. 4). High-resolution digital surface models show the morphology and roughness of the terrain strongly resemble the glacially scoured cnoc-and-lochan terrain of the Scottish NW Highlands and Inner Hebrides (e.g. Loch Laxford region, Raasay, Rona, Sleat on Skye), strongly modified by Pleistocene ice streams or their tributaries (Bradwell *et al.*, 2007; Bradwell, 2013; Dove *et al.*, 2015).

Four samples were taken from relatively high ground (84–94 m asl) on Muckle Roe (T1HAM01, 02, 03, 06) to constrain the timing of ice-mass retreat across the inner part of St Magnus Bay and back to the Shetland Mainland (cf. Papa Stour, above). Three of the samples were from large glacially transported granite/granodiorite boulders perched directly on pink granitic bedrock (i.e. Muckle Roe-derived material, not strictly erratics) (Fig. 5). T1HAM06 was from a smaller white quartz-feldspar-rich granite boulder. Disturbance of the boulders since deposition is possible but unlikely.

The four Muckle Roe samples have exposure ages of  $17.3 \pm 1.0$ ,  $18.2 \pm 1.0$ ,  $17.4 \pm 1.2$  and  $14.7 \pm 0.8$  ka (Table 4; Figs. 5 and 6). These four ages have a reduced- $\chi^2$  of 7.85 suggesting that geological uncertainty is contributing to the spread. A gESD test for outliers does not identify any outliers at  $p=0.05$ , but at  $p=0.1$  the youngest sample (T1HAM06) is flagged as an outlier. The three remaining samples compare closely with overlapping analytical uncertainties and a reduced- $\chi^2$  of 0.52 indicating that they are from a single population (with two degrees of freedom). We therefore consider their uncertainty-weighted mean age ( $17.6 \pm 1.0$  ka) to be an accurate robust representation of the true exposure age (Fig. 6). The precise glaciological interpretation of this group of exposure ages is complicated by the fact that their mean age is slightly older than the mean exposure age from Papa Stour ~12 km to the west and therefore further 'down-glacier' (see above). It is worth noting that previous TCN geochronologies in northern Scotland have reported stochastic variation of 0.3–1.2 ka calculated age even from boulders on the same moraine landform (Bradwell *et al.*, 2008; Ballantyne *et al.*, 2009; Ballantyne, 2010), which makes separation of events <1.0 ka difficult. The mean exposure ages from Muckle Roe and Papa Stour have overlapping (external) uncertainties ( $16.8 \pm 0.8$  ka vs  $17.6 \pm 1.0$  ka) making it difficult to

distinguish on statistical grounds whether deglaciation occurred first on Papa Stour (20 m asl) or, possibly due to early emergence of higher ground (100 m asl), on Muckle Roe first. The similarity of these two groups of ages, ~10 km apart, indicates that deglaciation probably occurred at approximately the same time at both sites (i.e. between 17.6 and 16.8 ka). What is certain, based on the clear submarine geomorphology and sound glaciological principles, is that the calving ice-margin retreated inshore from west to east (or NW to SE) within St Magnus Bay during the latter stages of deglaciation (Figs. 3 and 6).

### Skella Dale

Approximately 7 km east of Muckle Roe, a suite of conspicuous moraines occur in the E–W-trending valley of Skella Dale (Fig. 2). The moraines were mapped by Golledge *et al.* (2008) extending 2 km upvalley to a col at ~200 m asl. They ascribed the Skella Dale moraines to their 'Landsystem 3' produced during late-stage active, oscillatory, glacier retreat, possibly during the Younger Dryas Stadial (Greenland Stadial-1) (Golledge *et al.*, 2008).

Two large, quartz-rich, psammite boulders within the conspicuous moraine complex in Skella Dale, central Mainland, were sampled in 2006 (and re-sampled again in 2014) (Fig. 5). A third suitable target could not be found in the vicinity. Owing to their large size (>8 m<sup>3</sup>), disturbance of either boulder is very unlikely since deposition. We note that unusually large angular (i.e. non-rounded) boulders are more typical of supraglacial transportation and deposition (Putkonen and Swanson, 2003; Darvill *et al.*, 2015).

The Skella Dale samples yield apparent exposure ages of  $19.1 \pm 1.6$  and  $17.8 \pm 2.0$  ka, with relatively large but overlapping analytical uncertainties. These two ages yield a mean age of  $18.6 \pm 1.4$  ka, but owing to the small number of samples ( $n=2$ ) cannot be tested for clustering or outliers. Taken at face value these two ages *could* constrain the retreat of an ice-mass margin from the head of St Magnus Bay back to the central hills of Mainland Shetland by ~18.5 ka BP. However, our clusters of TCN exposure ages from Muckle Roe and Papa Stour further west indicate deglaciation *after* this time, around 17.6–16.8 ka BP (see above). This age conflict places considerable uncertainty on the accuracy of the two apparent exposure ages from Skella Dale. (See the Interpretation section for further discussion).

### North Roe

All but an island, North Mave, Shetland's large (204 km<sup>2</sup>) NW peninsula, is connected to the rest of Mainland by a narrow isthmus only 80 m wide and 200 m long. The northern part of this peninsula, beyond the deeply incised fjord of Ronas Voe and the rounded granite massif of Ronas Hill (450 m asl), is known as North Roe (Figs. 1 and 2). The landscape of this area is wild and varied, as is the geology – consisting of a large Devonian granite body intruded into ancient Archaean gneisses and Precambrian meta-sediments (Fig. 4). Like Muckle Roe the landscape of North Roe is rocky and rugged, and in places strongly streamlined by glacial action (Golledge *et al.*, 2008). The bedrock streamlining indicates erosion by warm (wet)-based glaciers flowing in a WNW direction and is most notable at lower elevations (<150 m asl). Hill-shaded DSM (NEXTMap GB) imagery shows a marked corridor of strongly directional glacial streamlining in the lower ground around Roer Water extending to the present-day coastline (Fig. 4). In the field, the landscape strongly resembles glacially scoured basement gneiss cnoc-and-lochan terrain seen in NW

Scotland (Bradwell *et al.*, 2007; Bradwell, 2013). Glacially transported boulders resting on ice-abraded bedrock, suitable for TCN exposure-age dating, are common at this locality.

Five samples from glacially transported boulders in the valley of Roer Water (T1MAA01–05) constrain the timing of ice-mass retreat in NW Shetland (cf. Papa Stour, above). Four of the samples are from ice-transported granitic blocks perched directly on a single large (~25 m<sup>2</sup>) ice-abraded granitic bedrock slab and are probably locally derived material, not strictly erratics. One was a whole cobble (<0.3 m<sup>3</sup>) (T1HAA02), the others were taken from the tops of boulders (ranging from 0.5 to 1.5 m<sup>3</sup> in size) (Fig. 5). The fifth sample is from a large perched glacially transported boulder <200 m away. Disturbance of this material since deposition is possible but unlikely.

The five North Roe samples have apparent exposure ages of  $15.3 \pm 0.8$ ,  $16.9 \pm 1.0$ ,  $14.3 \pm 0.9$ ,  $17.7 \pm 1.1$  and  $16.4 \pm 0.9$  ka (Table 4; Figs. 5 and 6). A gESD test for outliers did not identify any of these samples as outliers, but the youngest sample (T1MAA03) was identified as an outlier by our Bayesian age model (OxCal 4.3, run in outlier mode). The five exposure ages have an uncertainty-weighted mean of  $15.8 \pm 0.7$  ka. Four of these ages (excluding the youngest) have a reduced- $\chi^2$  of 2.95 indicating that they are probably from a single population (with three degrees of freedom) and yield an uncertainty-weighted mean age of  $16.4 \pm 0.8$  ka. The 'young' apparent exposure age (T1MAA03) suggests deposition, and therefore deglaciation of low ground, during Greenland Interstadial 1, which conflicts with other published dating evidence from Shetland suggesting deglaciation before this time (Birnie *et al.*, 1993). We therefore consider the uncertainty-weighted mean age of the four remaining plausible ages ( $16.4 \pm 0.8$  ka) to be an accurate and robust representation of the true exposure age, although we accept that other interpretations are possible. These four exposure ages closely constrain the timing of deglaciation in NW Shetland to ~16.4 ka BP (Fig. 6).

#### Fair Isle

Given its isolated location midway between Shetland and Orkney (centred on 59.55°N, 1.62°W), Fair Isle is a small but crucial landmass for constraining the deglaciation of the northern UK continental shelf and both island groups. Unfortunately, we were not able to visit Fair Isle during the 2014 field campaign owing to time constraints and poor weather. Targets for TCN analysis were identified from remote sensing imagery and previous literature (Flinn, 1970, 1978; Mykura, 1976), but samples could not be collected within the strict project timescale. The sample allocation ( $n=4$ ) was therefore re-apportioned to the other sites in Shetland.

#### OSL geochronology

Suitable sites for OSL dating of MIS 2–3 deglaciation are surprisingly rare on Shetland owing to the lack of sorted sand-fraction sediments within well-defined deglacial landform-sediment assemblages. Only four samples, from two sites, were taken and analysed in this study (Table 5; Fig. 6); one of these sites (Sel Ayre) has been the subject of previous OSL analysis (Duller *et al.*, 1995).  $D_e$  distributions were found to be highly scattered with overdispersion (OD) values of 100 and 83% for Gon Firth samples, and 100 and 71% for Sel Ayre samples – interpreted as indicating poorly bleached sediments. While a minimum age approach would normally have been adopted in such instances (e.g. Bateman *et al.*, 2018) it was noted that all samples had a low  $D_e$  component which gave

ages too young to be considered coherent with the site geology. Instead, FMM (Galbraith and Green, 1990) was used to isolate and remove this young component. Ages are reported based on the IEU model of the remaining data with starting parameters of  $a=0.3344$  and  $b=-0.064$  as determined experimentally from dose recovery tests (see Supporting Information).

#### Sel Ayre

Sel Ayre is located at the western extremity of Mainland Shetland (Fig. 2) and, along with Fugla Ness in North Roe, is one of only two pre-Late Weichselian (pre-MIS-2) sites known in Shetland (Duller *et al.*, 1995). The site, in a 90-m-high sea-cliff section, occupies a large pre-glacial channel filled (from bottom to top) with (i) periglacially derived breccia, (ii) peat, (iii) organic sand and gravel, (iv) diamicton, interpreted as till indicating ice-sheet flow from SE to NW (Hall *et al.*, 1993), and (v) Holocene peat. Previous luminescence measurements from the upper organic sands proved difficult, and infra-red stimulated luminescence measurements on feldspars are probably maximum estimates, producing reported ages of 98–105 ka BP (Duller *et al.*, 1995; Hall *et al.*, 2002). For a detailed sedimentological and biostratigraphical description of this site see Hall *et al.* (1993), Duller *et al.* (1995) and Hall *et al.* (2002). Two samples (Shfd14142 and Shfd14143) were collected in 2014 from the mid-to-upper sands and gravels (unit 3), slightly above the main organic unit but below the glacial diamicton (Sel Ayre Till). It was expected that the samples would constrain ice-sheet advance across Shetland before the Last Glacial Maximum (LGM).

The two OSL samples from the Sel Ayre sequence yield widely differing ages indicating sediment deposition at  $13.0 \pm 1.4$  and  $22.7 \pm 2.1$  ka BP (Table 5). Taken at face value, the youngest age is implausible as it places ice-sheet overriding after ~13 ka, at a time when all other sites on Shetland indicate ice-free conditions (e.g. Birnie *et al.*, 1993; Whittington *et al.*, 2003). The oldest age is plausible, placing the timing of ice-sheet advance after ~23 ka BP. Given that both samples proved problematic from an OSL perspective and show different ages from the same stratigraphically equivalent sedimentary unit, caution is required when interpreting them. However, the older age ( $22.7 \pm 2.1$  ka) is not inconsistent with TCN age constraints from Papa Stour <5 km away (see above), suggesting deglaciation by ~17 ka BP, and the 'minimal' <sup>14</sup>C assay from Sel Ayre ( $22\,450 \pm 80$  a <sup>14</sup>C BP; Hall *et al.*, 1993) – although the latter is thought to be affected by young carbon (Hall *et al.*, 2002).

#### Gon Firth

Gon Firth is a coastal inlet at the head of St Magnus Bay in central Mainland Shetland (Fig. 2). The site is within a 3-km<sup>2</sup> area mapped as till and hummocky moraines (BGS, 1982, 2018), with numerous small recessional morainic mounds and ridges trending broadly north–south across the area. These moraines probably represent the final stages of ice-mass decay towards the interior of Shetland (Colledge *et al.*, 2008). A small pit excavated into one of these moraines revealed massive to weakly stratified gravel-rich cobble and boulder diamicton with occasional thin units of rippled, subsequently deformed, sands. These sand units probably represent glaciofluvial deposition at, or near, the ice front during or slightly before moraine formation. Two OSL samples (Shfd14140 and Shfd14141) were collected from the rippled sand unit. It was expected that the samples would constrain the final stages of ice-mass decay in Shetland.

The two OSL samples from the moraine at Gon Firth, collected at two different points within the same stratigraphic unit, yield ages within error of each other:  $13.8 \pm 1.3$  and  $16.4 \pm 1.8$  ka (Table 5). Taken at face value, the broad age range covered by these estimated ages is glaciologically plausible, being similar to, but younger than, the TCN exposure ages from the periphery of western Shetland (cf. Papa Stour, Muckle Roe and North Roe, above). The age range of these two OSL samples, with an arithmetic mean of  $15.1 \pm 1.1$  ka, also corresponds with biostratigraphical and radiocarbon dating evidence from organic sites in central Shetland which indicate deglaciation before the Lateglacial Interstadial  $\sim 14.8$  ka BP (e.g. Birnie *et al.*, 1993; Hulme and Shirriffs, 1994; Whittington *et al.*, 2003).

### Submarine glacial geomorphology

Newly available digital multibeam and single-beam echosounder bathymetry datasets, largely acquired by the UK Maritime and Coastguard Agency's Civil Hydrography Programme, have revealed the pattern of glacial landforms preserved on the seafloor around Shetland in more detail (Figs. 2 and 3). In addition to these datasets, continuous high-resolution multibeam echo-sounder data were collected during scientific cruise JC123. Using these datasets we have mapped the offshore glacial landforms ( $n > 1000$ ) within the study area (Transect 1) and the adjacent areas to ensure spatial continuity with other ice-sheet sectors (i.e. Transects 8 and 2) – significantly revising those mapping compilations of Bradwell *et al.* (2008), Clark *et al.* (2012) and Sejrup *et al.* (2016) where they cover the same geographical area. The revised pattern, morphology and spatial relationships of seafloor moraines on the West Shetland and North Sea continental shelves changes our view of ice-sheet glaciation in this region (Fig. 3). Specifically, the mapping extends and clarifies the relationship between seabed moraines NE and NW of Shetland, in the northern North Sea Basin east of Shetland, and in the waters between Shetland and Orkney – areas that have previously escaped detailed scrutiny. Our palaeo-glaciological pattern reconstruction supports previous workers' findings that the northern sector of the BISS was confluent with the FIS to the east during one or more earlier phase(s) of Weichselian glaciation (e.g. Boulton *et al.*, 1991; Carr *et al.*, 2006; Bradwell *et al.*, 2008; Clark *et al.*, 2012; Sejrup *et al.*, 2016; Merritt *et al.*, 2017). However, this connection was lost at some point, as the two ice sheets decreased in size and separated – as also asserted by previous workers (Bradwell *et al.*, 2008; Clark *et al.*, 2012; Sejrup *et al.*, 2016; Merritt *et al.*, 2017). We find that following ice-mass separation, the most recent phase of ice-mass growth and decay left the strongest geomorphological imprint in the shelf-wide seabed geomorphology around Shetland.

We present this new glacial landform pattern information here (Fig. 3) mainly to place our new chronological data in context, but do not describe the geomorphological results in detail. A full presentation of the submarine geomorphology and its relationship to the Quaternary geological (sub-seabed) stratigraphy around Shetland forms work in progress.

### Marine sedimentology and geochronology

To prove the Quaternary stratigraphy at key locations and recover material for dating purposes, 41 seabed cores were taken within the study area (Transect 1) during scientific cruise JC123. This total was made up of 38 vibrocores (VC) with an internal diameter of 8 cm, and three piston cores (PC) with an internal diameter of 12 cm. All cores collected

had 100% continuous recovery. Cores ranged from 0.50 to 7.80 m in length. In the interest of space, the results are presented here in outline form simply to place our chronological data in context, focusing on key cores that yielded continuous deglacial sediment sequences and finite  $^{14}\text{C}$  dates.

In total, 35 marine carbonate samples from 23 cores within Transect 1 were analysed using AMS radiocarbon analysis (at NERC Radiocarbon Facility and SUERC, East Kilbride). Twenty-four finite dates were produced ranging from  $10\,839 \pm 37$  to  $31\,318 \pm 145$   $^{14}\text{C}$  a BP (uncalibrated ages; see Table 6); 11 non-finite ages were also produced. The remaining 17 cores were not deemed to be stratigraphically suitable for constraining the age of deglaciation or did not yield datable material. The following 'offshore results' section detailing all the radiocarbon dates is organized by sub-transect, clockwise from North. To aid brevity, the prefix 'JC123' has been omitted from all core names hereafter (i.e. 074VC = JC123-074VC). All measurements are from core-top down, to the nearest whole centimetre. All reported radiocarbon ages are presented calibrated, in calendar years BP, and corrected for marine reservoir effect, with  $\Delta R = 0$  (see Methods and Table 6 for details). However, by way of a sensitivity test, we also present a range of age calibrations ( $\Delta R = 0$ ;  $\Delta R = +300$ ;  $\Delta R = +700$ ), to explore the impact of using different  $\Delta R$  values (Table 7), as performed by others (e.g. Small *et al.*, 2013; Callard *et al.*, 2018). These different  $\Delta R$  values have only a modest impact on the overall reported ages. Owing to the current uncertainties surrounding the use of different  $\Delta R$  values in North Sea and North Atlantic waters (Stern and Lisiecki, 2013), herein we refer only to calibrated ages with  $\Delta R = 0$  for clarity and consistency (Table 6).

#### Sub-transect 1 – NE of Unst

The geomorphology of the continental shelf north and east of Unst is extremely complex hosting some of the best-preserved seabed moraines in NW Europe. These moraines were originally mapped using Olex variable-resolution single-beam bathymetry data by Bradwell *et al.* (2008) and were thought to relate to dynamic repeated oscillations of the northernmost marine sector of the BISS during overall shoreward retreat. More recently, Sejrup *et al.* (2016) related these moraines to a regional readvance of ice sourced on Shetland following rapid grounding-line retreat and withdrawal of the Norwegian Channel Ice Stream to the east. Sejrup *et al.* (2016) inferred ice-mass growth over Shetland at a time of Norwegian Channel Ice Stream collapse, possibly in response to reduced ice-sheet buttressing and changing ice-divides. They placed this collapse event between 18.5 and 17 ka BP. However, the status and timing of this regional readvance in the northern North Sea Basin, along with the configuration and extent of the ice mass at this time, requires further testing.

#### Core 074VC.

This core was the furthest north core taken within the whole Britice-Chrono project: located at  $61.47888^\circ\text{N}$ ,  $0.08535^\circ\text{E}$  in a water depth of 190 m. New MBES data from JC123 support previous mapping (Johnson *et al.*, 1993; Stoker *et al.*, 1993), showing that the seabed in this area is heavily iceberg scoured (Fig. 7). Numerous, large, curvilinear ploughmarks, 1–3 m deep, up to 100 m wide and 3000 m long, cross the MBES swath corridor in randomly orientated directions. Less well-preserved but

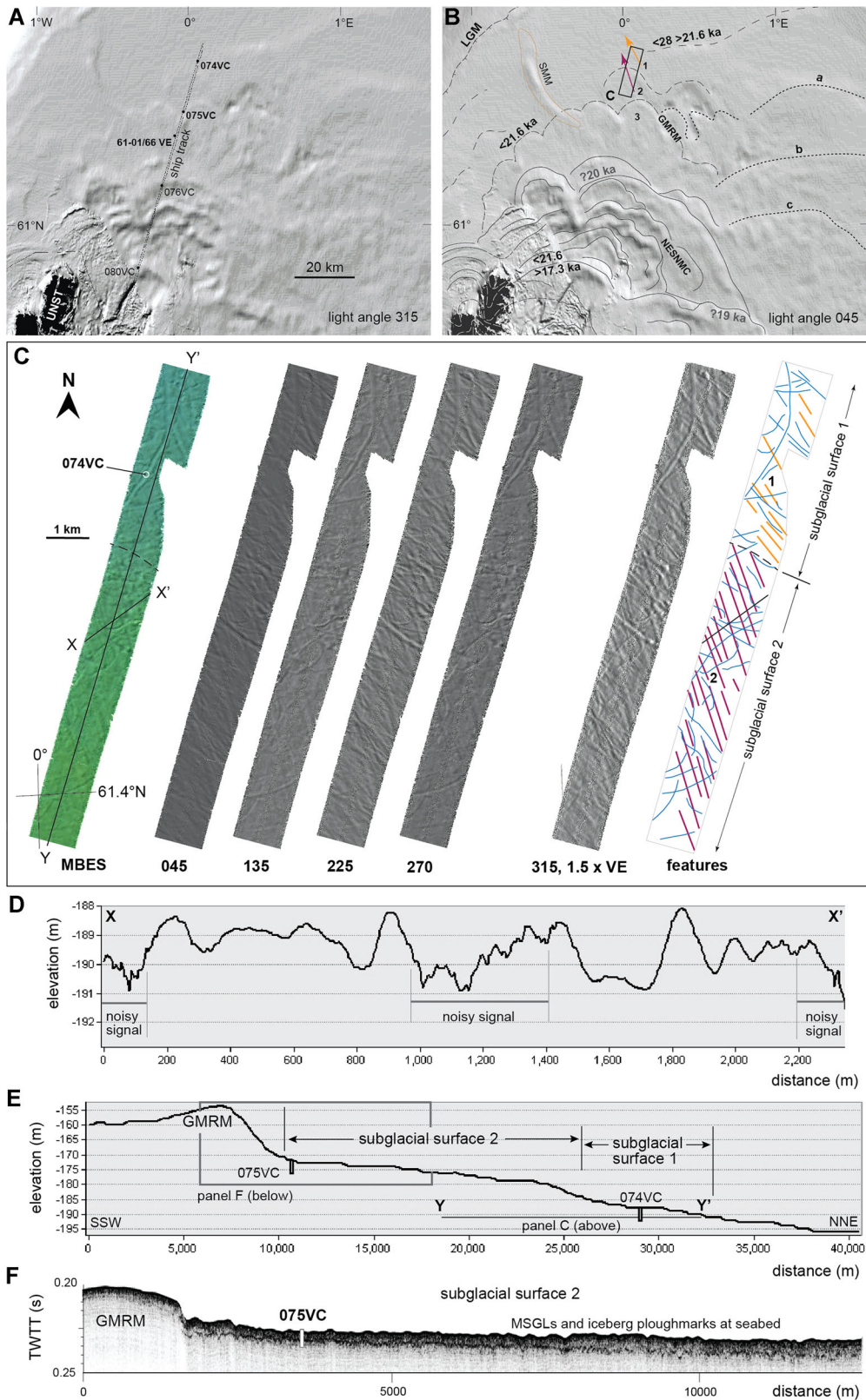


**Figure 7.** Marine geophysical data from the continental shelf NE of Unst. A. Bathymetric basemap showing location of multibeam echo-sounder (MBES) line (ship track) and selected core sites; hill-shaded greyscale EMODnet elevation model, light angle from NW/315°. B. Summary of submarine geomorphological and pseudo-stratigraphical relationships NE of Unst, at same scale as A. Subglacial surfaces, long dashed lines, labelled 1, 2 and 3. Large, lobate till aprons or possible low-relief grounding-zone wedges, at ca. 1°E, labelled a, b and c. Inferred ages of key moraine stages shown. LGM = Last Glacial Maximum ice-front position; SMM = probable shear margin moraine; GMRM = Greenwich Meridian Readvance Moraine; NESNMC = NE Shetland nested moraine complex. EMODnet bathymetry basemap; hill-shaded greyscale elevation model, light angle from NE/045°. C. MBES data collected on JC123 showing geomorphology of subglacial surfaces 1 and 2. Greyscale digital surface model (DSM) shown with four different lighting directions to aid geomorphological interpretation and to avoid azimuth bias. Final DSM is lit from NW/315° with 1.5× vertical exaggeration. Two sets of subglacial bedforms [glacial lineations; orange (1), purple (2)] and cross-cutting iceberg ploughmarks (blue) mapped from MBES data. D. Bathymetric seabed profile across MBES data, perpendicular to orientation of subglacial bedforms, shown in C from X to X'. Note amplitude of glacial lineations is typically 1–3 m. E. Bathymetric seabed profile in the direction of the MBES data collection swath, shown as Y–Y' in C. F. Geophysical sub-bottom profile along line of MBES swath showing typical acoustic facies of subglacial surfaces, irregular seabed morphology and location of core 075VC. For location of sub-bottom profile see grey box in E. TWTT = two-way travel time; GMRM = Greenwich Meridian Readvance Moraine. [Color figure can be viewed at [wileyonlinelibrary.com](http://wileyonlinelibrary.com)].

still clearly visible in the MBES data are subtle, closely spaced parallel lineations, trending 340–350° (NNW–SSE). We map a field of seabed lineations, between cores 074VC and 075VC, with individual ridges ranging in height from 1 to 3 m, in width from 100 to 300 m and in length from 1000 to >2700 m, stretching beyond the width of the MBES swath coverage (Fig. 7). Some lineations (ridges) appear to start from small seabed protuberances and some are flanked by narrow depressions (grooves). We interpret these landforms as large-scale flutings or mega-scale glacial lineations formed at the base of a rapidly flowing grounded ice sheet as it moved in a general NNW direction. The seabed in this region therefore represents one or more subglacial surfaces (i.e. the former ice sheet bed), subsequently scoured by large iceberg keels, and experiencing very little sediment deposition since.

Core 074VC (3.29 m long) was taken on subglacial surface 1 (Fig. 7) from within a long, wide iceberg scour, which cuts across the glacial lineations at an oblique angle (ca. 060°). The ploughing iceberg keel would have removed or redistributed the upper 1–2 m of glacial sediment, allowing the core to penetrate deeper (older) material beneath. The core consists almost entirely of firm dark grey to black, occasionally gravelly, mud coarsening upwards to slightly silty mud (2.90 m). Faint occasional colour laminations are seen under optical examination below 1.40 m. Rare isolated clasts (<20 mm in diameter) are visible in the core from 0.40 m to core base. Mud shear strengths are relatively high and variable ranging from 60 to 150 kPa. P-wave velocities – a useful proxy for the degree of consolidation or undrained sediment strength – are also relatively high ranging from 1600 to 1800 m s<sup>-1</sup> and, like the shear strength values, do not increase progressively with depth, suggesting they relate to depositional or formational processes rather than normal compaction processes. Sediment densities (measured by MSCL gamma-ray attenuation) are also relatively high, typically ranging from 2.1 to 2.3 g cm<sup>-3</sup> with occasional peaks signifying the presence of large clasts. X-radiography has not yet been conducted on this core. The dense muddy lithofacies is unconformably capped by 0.37 m of fine- to medium-grade well-sorted sand and shell hash – representing erosion followed by deposition of a thin postglacial marine sand sheet on the subglacial surface in this area.

A single broken shell (of undetermined species) within the firm black mud lithofacies, at a depth of 3.00 m, returned a calibrated age of 29.76 ± 0.37 ka cal BP. Given the poor state of preservation, along with several other shell fragments in the same sediment unit, and its sedimentological setting, within a firm clast-poor muddy diamict, we interpret this shell fragment as being reworked, probably incorporated within a deformation till, by one or more glacier advance(s). The finite age of this shell provides a *maximum* age for glacier advance at this locality (i.e. shell age pre-dates glacier advance). We therefore conclude that the glacially lineated surface formed *after* 29.8 ka BP. The obvious major hiatus close to the seabed (~0.35 m) has made it stratigraphically impossible to obtain meaningful deglacial ages for this location. However, we can conclude that this region of North Sea continental shelf was glaciated during the LGM (MIS 2–3) by a grounded ice mass advancing from the south or SE sometime after ~29.8 ka BP, but before ~17.5 ka BP when the ice sheet had retreated back to the outlying islands of Shetland (Out Skerries).

#### Core 075VC.

This is a 3.28-m-long vibrocore, taken 18 km SSW of core 074VC, and recovered 2.93 m of firm dark grey to black

massive gravelly mud, becoming more gravelly or diamictic in places with occasional shell fragments, overlain by 0.35 m of fine-grained shelly sand (Fig. 8). No sedimentary or directional structures were seen under optical examination within the dense mud facies. No definitive deformation structures were identified in X-radiographs. Numerous gravel clasts (<20 mm in diameter) are clear in X-radiographs from 0.40 m to core base, increasing in frequency from ca. 1.00 to 2.40 m and decreasing in frequency below 2.50 m (Fig. 9). Gravel is rare or absent below 2.80 m. Shear strengths in this muddy lithofacies are relatively high but variable, ranging from 50 to 140 kPa, and do not increase progressively with depth, suggesting that values are not simply compaction related. We ascribe this relatively high-shear strength, massive, gravelly, slightly shelly mud facies to the incorporation and deformation of pre-existing sediments by an advancing ice sheet. Similar relatively clast-poor but moderate to high-strength diamicts, interpreted as glaciomarine deformation tills, have been identified in equivalent settings on the NW European continental shelf by other workers (e.g. Ó Cofaigh and Evans, 2007; Peters *et al.*, 2015; Arosio *et al.*, 2018). Numerous large iceberg scours are seen overprinting subtle glacial lineations in the MBES data (Fig. 7), emphasizing that the seabed in this region north of Shetland comprises one or more subglacial surfaces, shown in cores 074VC and 075VC, with only a thin (<0.40 m) postglacial sediment cover (Fig. 8).

A single shell fragment (of undetermined species) within the firm black gravelly mud lithofacies recovered in the vibrocorer shoe-sample, at a depth of ~3.30–3.40 m, returned an age of 28.31 ± 0.27 ka cal BP (Fig. 8). We interpret this date on a subglacially reworked shell fragment as a *maximum* bounding age for grounded glacier advance at this locality. Numerous other small broken shell fragments were sub-sampled within the same gravelly mud facies at 1.41, 1.46, 1.73, 1.88, 2.26, 2.47 and 2.52 m, but as these were in the same condition as the shoe-sample shell they were not put forward for radiocarbon assay. Based on the evidence in this core, and supported by core 074VC (above), we conclude that this region of continental shelf was glaciated during the LGM (MIS 2–3) by a grounded ice mass advancing from the south or SE sometime after ~28.3 ka BP and well before 17.3 ka BP.

#### Cores 076VC–082VC.

Unfortunately, these cores either did not yield any material for radiocarbon dating, or in three cores (076VC, 078VC, 079VC), the samples yielded marine carbonate material that when analysed was indistinguishable from background radiocarbon levels. These non-finite ages from reworked shells within glacial diamicts provide only weakly constrained *maximum* bracketing dates for the onset of glaciation. In other words, deposition (or pervasive deformation) of the mud-rich facies by advancing grounded ice occurred sometime after ~50 ka BP.

Shell material in an important core (BGS 61-01/66 VE) (Fig. 1) between cores 075VC and 076VC, just inshore of the Greenwich Meridian Readvance Moraine (GMRM) (Fig. 7), was AMS-radiocarbon dated in the 1990s as part of a doctoral research project on the deglaciation of Shetland (Ross, 1996). Although not published, these dates shed important light on the timing of deglaciation NE of Unst. Four downcore dates were presented in stratigraphic order (Ross, 1996, p. 122); the oldest of these ages, a broken *Trodonia elliptica* mollusc shell (18 230 ± 280 <sup>14</sup>C a BP), is re-calibrated here as 21.61 ± 0.31 ka cal BP. The mollusc was recovered from a dense gravelly sandy diamict with an undrained shear strength of 450 kPa – ~50 times stiffer than the overlying glaciomarine mud facies

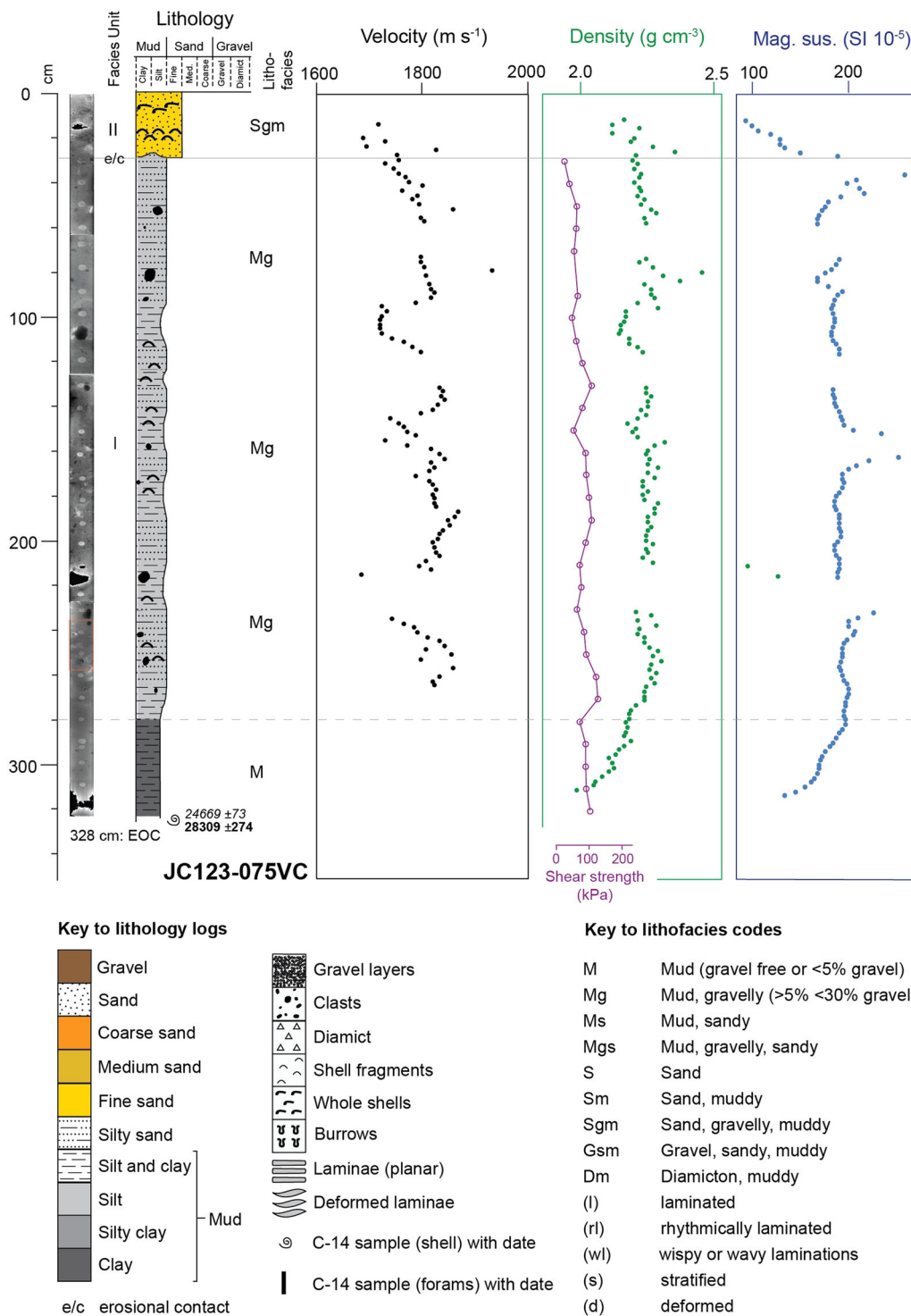


**Figure 8.** Sedimentology, geochronology and geophysical properties of seabed core JC123-075VC. From left to right: X-radiograph, and interpreted lithofacies boundaries, lithological log, main lithofacies codes, P-wave velocity, shear strength, bulk density and magnetic susceptibility values all plotted on same depth scale. Ages of AMS-dated samples given in radiocarbon years (italic) and calibrated calendar years BP (bold font) (Table 6). Physical property data measured using a Geotek MSCL-S at 2-cm intervals. Gaps are missing data. Key relates to all subsequent core-lithology figures. [Color figure can be viewed at wileyonlinelibrary.com].

(Ross, 1996). Although difficult to distinguish from ice-proximal debris-rich grounding-line deposits, we interpret the stiff unit as a subglacial deformation till based on the unusually high shear strength and affinity with subglacial facies seen in adjacent cores. [Ross (1996) is equivocal in his interpretation of this unit, on balance, assigning it to a ‘nearby ice margin’.] The dated shell from within the subglacial facies demonstrates that an advancing (or oscillating) grounded ice mass incorporated this material and deposited it at the

vibrocore site sometime *after* 21.6 ka BP, but clearly *before* the deglaciation of Out Skerries at ~17.3 ka BP.

On the basis of the new offshore geomorphological and stratigraphic evidence presented here we ascribe the large, arcuate, highly lobate till apron and moraine ridge (GMRM) (Fig. 7) to a significant readvance, possibly a surge, of ice from the south ca. 20–21 ka BP. The 1.5-km-wide swath of JC123 MBES data shows the seabed inshore of the GMRM to be curiously featureless for a distance of 14 km – devoid of

recessional moraines, glacial bedforms or small-scale features normally associated with surging ice lobes (cf. Evans and Rea, 2005; Dowdeswell *et al.*, 2016; Ottesen *et al.*, 2017). However, the indented, scalloped morphology of the GMRM within a larger sequence of nested moraines, combined with the presence of elongate streamlined forms and lineations imaged on the MBES data 20–30 km inshore of core 074VC, are geomorphologically consistent with a short-lived dynamic advance of the ice margin in this area. The irregular outline but broadly arcuate shape of the GMRM can be traced for around 150 km from ca. 0.8°E to ca. 0.95°W, where it is overprinted by a younger recessional moraine ~20 km north of Unst. The correlation between the GMRM and the sequence of conspicuous arcuate moraines to the NW of Shetland is still uncertain and requires further investigation. However, the most prominent, near-continuous, arcuate moraine offshore NW Shetland, part of a larger complex of stacked and partly overprinted moraines within the Otter Bank Formation (Stoker *et al.*, 1993), clearly relates to a significant readvance or stillstand of grounded ice 20–22 km from the NW tip of North Roe (Mainland Shetland). We relate this moraine, by geomorphological and seismostratigraphical connection, to one of the prominent ridges within the nested NE Shetland moraine complex, ~20 km inshore of the GMRM, placing its formation also sometime between 21.6 and 17.3 ka BP (Fig. 7).

#### *Sub-transect 2 – East Shetland to Norwegian Channel*

The submarine geomorphology of the continental shelf east of Shetland is still incompletely mapped with Quaternary geology here only locally characterized (Johnson *et al.*, 1993; Graham *et al.*, 2011; Stoker *et al.*, 2011; Clark *et al.*, 2012). Following a transect due east from Shetland at 60.5°N, the shelf is clearly seen to vary in elevation in an irregular way (i.e. does not progressively deepen with distance offshore). Nearshore troughs and deeps (140–160 m bsl) are bounded to the east by a broad bedrock high (Pobie Bank: 90–110 m bsl) which slopes gently east towards a wide bathymetric channel (typically 130–160 m bsl) midway across the northern North Sea Basin (at ca. 1.0°E), referred to here as the East Shetland Channel (Fig. 1). East of this, in Norwegian waters, the seafloor rises gradually again to the Viking and Bergen banks (90–110 m bsl) before rapidly descending to depths of around 300–350 m bsl in the Norwegian Channel (Fig. 1).

Bradwell *et al.* (2008) used single-beam bathymetric surface models (Olex) to map the complex but well-preserved geomorphology on the continental shelf east of Shetland at a broad scale. Their work identified large arcuate moraines and extensive till lobes marking numerous positions of an oscillating grounded ice-sheet margin(s) retreating back towards the Shetland landmass. These features are geomorphologically similar and, by inference, probably of a similar age to the moraines preserved NE of Unst. Bradwell *et al.*'s (2008) mapping was extended and re-interpreted by Sejrup *et al.* (2016) across other parts of the northern North Sea Basin. Importantly, both empirical evidence and modelling experiments indicate that this region represented the zone of confluence and subsequent separation between the BIIS and the larger FIS (Boulton and Haggdorn, 2006; Bradwell *et al.*, 2008; Clark *et al.*, 2012; Patton *et al.*, 2016; Sejrup *et al.*, 2016).

#### **Core 083PC.**

Taken in a water depth of 200 m, on the western slope of the Norwegian Channel, this core recovered 7.80 m of massive bioturbated mud, with silt/fine sand laminations below 4.00-m

depth. No basal diamict was encountered. Two shells (of undetermined species) from within the lower part of the laminated section (6.74 and 7.62 m) returned radiocarbon ages, in stratigraphic order, both from within Greenland Stadial 1 ( $12.64 \pm 0.08$  and  $12.81 \pm 0.12$  ka cal BP; Table 6).

#### **Cores 084VC–086VC.**

These three cores taken from the shallower waters (125–135 m bsl) immediately west of the Norwegian Channel yielded differing stratigraphies. Core 084VC recovered only Holocene sand; by contrast, cores 085VC and 086VC in very similar localities recovered 0.61 and 2.12 m of firm to stiff (100–160 kPa) dark grey to black massive, in places weakly colour banded and occasionally deformed, mud with rare gravel clasts (<1 per 0.2 m of core) seen in X-radiographs. This facies is interpreted as an unusually clast-poor subglacial sediment (deformation till) based on its relatively high shear strength and structureless composition. Two samples of marine carbonate from core 086VC were submitted for radiocarbon assay: an intact shell from core base (within the shoe sample); and a sample of cold-water, not monospecific, foraminifera from a depth of 2.60–2.64 m. Both samples returned non-finite ages (>50 ka BP), indistinguishable from background radiocarbon values (Table 6), indicating reworking of old shell material.

#### **Core 093VC.**

This core, taken at the foot of the western slope of the Viking Bank at 130 m bsl, recovered 1.97 m of sediment. Core 093VC contains two distinct facies: (I) a dark grey, firm (70–140 kPa), massive mud with rare gravel clasts and occasional fine sandy laminae showing evidence of weak deformation; overlain by (II) 0.56 m of massive to crudely bedded sand with a condensed 'shell hash' base (0.20 m thick). Based on its relatively high shear strength and X-radiographic character, the dense gravel-poor mud unit is interpreted as a subglacial deformation till – probably reworking glaciomarine sediment. One broken shell from a depth of 1.35 m returned a non-finite radiocarbon age (>50 ka BP) (Table 6), as in core 086VC, supporting the notion that this firm glacial mud includes reworked pre-MIS2-3 shell material.

#### **Core 092VC.**

This was taken roughly midway between Shetland and the Norwegian Channel in the broad deeper-water East Shetland Channel separating the Pobie Bank from the Viking Bank. This important core (Fig. 10) recovered 5.96 m of highly variable sediment which can be broadly classified into four main facies on the basis of geophysical properties, visible and X-radiographic sedimentology. From the base upwards, these are (I) dark grey to black, firm, massive mud facies, with a relatively high shear strength (80–120 kPa) rare clasts and occasional shells, akin to the subglacially deformed deformation tills seen in cores 085VC, 086VC and 093VC. In places, thin sandy layers within this largely homogeneous mud unit show evidence of deformation or a weak strain fabric. Around 2.80–3.00 m this firm mud facies grades into (II) a lighter grey-green, soft (20–40 kPa) gravelly mud unit with high silt content and clear density laminations seen in X-radiographs. At 2.10 m this unit is abruptly truncated by (III) a thick massive sandy facies with a condensed 'shell hash' base, that fines upwards into muddy shell-rich sand and then, at 1.40 m, into (IV) grey-brown, low-density, gravel-free mud with evidence of wavy laminations, occasional shells and bioturbation increasing upwards to the seabed.

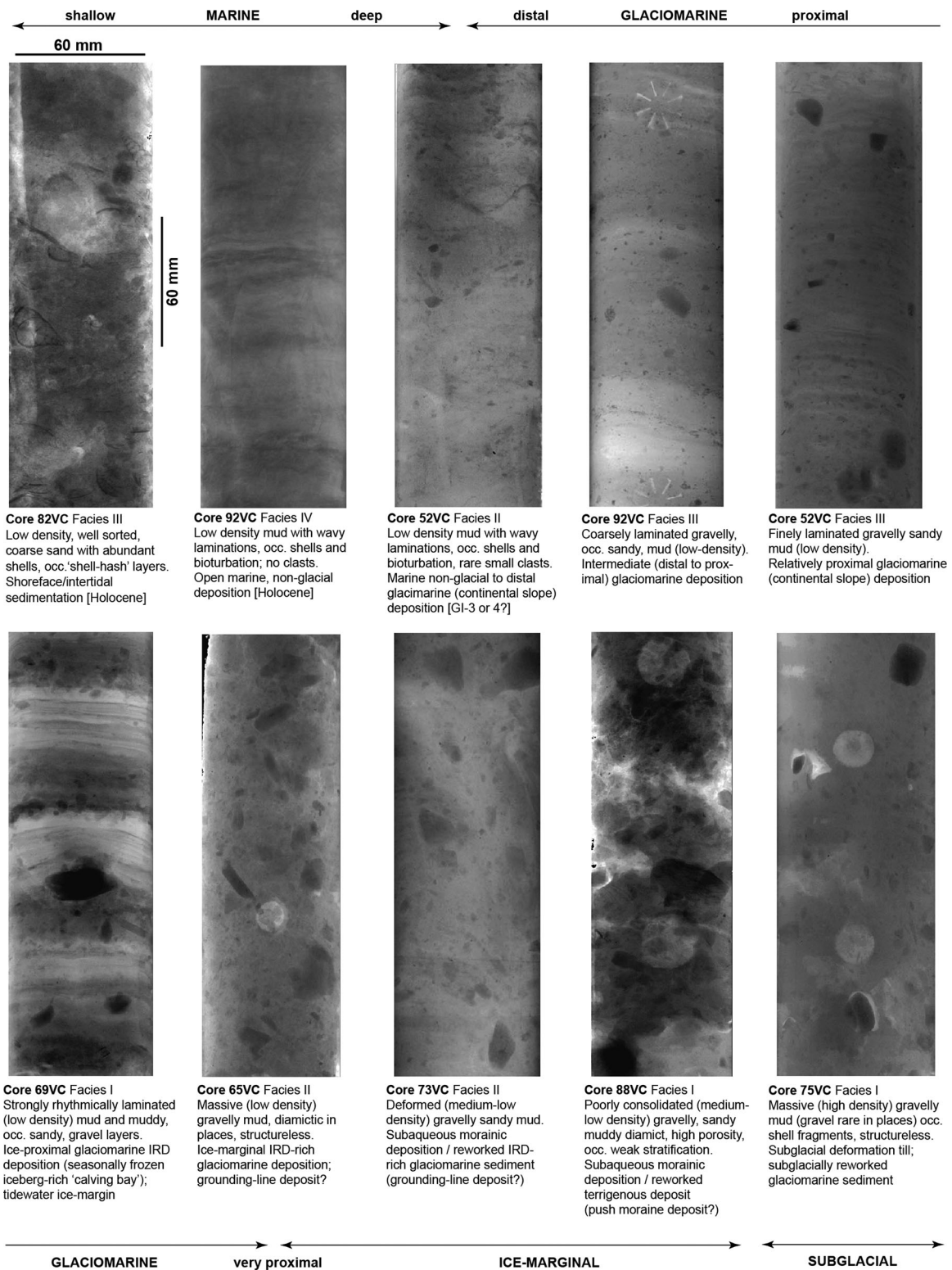


**Figure 9.** Selected image-processed X-radiographs from key marine cores showing different representative sedimentological facies in cores from the continental shelf around Shetland (T1). Brief sediment descriptions and interpretations are provided below each image. Dark pixels are higher density sediments (with greater X-ray attenuation coefficient); lighter pixels are lower density sediments or voids. The facies chosen show a wide variety of depositional settings encountered: from (non-glacial) marine to glaciomarine to ice-marginal to subglacial. All images to the same scale. [Color figure can be viewed at [wileyonlinelibrary.com](http://wileyonlinelibrary.com)].

Radiocarbon analyses were undertaken on three marine carbonate samples taken from this core. From core-base upwards: a shell fragment from Facies I (5.50 m), interpreted as deformation till, returned a non-finite (background) age as expected (Table 6; Fig. 10). Second, a sample of cold-water

foraminifera from Facies II (2.60 m), interpreted as ice-rafted debris (IRD)-poor proximal to distal glaciomarine sediment, returned a calibrated radiocarbon age of  $18.01 \pm 0.16$  ka cal BP (Table 6). Third, a single articulated shell (of undetermined species) within the transition from Facies III to IV (1.50 m)

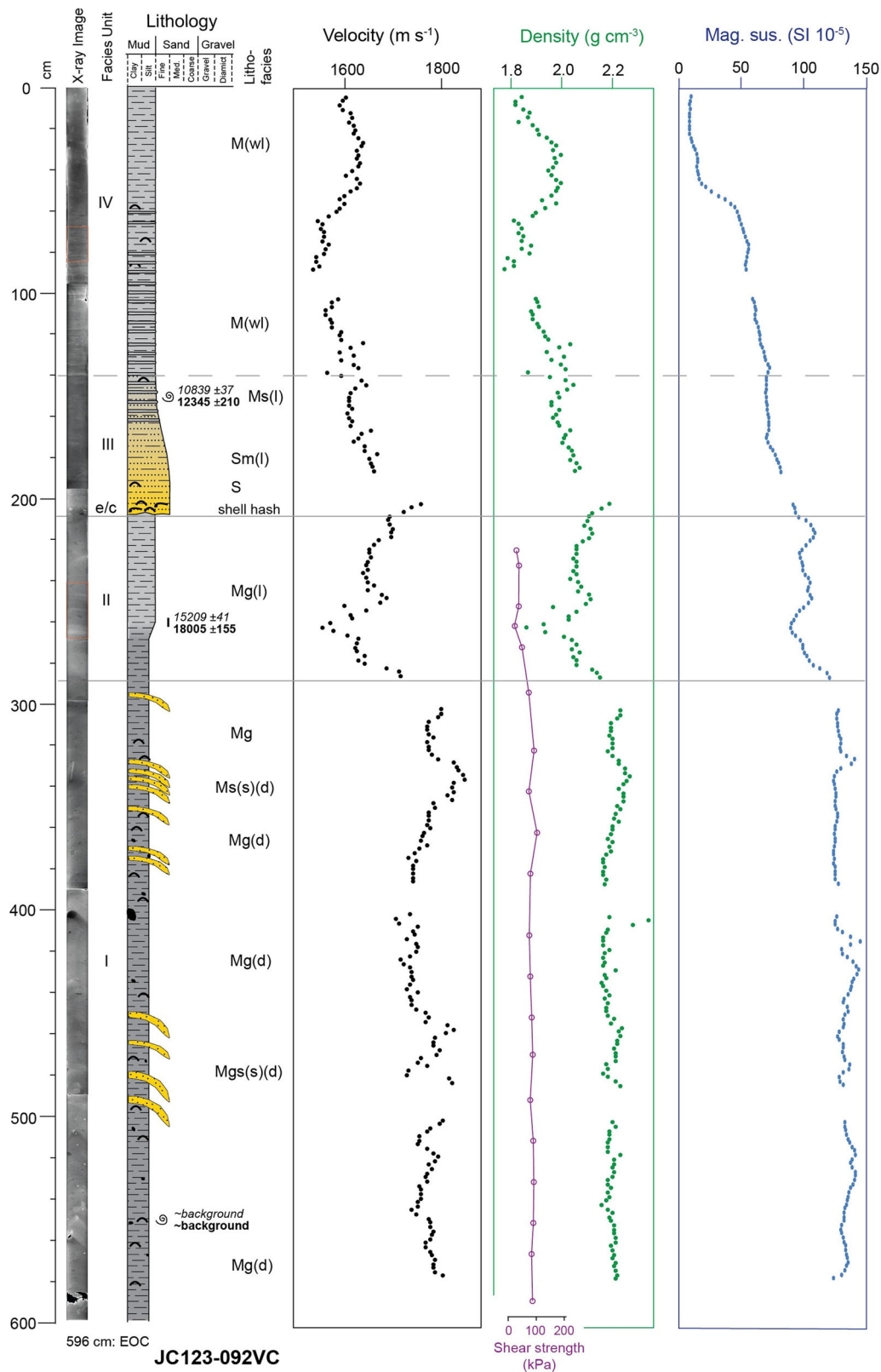


**Figure 10.** Sedimentology, geochronology and geophysical properties of seabed core JC123-092VC. From left to right: X-radiograph, and interpreted lithofacies boundaries, lithological log, main lithofacies codes, P-wave velocity, shear strength, bulk density and magnetic susceptibility values, all plotted on same depth scale. Ages of AMS-dated samples given in radiocarbon years (italic) and calibrated calendar years BP (bold font) (Table 6). Physical property data measured using a Geotek MSCL-S at 2-cm intervals. Gaps are missing data. For key see Fig. 8. [Color figure can be viewed at [wileyonlinelibrary.com](http://wileyonlinelibrary.com)].

returned an age of  $12.35 \pm 0.21$  ka cal BP – within Greenland Stadial 1 (Table 6). The style and timing of deglaciation in the central northern North Sea is well captured by the sedimentology of core 092VC, and the three  $^{14}\text{C}$  ages are in stratigraphic order. The key AMS date from foraminifera within the

glaciomarine unit, immediately overlying the subglacial facies, constrains final ice-sheet retreat in this location to (shortly) before 18.0 ka BP. Equally importantly, however, the detailed sedimentology combined with the submarine geomorphology and wider Quaternary geological evidence strongly support

the opening of a large marine embayment or open-water marine corridor between the previously conjoined FIS and BISS before 18 ka BP. We find no evidence for subsequent grounded glaciation at this location (61.4°N, 1.1°E), from either side of the North Sea Basin, after 18 ka BP.

#### Cores 090VC and 091PC.

Between 0.8°E and 1.0°E one vibrocore (4.98 m long) and one piston core (2.19 m long) recovered Quaternary sediment sequences from either side of a prominent seabed moraine marking the maximum eastward advance of a relatively late-stage independent Shetland Ice Cap (Figs. 2 and 3). This geomorphologically continuous large moraine, ca. 100 km due east of Shetland, can be confidently traced for ~65 km to the NW where it joins with the sequence of large nested moraines NE of Unst. Here the connection becomes less clear – with two scenarios possible: (i) the moraine kinks to the north correlating with the irregular sawtooth moraine arc located between cores 077VC and 078VC (Fig. 7), or (ii) the moraine continues to the east correlating with a substantial, but younger, moraine adjacent to core 080VC and thereafter to connect with the North Unst Moraine (Fig. 7) (see TCN Results: Unst). The latter scenario is preferred, based on the overprinting relationships at ca. 60.7°N, 0.4°E, and the law of parsimony – but both scenarios could be closely related in time (<0.5 ka).

Although no basal diamict was recovered in either core, large barnacle plates sub-sampled in core 090VC from within weakly stratified silty/sandy mud facies with distinctive shell-rich layers – interpreted as transitional distal glaciomarine to modern marine (non-glacial) facies – returned a calibrated radiocarbon age of  $13.60 \pm 0.14$  ka cal BP (Fig. 11). This single date can only be viewed as a loose minimum age for deglaciation in this location, based on our TCN exposure ages

from Out Skerries, indicating ice-free conditions at ~17.3 ka BP, 95 km inshore (hence upglacier) of this core site. Core 091PC did not yield any material suitable for radiocarbon assay.

#### Cores 089VC.

Around 20-km further west on this sub-transect, in a water depth of 147 m, core 089VC recovered only 1.50 m of continuous sediment but did capture several different facies. From core-base upwards: 0.50 cm of firm to stiff (120–160 kPa) overconsolidated massive gravelly mud (Facies I), overlain by 0.20 m of massive soft mud with rare isolated gravel clasts (Facies II), overlain by 0.70 m of crudely stratified sand and muddy sand with occasional shell-rich ‘hash’ layers (Facies III). Two marine carbonate samples were  $^{14}\text{C}$ -age assayed – an intact single valve (*Astarte* species) and 0.010 g of cold-water (not-monospecific) foraminifera – from very similar stratigraphic depths (0.92 and 0.96 m), immediately above the stiff basal diamict interpreted as a subglacial till. The samples returned calibrated ages of  $15.94 \pm 0.17$  ka and  $16.31 \pm 0.19$  ka cal BP, respectively (Table 6). Taken at face value, the close association between these dated shells in Facies II and the upper surface of the stiff subglacial diamict (Facies I) suggests that deglaciation at this site occurred shortly before ~16.3 ka BP. However, we cannot rule out the possibility of an erosional or non-depositional hiatus occurring between Facies I and II, which would put the timing of deglaciation here substantially earlier.

#### Core 088VC.

A further 20 km west, on the eastern flank of the Pobie Bank in water 123 m deep, this core recovered 2.40 m of sediment from the proximal slope of a small seabed moraine consisting of four main facies. From base upwards: (I) variable (soft to



**Figure 11.** A selection of marine shells from four different cores chosen for AMS  $^{14}\text{C}$  analysis. Ages quoted in radiocarbon years; scale graduated in millimetres. [Color figure can be viewed at [wileyonlinelibrary.com](http://wileyonlinelibrary.com)].

firm) shear strength (20–100 kPa), poorly consolidated, sand and gravel-rich, muddy diamict, with weak stratification in places; overlain by (II) 0.50 m of massive sand intercalated with moderately well-sorted thin gravel layers and occasional outsized clasts; overlain by (III) 0.50 m of massive mud with occasional gravel clasts; and finally capped by (IV) 0.78 m of crudely stratified well-sorted medium to very coarse-grained sand with one discrete ‘shell-hash’ layer.

The basal diamict in this core is interpreted as a morainic deposit, consisting of locally derived terrigenous material, primarily on the basis of its X-radiographic sedimentology, highly variable P-wave velocity and density, and generally low to moderate shear strength. Facies II indicates a glacier-fed (or grounding-line) subaqueous fan closely associated with a retreating ice-margin. A well-preserved *Hiatella arctica* shell sub-sampled at a depth of 1.40 m within the upper part of this facies returned a calibrated radiocarbon age of  $15.99 \pm 0.18$  ka cal BP (Fig. 11). Interestingly, this supports the deglaciation age from core 089VC, although the existence of an erosional hiatus between Facies I and II or within the lower part of Facies II is possible. Taken at face value these two cores (088VC and 098VC), weakly supported by moraine patterns (Fig. 3) and existing seismostratigraphy (Johnson *et al.*, 1993; Peacock, 1995), indicate relatively late-stage deglaciation (~17–16 ka) – perhaps of a subsidiary ice-centre on Pobie Bank, east of Shetland.

#### Cores 087VC and 082VC.

The innermost two cores from this sub-transect, 087VC and 082VC, were taken from the deeper-water channel 15–25 km east of Unst and recovered 2.25 and 2.52 m of sediment, respectively. They both captured only Holocene (not deglacial) sediments and no samples were submitted for radiocarbon analysis.

#### Sub-transect 3 – Otter Bank

The Quaternary geology and geomorphology of this part of the NW UK continental shelf has been studied for over 30 years. Attention has focused, most notably, on the sequence of broad mid-shelf moraines within the Otter Bank Formation (Stoker and Holmes, 1991; Stoker *et al.*, 1993; Bradwell *et al.*, 2008; Ritchie *et al.*, 2011). The geomorphology of these moraines has been mapped in more detail as part of recent regional ice-sheet reconstructions (Bradwell and Stoker, 2015). We took 10 sub-seabed cores along a ~50-km-long transect from NW of Orkney to the continental slope, between and adjacent to the well-preserved Otter Bank Formation moraines.

#### Core 052VC.

This important but stratigraphically complex core was taken in 480 m water depth on the mid-section of the West Shetland continental slope. The core recovered 3.64 m of intercalated sediment classified into six main facies on the basis of visual logs, X-radiography and geophysical properties (Fig. 11). From core-base upwards: (I) soft (<40 kPa), massive gravelly mud becoming diamictic in places, with an abrupt (probably erosional) upper contact; overlain by (II) soft, low-density mud with wispy laminae, shells, bioturbation and rare gravel clasts; a gradational boundary into (III) stratified higher-density sandy, gravelly mud, with occasional gravel-rich mud to diamictic intervals; overlain by (IV) lower density massive gravelly mud; grading upwards into (V) gravel-free low-density bioturbated mud with wispy laminae and occasional shells; capped by (VI) a thin unit of slightly gravelly sand. These facies are interpreted to

represent the following depositional regimes, respectively: (I) glaciogenic ice-proximal debris flows (turbiditic units) or ice-proximal IRD-rich rain-out; (II) extra-glacial or very ice-distal biosiliceous hemipelagic open water sedimentation with rare IRD; followed by (III) transitional, pulsed, ice-proximal IRD-rich sedimentation (or glaciogenic debris-flow deposition) and (IV) ice-distal IRD-poor sedimentation; followed by (V) non-glacial hemipelagic open-water sedimentation, overlain by (VI) current-reworked sand. The lowermost facies indicates ice-sheet-fed debris-flow activity or IRD-rich diamict deposition on the upper-to-mid West Shetland slope. The rapid upcore transition (3.20–3.14 m) into hemipelagic muds with markedly decreasing amounts of IRD (above 3.14 m) suggests a rapid retreat of the grounded or floating ice margin from the shelf break, with only a brief period of glaciomarine conditions and IRD deposition (<10 cm thick). A sample of cold-water (not monospecific) Arctic-affinity foraminifera from within this brief IRD-pulse at the base of the hemipelagic sediments (Facies II), immediately above Facies I, returned an age of  $31.20 \pm 0.18$  ka cal BP (Fig. 12; Table 6).

Taken at face value, this date indicates ice-sheet advance to, and subsequent retreat from, the shelfbreak (Facies I) before ~31 ka BP. However, as this date is a single ‘minimum’ constraint we cannot say how long *before* 31 ka BP this event took place, or whether an erosional/non-depositional hiatus occurred between Facies I and II. Hence, although a Greenland Stadial (GS) 5 or GS-6 age (~32 ka BP) is possible for ice advance to the shelf-edge here based on the evidence in this core, we cannot rule out the likelihood that this scenario occurred considerably earlier during MIS 3 (i.e. pre-35 ka BP). An alternative, less parsimonious, but preferred interpretation is that the foraminifera sampled were reworked and incorporated by the advancing ice-sheet, to be subsequently re-deposited within the glaciomarine iceberg-rafted sand-fraction during deglaciation. This would place the timing of ice-sheet advance here *after* ~31 ka BP, possibly within the severe full-glacial cold period between Greenland Interstadial (GI) 3 and GI-2 (27.8–23.3 ka BP; Lowe *et al.*, 2008). On this basis, the predominantly hemipelagic extra-glacial sediment (Facies II), indicative of a rapid return to open-water milder conditions, may relate to a brief but abrupt regional warming event (<28 ka and >23 ka BP) not seen in the Greenland ice-core records.

The gradual transition from Facies II to Facies III at 2.50–2.40 m indicates a return to extensive, possibly shelf-edge, ice-sheet glaciation at this location and across the wider West Shetland Shelf. Punctuated proximal glaciomarine sedimentation continued for some time with layered terrigenous sediments (silt, sand and gravel) recording relative fluxes of IRD and meltwater-plume-derived deposits to the upper to mid-slope. A sample of cold-water (not monospecific) Arctic-affinity foraminifera from the more distal, massive, IRD-rich gravelly mud unit immediately above Facies III (at 1.80–1.86 m) yielded a calibrated age of  $23.79 \pm 0.22$  ka cal BP (Fig. 12; Table 6). We interpret this date as capturing a period of concentrated iceberg rafting soon after ice-sheet maximum (Facies III, at 2.30–1.90 m), possibly associated with a widespread marine-margin break up in this sector. It is perhaps significant that this date coincides with the timing of Heinrich Event 2 (ca. 23.0–24.5 ka BP) – seen widely in the deepwater record across the NE Atlantic (e.g. Peck *et al.*, 2007; Scourse *et al.*, 2009).

#### Cores 053VC, 054VC and 056VC.

Taken on the outer continental shelf, adjacent to several large morainic banks within the Otter Bank Formation, in water

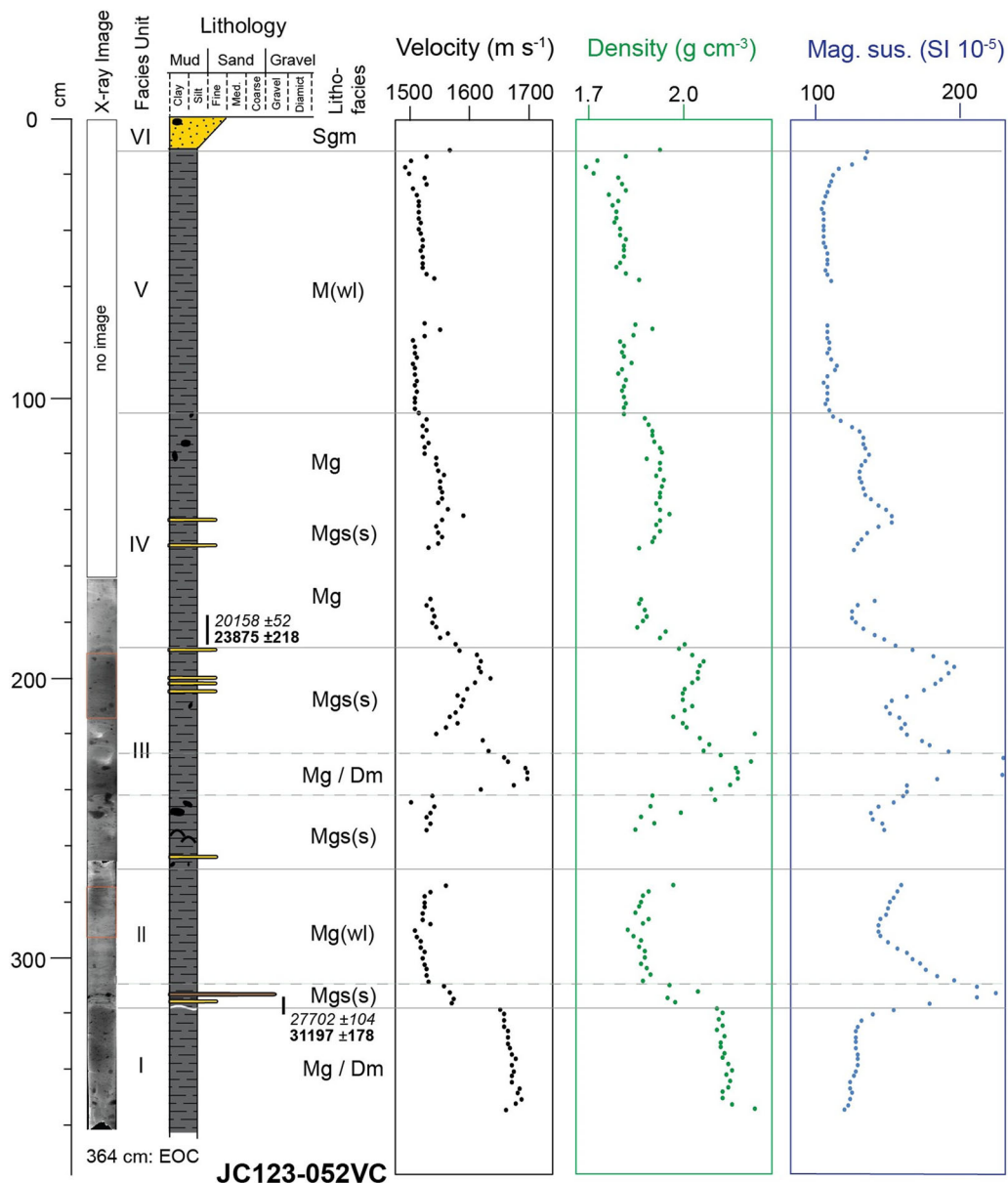


**Figure 12.** Sedimentology, geochronology and geophysical properties of seabed core JC123-052VC. From left to right: X-radiograph, and interpreted lithofacies boundaries, lithological log, main lithofacies codes, P-wave velocity, bulk density and magnetic susceptibility values, all plotted on same depth scale. Ages of AMS-dated samples given in radiocarbon years (italic) and calibrated calendar years BP (bold font) (Table 6). Physical property data measured using a Geotek MSCL-S at 2-cm intervals. Gaps are missing data. For key see Fig. 8. [Color figure can be viewed at [wileyonlinelibrary.com](http://wileyonlinelibrary.com)].

depths of 156–158 m, these three cores produced a number of radiocarbon dates (Table 6). All three yielded non-finite (or background) AMS radiocarbon dates on shell fragments incorporated into basal sediments interpreted as subglacial till. Core 054VC also produced three statistically identical young dates on shells at core depths of 1.80, 2.28 and 2.34 m – all of which when calibrated fall within GS-1 (11.7–12.9 ka BP) and are therefore ‘loose minimum’ dates on deglaciation (Tables 6 and 7). By contrast, core 056VC produced two important dates from shell material within soft, low-density, weakly stratified glaciomarine mud (Fig. 13). The lowest radiocarbon assay, on cold-water benthic foraminifera, immediately overlying the subglacial facies at a depth of 2.56–2.60 m, returned a calibrated age of  $24.80 \pm 0.31$  ka cal BP. A second assay, on a single intact shell (at 2.48 m) within the same clast-poor weakly stratified glaciomarine mud facies yielded an age of  $22.96 \pm 0.23$  ka BP (Figs. 11 and 13; Table 6). We interpret both ages as meaningful ‘close

minimum’ dates on the timing of deglaciation. Core 056VC therefore provides good chronological constraints on grounded ice-sheet retreat from the outer shelf in this sector – the oldest date constraining ice-sheet withdrawal at ca. 25 ka and, by inference, Late Weichselian ice-sheet maximum extent, at or close to the continental shelfbreak, shortly before this period (i.e. ~25–26 ka BP).

#### Cores 057VC–059VC.

These three cores were taken on the inshore (ice-proximal) slope of the innermost large seabed ridge within the Otter Bank Formation nested moraine complex (Figs. 2 and 3), first identified by Stoker and Holmes (1991) and remapped by Bradwell *et al.* (2008). Unfortunately, owing to seabed cables, cores could not be positioned in the optimum sites. Hence, only one vibrocore, 059VC, recovered a useful deglacial sequence, with 2.40 m of Holocene shelly sands overlying soft

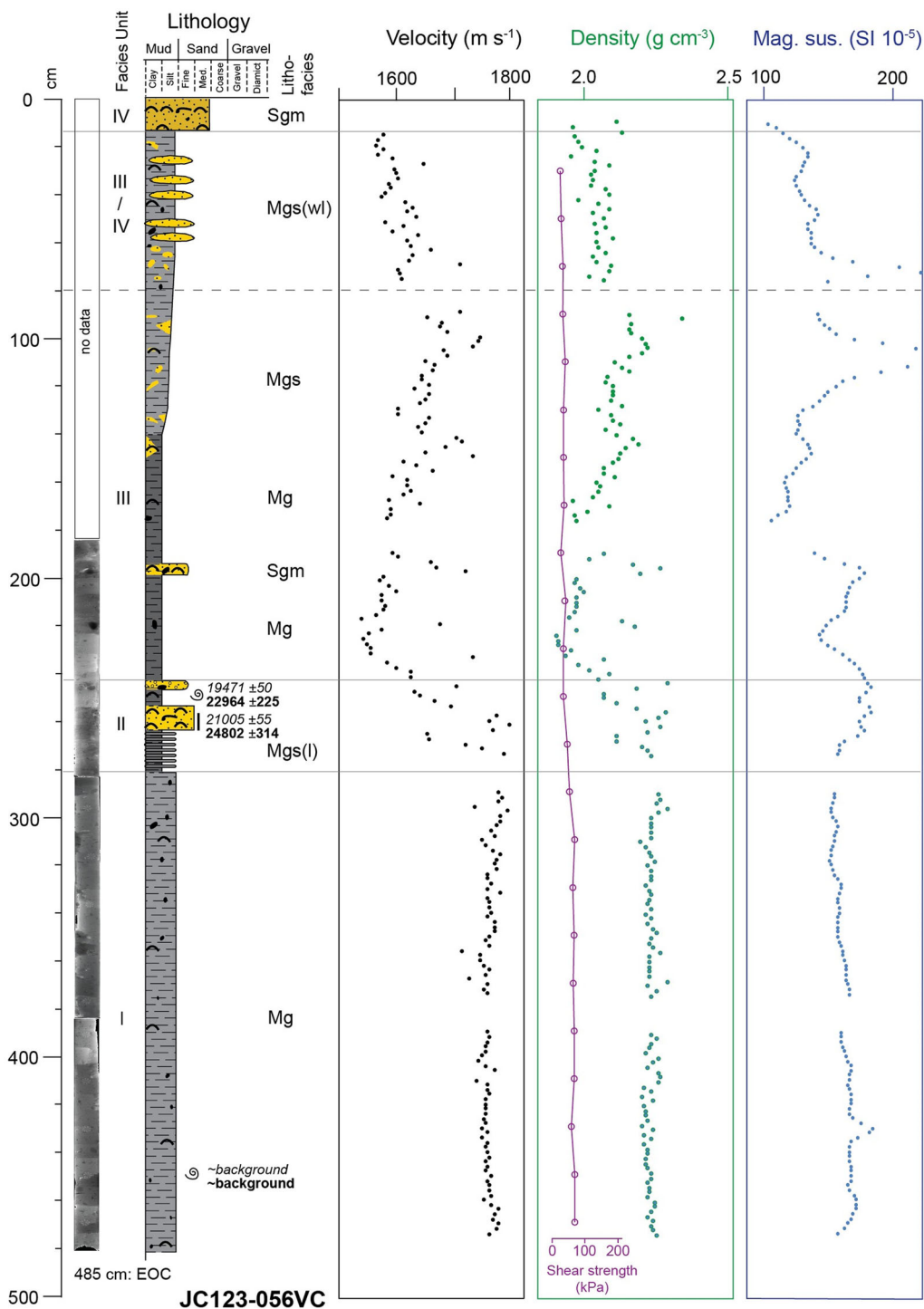


**Figure 13.** Sedimentology, geochronology and geophysical properties of seabed core JC123-056VC. From left to right: X-radiograph, and interpreted lithofacies boundaries, lithological log, main lithofacies codes, P-wave velocity, shear strength, bulk density and magnetic susceptibility values, all plotted on same depth scale. Ages of AMS-dated samples given in radiocarbon years (italic) and calibrated calendar years BP (bold font) (Table 6). Physical property data measured using a Geotek MSCL-S at 2-cm intervals. Gaps are missing data. For key see Fig. 8. [Color figure can be viewed at [wileyonlinelibrary.com](http://wileyonlinelibrary.com)].

clast-poor massive muds (0.50 m thick), overlying firm to stiff rhythmically laminated, but undeformed, slightly sandy mud with occasional isolated gravel clasts (1.20 m thick). The lowermost laminated facies yielded unusually high and variable shear strengths (80–160 kPa) suggesting overconsolidation by grounded ice or possibly by iceberg turbation, rather than simply sediment compaction. However, no definitive subglacial facies was recovered. Only one large shell fragment was radiocarbon dated, from the base of the stiff laminated mud facies (shoe sample), yielding an age of  $17.56 \pm 0.17$  ka cal BP (Table 6). We cannot reconcile this age as reworking of

older shell material by an ice-sheet readvance – the date is so much younger than those from elsewhere on the continental shelf and on Shetland and Orkney. Such an interpretation would require an ice sheet re-advance to the mid-shelf ~80 km NW of Orkney *after* 17.5 ka BP, at the same time as TCN exposure ages place the ice margin on land in Orkney (Phillips *et al.*, 2008). Similarly, our new onshore dating evidence indicates that the dynamic ice mass centred over Shetland would also have been predominantly terrestrial by ~17 ka BP. Detailed moraine mapping and ice-front reconstructions suggest strongly that the large Otter Bank Formation moraines

are time-equivalent to other features shown to be >20-ka years old (Bradwell and Stoker, 2015; and this study). We therefore infer that the dated shell from the base of core 059VC is simply a *minimum* deglaciation age from an incompletely recovered, unusually dense, possibly iceberg-turbated, glaciomarine sediment facies. Ice-sheet withdrawal from this mid-shelf moraine, and the wider area, occurred therefore sometime before 17.5 ka BP.

#### Cores 060VC–062VC.

These three cores were taken from the inner part of the Otter Bank/Stormy Bank Formation moraine complex (Stoker *et al.*, 1993) (Fig. 2), in water depths of 116, 123 and 147 m, respectively. Cores 060VC and 062VC failed to recover substantial or meaningful glacial-to-deglacial sediment sequences. As such, no material was submitted for radiocarbon assay. Core 061VC was taken between two conspicuous seabed moraines and penetrated 1.90 m of stiff, red-brown, poorly sorted, gravelly muddy diamict with occasional large sub-rounded clasts and rare shell fragments; overlain by 2.50 m of crudely bedded, sometimes gravelly, coarse to fine sand with occasional shelly layers. One shell fragment from within the diamictic unit, interpreted as a subglacial till, returned a calibrated radiocarbon age of  $34.82 \pm 0.31$  ka cal BP (Table 6). This single date on a glacially reworked shell, 60 km NW of Orkney, supports a small number of other dates (Rise and Rokoengen, 1984; Sejrup *et al.*, 1994, 2009) that point towards a period of restricted glaciation or largely ice-free continental shelf in the northern North Sea Basin ca. 35 ka BP.

#### Sub-transect 4 – St Magnus Bay

St Magnus Bay is a large approximately circular deep-water embayment, 20 km north–south and 18 km east–west. Present-day water depths in the centre of the bay are up to 170 m, exceeding those on the continental shelf to the west except at the shelf edge. This deep-water bay is partially hydrodynamically enclosed along its western margin by a bedrock sill where water depths shallow to 85 m. Ten sub-seabed sediment cores (064PC–073VC) were recovered from a 60-km-long sub-transect, starting in St Magnus Bay, heading offshore into shallower waters typically 100–120 m deep (Fig. 2). Sediment recovery was good but penetration depths were highly variable, with cores ranging in length from 5.9 to 0.5 m.

As in other sub-transects, cores targeted sediment basins, acoustically recognized in sub-bottom profiles, between well-imaged moraines. In St Magnus Bay, a suite of around 20 seabed moraines record punctuated recession of a grounded tidewater glacier margin in a generally easterly or SE direction (Fig. 14). The moraines are particularly well developed and well preserved north of Papa Stour and bear strong morphological resemblance to those subaqueous (de-Geer type) moraines seen in the Summer Isles region of NW Scotland and in the Bay of Fundy, eastern Canada (Bradwell *et al.*, 2008; Bradwell and Stoker, 2015; Todd, 2016).

#### Core 064PC.

Taken from the deepest part of St Magnus Bay (Fig. 14), only 6.5 km west of Shetland (Muckle Roe), this core recovered 5.92 m of soft (20–40 kPa) grey to dark grey weakly laminated mud. Very little grain-size variation occurs but magnetic susceptibility values show a clear step-like decrease from 100 to 50 SI  $10^{-5}$  at around 2.90–2.80 m. P-wave velocity readings are low ( $\sim 1500$  m s<sup>-1</sup>) and incomplete below 3.20 m – probably indicating the presence of trapped gas. X-radiographs show faint and wispy, occasionally bioturbated, laminations in

the stratigraphically oldest sediments (>4.40 m), with occasional isolated shells seen but no gravel clasts (dropstones), indicating non-glacial marine conditions.

A single well-preserved shell (of undetermined species) with articulated valves, at a depth of 5.02 m, returned a calibrated age of  $14.79 \pm 0.32$  ka cal BP (Table 6). In addition, a sample of non-monospecific foraminifera from the base of the core (5.64–5.73 m) returned a calibrated age of  $14.57 \pm 0.36$  ka cal BP, indicating that the oldest recovered sediment facies was deposited during the earliest, probably mildest, part of GI-1 – GI-1e (14.69–14.08 ka BP; Lowe *et al.*, 2008). The incomplete deglacial stratigraphy and lack of basal till or glaciomarine facies in this 6-m-long core make this age constraint only a loose *minimum* for the deglaciation of central–inner St Magnus Bay. On the evidence in this core, we infer that the ice cap on Shetland was no longer water-terminating in St Magnus Bay by  $\sim 14.7$  ka BP and, on the basis of our onshore TCN exposure-ages, had probably withdrawn to a predominantly terrestrial setting in central Shetland  $\sim 1.5$ – $2.0$  ka before this time (i.e. by 16.5 ka BP).

#### Cores 065VC–068VC.

Core 065VC recovered 2.62 m of sediment from between two of the prominent recessional moraines in St Magnus Bay. X-radiographs show 0.24 m of coarse crudely stratified sand and gravel, overlying 1.60 m of laminated mud (silt and clay) with occasional sand laminae (0.5–1.5 mm thick) and rare isolated dropstones. Deformation structures and muddy gravel-rich layers are seen towards the base of the unit. The whole laminated facies is interpreted as a condensed proximal-to-distal glaciomarine sediment sequence, becoming more distal upcore. The base of the core penetrated 0.50 m of relatively low-density, low-shear-strength (20–50 kPa) sandy mud-matrix diamict with abundant sub-rounded to sub-angular clasts, up to 30 mm in diameter – interpreted as a subaqueous morainic deposit or grounding-line (ice-contact) glacial debris flow. Unfortunately, this core did not yield any suitable material for radiocarbon assay. Cores 066VC, 067VC and 068VC also from within the moraine sequence (Fig. 14) were short (<1.0 m) and predominantly recovered sandy facies overlying high-strength (150–200 kPa) diamict with an erosional upper surface. Only one broken shell valve was recovered from within the stiff clay-rich diamict, interpreted as subglacial till, at the base of core 067VC (at 0.74 m). This radiocarbon assay yielded a non-finite age (Table 6), indicating that the shell was reworked and incorporated by an advancing glacier sometime after  $\sim 50$  ka BP. Neither cores 066VC nor 068VC yielded material suitable for radiocarbon dating.

#### Cores 069VC–072VC.

Moving progressively further offshore (Figs. 2 and 14), core 069VC captured a relatively long (5.60 m) and detailed deglacial glaciomarine sequence of strongly rhythmically interlaminated silty muds with occasional gravel layers and dropstones, becoming less gravelly upcore. No definitive subglacial facies was recovered at the base. A single articulated shell sampled at 1.65 m yielded a calibrated radiocarbon age of  $15.44 \pm 0.20$  ka cal BP (Table 6). Although possessing a promising stratigraphy, further examination downcore, including foraminifera counts, did not yield any additional material suitable for dating. In core 072VC, one broken shell fragment at a depth of 2.02 m from within a soft to firm (40–50 kPa) brown clast-rich mud, interpreted as ice-proximal iceberg-rafted facies, produced a radiocarbon age of  $16.24 \pm 0.17$  ka cal BP (Table 6). Both cores 069VC and 072VC

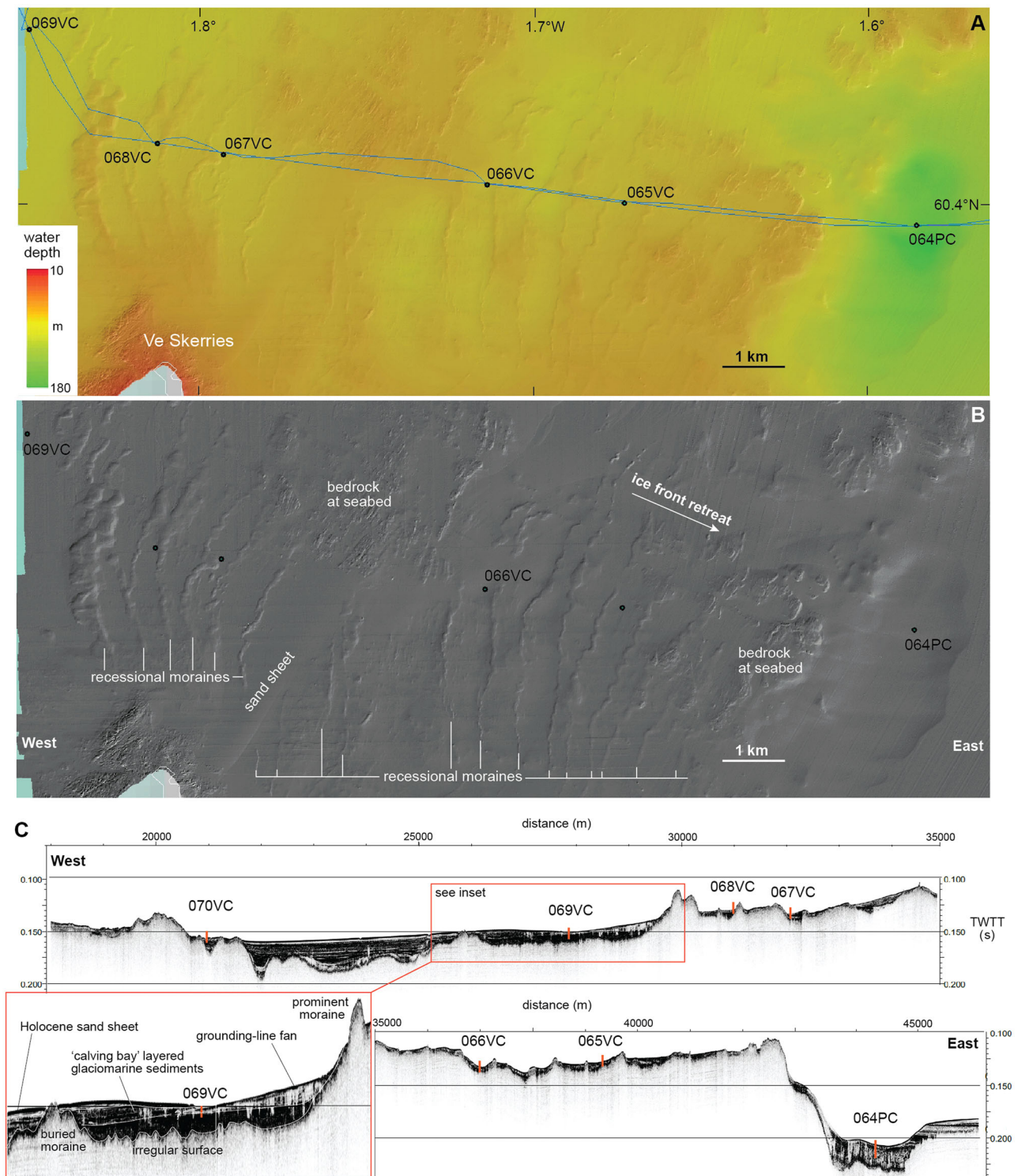


**Figure 14.** Marine geophysical data from central St Magnus Bay, west of Shetland; for location see Fig. 6. A. Depth-coloured MBES elevation model of seafloor showing JC123 ship's track and location of six cores collected. (MBES data are from Maritime and Coastguard Agency/UKHO, Crown copyright). B. Greyscale, hill-shaded, MBES bathymetry data highlighting the suite of ~20 recessional moraines charting punctuated retreat of a partly buoyant/lightly grounded tidewater ice-margin (DSM lit from SE/135°). C. JC123-acquired geophysical sub-bottom profile (along ship track in A) showing geological/stratigraphic context for core-site selection. Inset shows detail of sub-bottom glacial sediment architecture in vicinity of core 069VC adjacent to prominent seabed moraine. [Color figure can be viewed at [wileyonlinelibrary.com](http://wileyonlinelibrary.com)].

provide loose *minimum* ages for ice-sheet deglaciation before 16.2 ka BP on the mid-continental shelf 15–30 km west of St Magnus Bay. This is consistent with our terrestrial TCN exposure ages from Papa Stour and North Roe, indicating that deglaciation of westernmost Shetland had occurred by ca. 16.8–16.4 ka BP. Neither core 070VC nor core 071VC (3.40 and 2.50 m long) yielded any suitable material for radiocarbon dating.

#### Core 073VC.

This core was taken on the mid-West Shetland Shelf, 30 km NW of Mainland Shetland and 30 km SE of the shelfbreak, in a water depth of 113 m (Figs. 2 and 15). The core was located immediately inshore of a conspicuous large arcuate moraine, originally identified from Olex bathymetry data (Bradwell *et al.*, 2008) and part of a sequence of nested, occasionally overprinted, substantial moraines on the shelf between 60.5

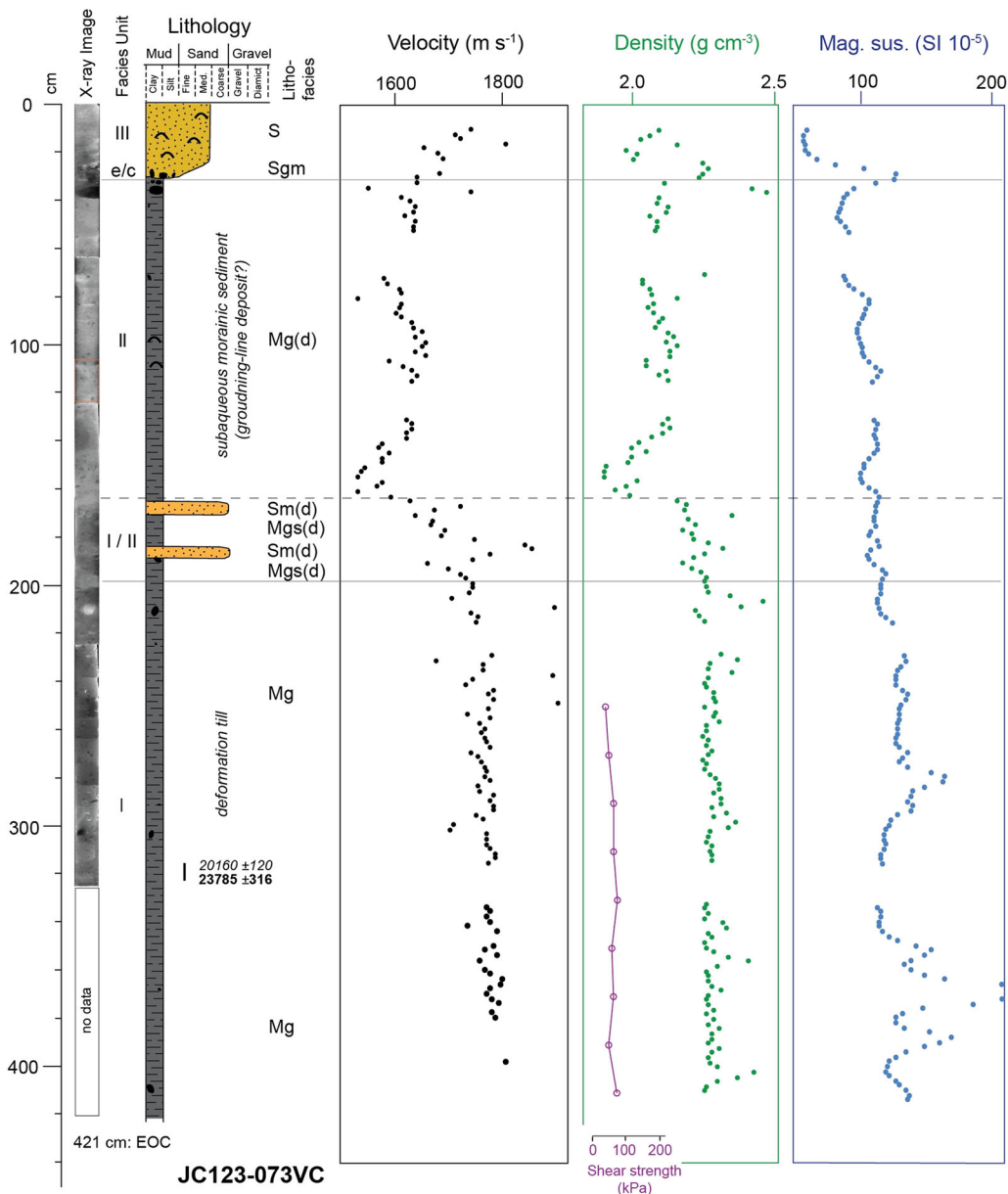


**Figure 15.** Sedimentology, geochronology and geophysical properties of seabed core JC123-073VC. From left to right: X-radiograph, and interpreted lithofacies boundaries, lithological log, main lithofacies codes, P-wave velocity, shear strength, bulk density and magnetic susceptibility values, all plotted on same depth scale. Ages of AMS-dated samples given in radiocarbon years (italic) and calibrated calendar years BP (bold font) (Table 6). Physical property data measured using a Geotek MSCL-S at 2-cm intervals. Gaps are missing data. For key see Fig. 8. [Color figure can be viewed at [wileyonlinelibrary.com](http://wileyonlinelibrary.com)].

and 61°N (Fig. 3) indicative of an oscillating ice-sheet margin. The seabed sediment (to a depth of 0.24 m) consists of medium to coarse shelly sand. The remainder of the core recovered almost 4.00 m of soft to firm (40–90 kPa), massive, dark grey to brown, silty mud with numerous gravel clasts. X-radiographs show that these sub-rounded to sub-angular gravel clasts range widely in size (2–80 mm in diameter), and are widely dispersed and randomly orientated throughout the core (Fig. 9). The gravelly mud is diamictic in places, with varying clast proportions downcore, and is weakly stratified in places with some evidence of deformation especially towards the top. P-wave velocity and gamma-ray attenuation (bulk density) data show a marked shift from dense, well-consolidated sediments to less dense, weakly consolidated sediments at ca. 1.60 m (Fig. 15). On this basis, and the X-radiograph sedimentology, we distinguish two gradational facies, interpreted as: (I) dark grey subglacial diamict, probably a deformation till formed as grounded ice re-advanced and reworked dropstone-rich glaciomarine muds; overlain by (II)

brown, lower-density, deformed gravelly mud, representing morainic or grounding-line facies deposited as the retreating ice-front built one of several small nested push moraines on the seafloor (Figs. 3 and 9).

A bulked sample of cold-water (not monospecific) Arctic-affinity foraminifera from within the deformation till (facies I) at a core depth of 3.15–3.25 m returned an age of  $23.79 \pm 0.32$  ka cal BP (Fig. 14). As this unit has been subglacially reworked, this date is interpreted to represent the *maximum* timing of ice advance; i.e. these foraminifera were incorporated into sediments deposited sometime *after* 23.8 ka BP. It is notable that this calibrated  $^{14}\text{C}$  age cannot be statistically distinguished (at  $2\sigma$ ) from the timing of GI-2 (23.5–22.9 ka), according to the revised Greenland ice-core chronology (Lowe *et al.*, 2008). This brief, less cold, interval would have probably been a period of overall glacier recession in the British Isles including Shetland. Assuming that the ice-sheet fluctuations were climatically driven, any regional-scale ice-sheet readvance west of Shetland is likely to have taken place after this period, as the climate

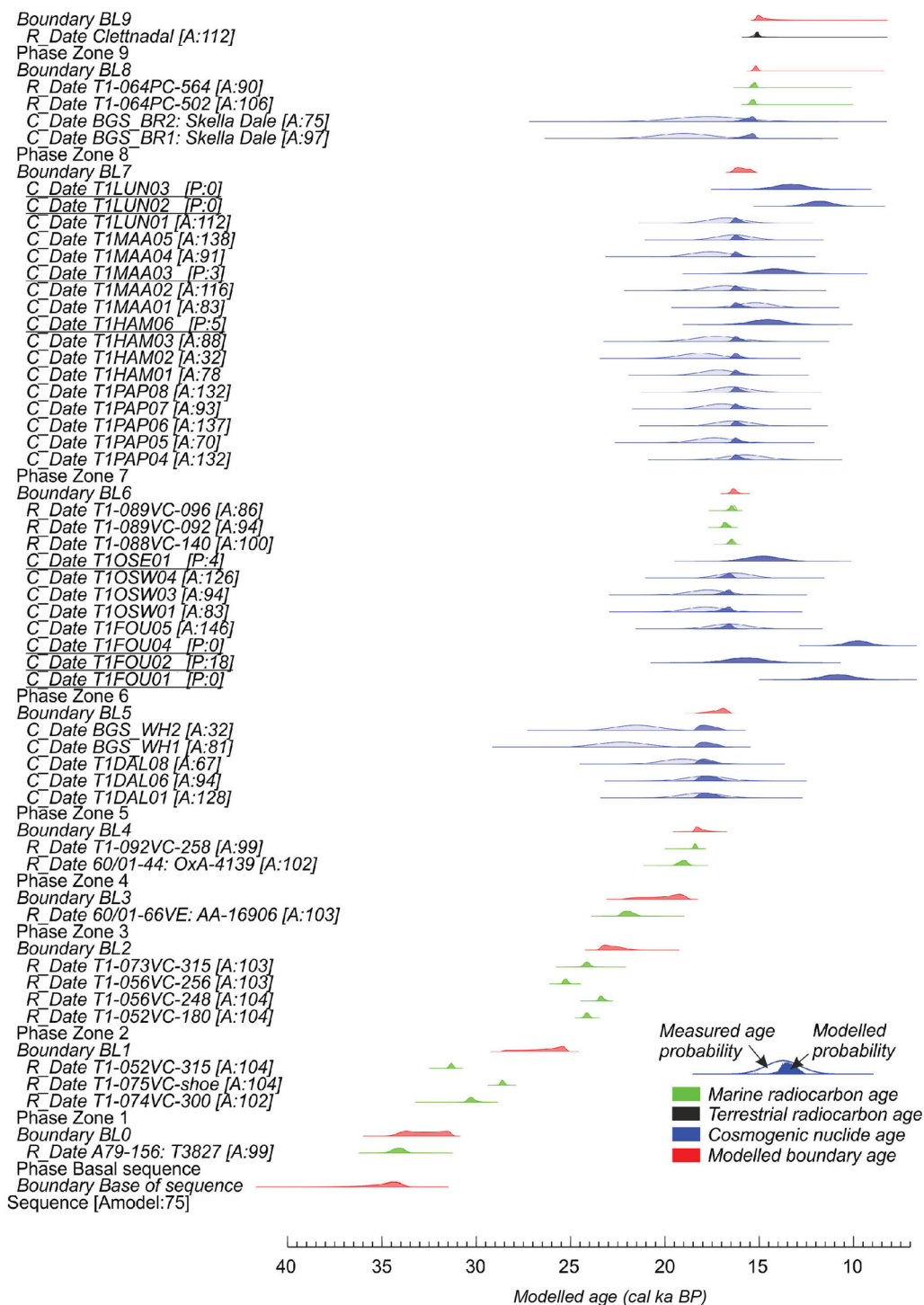


**Figure 16.** Bayesian age-model output for age measurements constraining the deglaciation of Shetland and the surrounding continental shelf, using OxCal 4.3 (Bronk Ramsey, 2013). Agreement index (A-values in square brackets) shown alongside chronosequence conformability.  $p$ -values <20 (in square brackets) denote outliers (underlined). Modelled age in ka cal BP on x-axis. [Color figure can be viewed at [wileyonlinelibrary.com](http://wileyonlinelibrary.com)].

deteriorated again in GS-2, around 22.5–21.5 ka BP. Unfortunately, there was insufficient datable material in the overlying facies to provide a bracketing deglaciation age at this location.

## Interpretation and palaeoglaciological reconstruction

We present a transect overview map showing the most complete assessment of ice-margin pattern information in the northernmost sector of the former BIIS (Fig. 3). In combination with this geomorphological mapping we have derived a new absolute chronology, using a probabilistic Bayesian chronose-

quence model (Fig. 16), to guide the final user-interpreted 'optimal' ice-sheet retreat sequence, based on all the available evidence (Figs 17 and 18). This Bayesian temporal model was developed independently of the age information reasoned from the geomorphology, with some iteration using age information given the complex radial retreat pattern. The motivation for the Bayesian modelling was to test hypotheses about the relative order of events (e.g. ice-mass retreat) and explore spatiotemporal correlations of former ice-margin positions around Shetland. The final prior model (Fig. 16) included all the geochronological measurements and comprised a uniform phase-sequence model punctuated by boundaries coded using OxCal 4.3 (Bronk Ramsey, 2013).

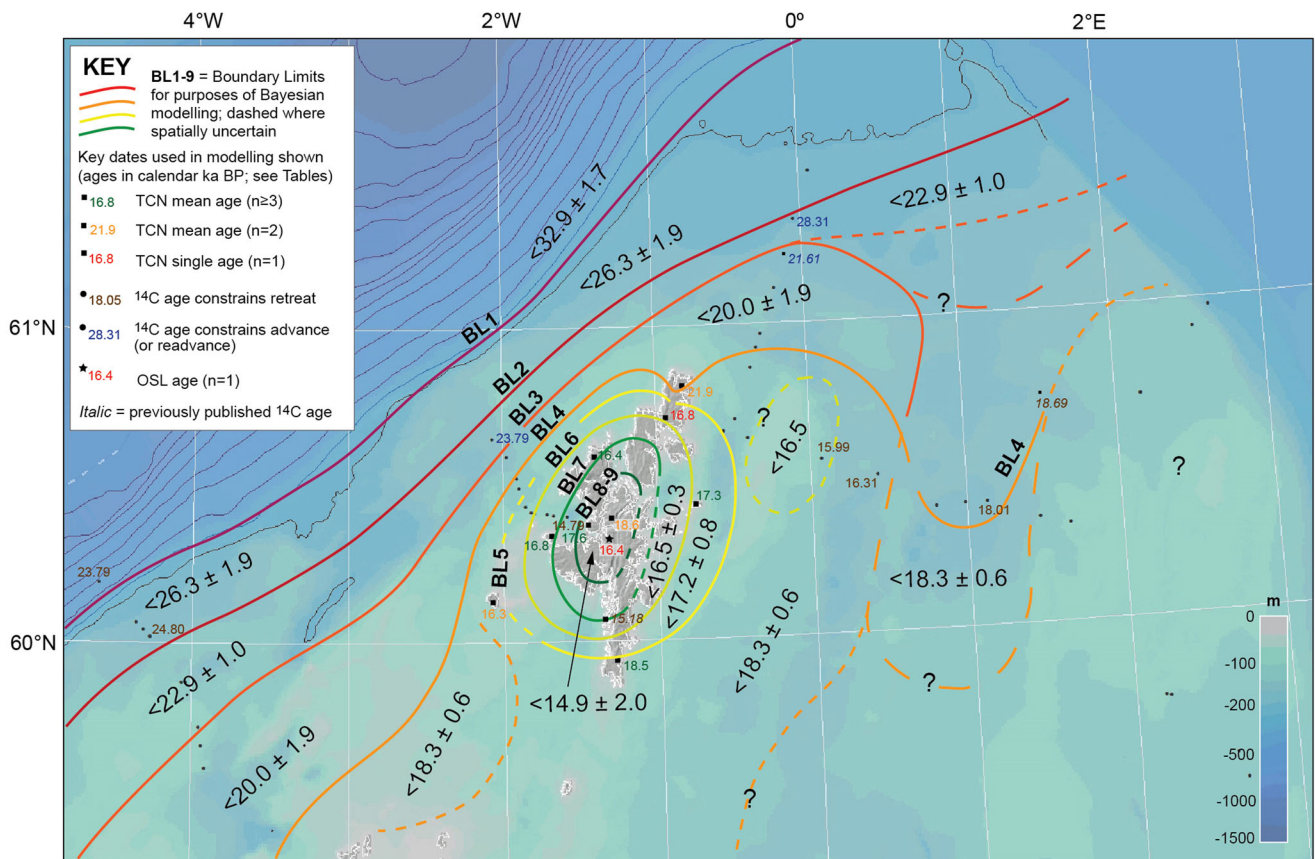


**Figure 17.** Bayesian modelling boundary limits (coloured lines, BL1–9) and modelled median ages with 2-sigma uncertainties (cal ka BP). Key dates used in modelling experiments also shown. Boundary limits guided by geomorphological reasoning and pattern information. See text for more details. Basemap uses BGS-NERC bathymetry (1-km cell size). Isobaths at 100-m water-depth intervals shown in Atlantic sector. Note: 100-m isobath on continental shelf has been omitted for cartographic clarity. [Color figure can be viewed at [wileyonlinelibrary.com](http://wileyonlinelibrary.com)].

The approach uses Markov chain Monte Carlo (MCMC) sampling to build up a distribution of possible solutions generating a probability, called a posterior density estimate for each sample, these are the product of the prior model and likelihood probabilities. This has produced modelled ages for boundaries (Fig. 16) delimiting several zones (coloured lines; Fig. 17). Each retreat zone or phase groups dating information for sites that share a common relationship with all other items in the model. Phases are separated by boundary commands, which generate modelled age probability distributions for Boundary Limits BL0 to BL9 (Table 8).

The sequence model was run in an outlier mode to assess outliers in time using a Student's *t*-distribution ( $p < 0.05$ ) to describe the distribution of outliers with a scaling of 10–10 000 years (Bronk Ramsey, 2009a). Complete outliers were given a probability scaling of  $p = 1$ , with ages showing a poor model fit given values of  $p < 0.25$ ,  $p < 0.5$ ,  $p < 0.75$  and  $p < 0.90$  on a scale of increasing severity. Outliers here, in part, reflect the site-specific treatments (see Results) but also assess the fit of individual age measurements in the different phases of grouped dating information, as well as their fit in the overall retreat sequence. Chronological measurements showing a strong fit to the model have individual agreement indices  $> 60$  (Bronk Ramsey, 2009b, 2013) ([A: values] on Fig. 16). Ultimately, Bayesian analysis produced a conformable age model with an overall agreement index of 75% exceeding the 60% threshold advocated by Bronk Ramsey (2009b, 2013). Note that owing to divergence between ages in the same stratigraphic position, the four OSL ages were not considered in the Bayesian modelling. [The OxCal input code can be accessed on request].

One of the main strengths of using an ice-mass-wide or transect/sectoral approach is that even though not all stages or 'isochrons' can be robustly constrained, all sites sit within a wider (geo-) morphostratigraphic framework – namely a coherent spatial pattern – and a developing probabilistic chronosequence of quality-checked absolute dates, giving them a sense of chronological 'place'. A similar approach has been successfully used by others seeking to reconstruct the pattern and timing of ice-sheet-wide retreat elsewhere (e.g. Bentley *et al.*, 2014; Hughes *et al.*, 2016; Stroeven *et al.*, 2016). To explore the wider connections and ensure maximum spatial continuity between adjoining BIIS sectors, namely: Transect 8 – NW Scotland (Bradwell *et al.*, in prep.); Transect 2 – Central North Sea Basin (Roberts *et al.*, in prep.); and the FIS (e.g. Sejrup *et al.*, 2016; Stroeven *et al.*, 2016; Becker *et al.*, 2018), the geographical area covered by the final reconstruction is deliberately larger than the T1 study area (as defined earlier; Fig. 1). [Note: all ages below refer to calendar years, i.e. the mean of the calibrated 2-sigma age range for <sup>14</sup>C dates; and the site-average uncertainty-weighted mean for TCN exposure ages].

The following sections highlight the main palaeoglaciological events and their timings in this sector of the BIIS (T1), with reference to the Bayesian modelled chronosequence, from before the Last Glacial Maximum to ice-mass disappearance (Figs. 16 and 17). The final map reconstruction (Fig. 18) summarizes the different key stages of ice-sheet/ice-mass retreat, based on all the available geomorphological and geochronological evidence: with solid lines and numbered stages (in calendar ka BP) where more secure, and dashed lines where inferred or projected. These lines

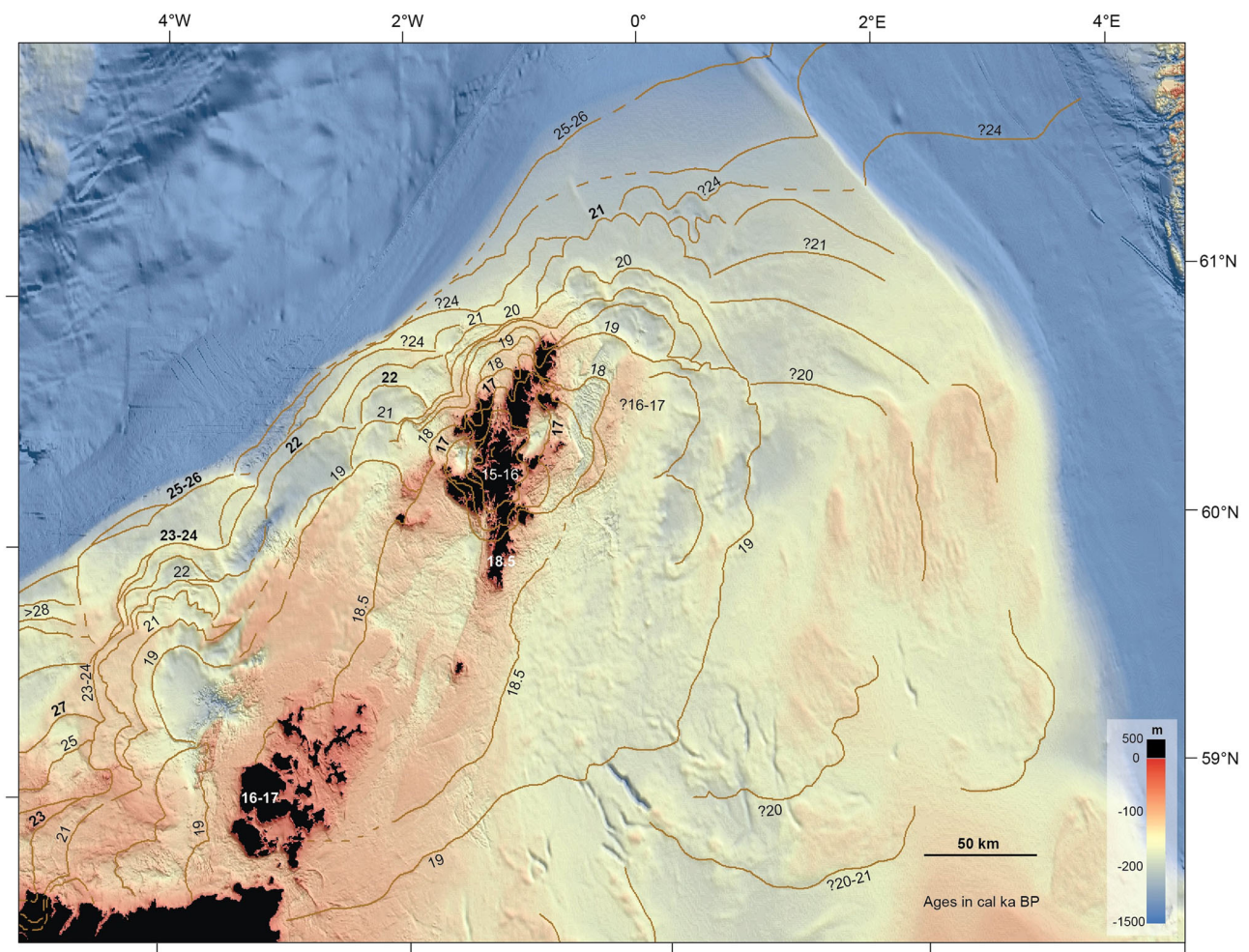


**Figure 18.** Summary palaeoglaciological reconstruction of ice sheet/ice cap deglaciation in the northernmost sector of the former BIIS (T1), centred on 60°N, 0°E. Reconstructed palaeo-ice margins (brown lines) based on all available geomorphological/geological evidence and Bayesian-age-modelled chronology (Figs. 16 and 17). Numbers are ages in cal ka BP. Bold numbers are firmly dated; roman numbers are less firmly dated but ‘in sequence’. Question marks indicate uncertainty owing to lack of dating constraint in surrounding areas. Surface-exposure age constraints from Orkney taken from Phillips *et al.* (2008). Map area presented is deliberately larger than T1 study area to show optimal connectivity with adjacent Britice-Chrono transects (i.e. T8 and T2). EMODnet present-day bathymetry basemap (not GIA corrected) with colour ramp chosen to highlight continental-shelf water depths (i.e. blue >200 m). Note: linear features in NW of image are survey artefacts. [Color figure can be viewed at [wileyonlinelibrary.com](http://wileyonlinelibrary.com)].

represent user-interpreted optimally reconstructed coeval ice-mass margins – effectively isochrons – at different times during deglaciation. Some are well constrained, based on one or more good-context geochronological sites; some are less well constrained, based only on spatiotemporal inferences, submarine landform correlations and/or wider seismo-stratigraphic relationships (e.g. Stoker *et al.*, 1993, 2011; Bradwell and Stoker, 2015). However, all are guided

**Table 8.** Bayesian age-modelled geochronological boundaries.

Boundary limit	Median modelled age (ka) with uncertainties ( $2\sigma$ )
Base of sequence	$34.8 \pm 2.7$
BL0	$32.9 \pm 1.7$
BL1	$26.3 \pm 1.9$
BL2	$22.9 \pm 1.0$
BL3	$20.0 \pm 1.9$
BL4	$18.3 \pm 0.6$
BL5	$17.2 \pm 0.8$
BL6	$16.5 \pm 0.3$
BL7	$16.0 \pm 0.6$
BL8	$15.3 \pm 0.6$
BL9	$14.9 \pm 2.0$

by and framed within our probabilistic Bayesian chronosequence model with ages and uncertainties in calendar ka BP (Figs. 16 and 17; Table 8).

*Before, and build-up to, LGM:  $34.8 \pm 2.7 - 26.3 \pm 1.9$  ka BP [Base to Bayesian Boundary Limit 1]*

We have little new information regarding the shape and size of the ice masses in this sector before the local LGM. Good-context ‘green’ radiocarbon dates from one previously published core site at 61.0°N, 1.8°E, ~50 km NW of Viking Bank, indicate ice-free marine conditions here ~34–35 ka BP (Rise and Rokoengen, 1984; Sejrup *et al.*, 2009) (Table 1). It is possible that the northernmost sector of the BIIS grew rapidly after this time, during GS-5 or GS-6, reaching the continental shelf edge (at 60°N, 4.5°W) between ~33 and 31 ka BP, before retreating some distance and readvancing again to the shelfbreak during the local LGM (GS-3) (see below). However, as a pre-LGM (~32 ka) event is only suggested by the stratigraphy and a single (possibly reworked) radiocarbon date in one continental slope core (052VC), and not in the geomorphological record, we cannot substantiate this assertion. What can be stated with certainty is that the local LGM in the

northernmost BIIS sector occurred after this time, very probably around 25–26 ka BP, as indicated by our Bayesian modeling (Figs 16–18) (see below).

#### *Local LGM and immediate aftermath: $26.3 \pm 1.9 - 22.9 \pm 1.0$ ka BP [BL1–2]*

The outermost system of moraines at the continental shelf-edge ~80 km west of Shetland and ~110 km NW of Orkney have been taken as good evidence of an extensive Weichselian ice sheet extending at least this far (e.g. Stoker and Holmes, 1991; Davison, 2005; Ritchie *et al.*, 2011; Clark *et al.*, 2012; Bradwell and Stoker, 2015). These moraines have previously been assigned to MIS 2–3, based solely on regional seismostratigraphical investigations; i.e. they are within the Otter Bank Formation (Stoker *et al.*, 1993, 2011). New AMS radiocarbon dates in cores 052VC and 056VC constrain the timing of shelf-edge glaciation at ~60°N to between 31.2 and 24.8 ka BP. By inference, and detailed geomorphological connectivity of moraines, this timing can be constrained further with AMS dates from cores 074VC and 075VC, 70–80 km NE of Shetland at ~61.5°N indicating that maximal ice-sheet advance was after 28.3–29.8 ka BP. The youngest *maximum* date and oldest *minimum* date therefore provide the closest (most plausible) age bracket for shelf-edge LGM glaciation west and north of Shetland, i.e. between 28.3 and 24.8 ka BP.

It is tempting to refine this timing further with reference to the Greenland ice-core isotopic record – a proxy for seasonal temperature variations in the mid- to high-latitude Northern Hemisphere. On glaciological and climatological grounds, it is very unlikely that the local BIIS LGM occurred during either of the brief relatively mild (D–O) interstadials, GI-4 and GI-3, at 28.9–28.6 and 27.8–27.5 ka BP, or in the short-lived stadial between (GS-4) (age defined in Rasmussen *et al.*, 2006; Lowe *et al.*, 2008). In sharp contrast, the NGRIP, GRIP and GISP2  $\delta^{18}\text{O}$  records all show a pronounced negative departure between 26.0 and 25.5 ka BP, midway through GS-3, with a nadir around 25.7 ka BP (Rasmussen *et al.*, 2006; Lowe *et al.*, 2008). We propose, based on all the available evidence, that this extremely cold ~500-year interval, preceded by ca. 1500 years of full-stadial conditions in the Northern Hemisphere, is the most likely period for maximal ice-sheet extent in the northernmost sector of the BIIS (60°N–62°N). Our Bayesian modelling strongly supports this assertion and we place a boundary here (BL1) to distinguish between pre-LGM and post-LGM ice-sheet behaviour. The BIIS and FIS were conjoined at this time across the northern North Sea Shelf, with the large Norwegian Channel Ice Stream probably being supported or glaciologically buttressed by a significant Shetland-centred (or perhaps northern North Sea Basin centred) ice-mass – a contiguous ice dome within the larger BIIS complex (Fig. 18). At its most extensive, the glacierized area probably included the entire continental shelf within the study area, approximately 85 000 km<sup>2</sup>.

Retreat from the ice-sheet maximum position (local LGM) occurred in several phases. Large seabed moraines on the outer shelf NW of Orkney ca. 60°N, 4°W can be traced to the west of Shetland ca. 61°N, 1.3°W reflecting this oscillatory ice-front behavior. Minimum and maximum ages from cores 056VC and 073VC constrain the timing of this post-LGM period of retreat (i.e. after 24.8 ka and before 23.8 ka BP), coincident with Heinrich Event 2 (centred on 24 ka BP; Scourse *et al.*, 2009). Although the precise magnitude of ice-sheet recession during this time, before subsequent advances, cannot be quantified, ice-front retreat must have been significant, perhaps receding 30 km or more, across the West Shetland continental shelf.

#### *Post-LGM retreat and fluctuations: $22.9 \pm 1.0 - 20.0 \pm 1.9$ ka BP [BL2–3]*

The ice sheet in this sector underwent significant oscillations during this period reducing in size considerably from ~85 000 to <50 000 km<sup>2</sup>. The size of the ice sheet ca. 23 ka BP cannot be robustly determined based on geomorphological evidence owing to subsequent readvances, but it is highly likely that the Shetland-centred ice mass receded to the inner shelf, well within the limits of the ice-sheet ‘footprint’ at 21 ka BP (see below). Reworked shells in core 073VC adjacent to one of the large mid-shelf moraines show that a major ice-lobe oscillation took place west of Shetland after 23.8 ka, and probably before 21.6 ka, although connection with palaeo-ice-margins to the north of Shetland is difficult owing to the truncated pattern of moraines. The margins of the BIIS and FIS may still have been physically conjoined for much of this time, probably in the vicinity of Bergen Bank, Bressay Bank and the Witch Ground (Fladen) Basin (Graham *et al.*, 2007; Merritt *et al.*, 2017), although the degree of glaciological connectivity is likely to have been low. Unfortunately, glacio-geomorphological relationships are still somewhat unclear and chronology is less robust in this geographical corridor (Fig. 17).

#### *Ice-sheet separation and dynamic oscillations: $20.0 \pm 1.9 - 18.3 \pm 0.6$ ka BP [BL3–4]*

This period saw wholesale changes in the glaciology of the northernmost BIIS sector and ice-sheet connection between the BIIS and FIS was lost. We propose that the volume, flow configuration, symmetry and outline shape of the ice masses changed markedly because of this ice-sheet separation, with unusual lobate ice-front morphology developing NE of Shetland and elsewhere on the shelf. Readvance of the northernmost ice-mass lobe, for example, took place after 21.6 ka BP (as dated in core 61-01/66 VE; Ross, 1996), but clearly well before 17.3 ka BP, when the ice margin had receded back beyond the northern and eastern extremities of the present-day Shetland landmass. This period was cold. Full-glacial conditions existed in the NE Atlantic, with temperatures –10 to –15 °C below present (Peck *et al.*, 2007; Scourse *et al.*, 2009), coincident with the Northern Hemisphere insolation minimum (Berger and Loutre, 1991). We suggest that much of the ice-mass loss that preceded this time (i.e. 25–23 ka BP) was reversed in this sector with the re-growth of a substantial, glaciologically independent, ice sheet (or ice cap) centred on the Orkney–Shetland platform. This ~50 000–60 000-km<sup>2</sup> ice mass was asymmetrical with respect to the high ground – being mainly, or overwhelmingly, situated to the east of the present-day Shetland landmass. Moraines related to this ice-sheet stage are found ~150 km east of Shetland, on the Viking Bank, which would have been subaerially exposed at this time of eustatically low sea levels (~100 m bsl); there are equivalent-age moraines located only 20–30 km offshore NW Shetland and 70–80 km offshore NW Orkney, emphasizing the ice-mass asymmetry with respect to Shetland. It should be stated that this ice-sheet configuration was not expected and has not been described fully before, although it has some similarities with the most recent reconstructions of Sejrup *et al.* (2015) working in the Witch Ground/Fladen region further south, Stage C of Sejrup *et al.* (2016; their fig. 3) and ‘Stage 5’ of Merritt *et al.* (2017; their fig. 9). The wider palaeoclimatic, glacio-isostatic and geotechnical implications of such a large, dynamic, grounded ice mass on the North Sea Shelf at a relatively late stage during the last glacial cycle (MIS 2) have not been considered, but ought to be the focus of further more detailed work.

### **Rapid ice-mass retreat and collapse: $18.3 \pm 0.6 - 16.5 \pm 0.3$ ka BP [BL4–6]**

Following a number of ice-margin oscillations of varying magnitude, AMS  $^{14}\text{C}$  dating in core 092VC constrains ice-sheet/ice-cap retreat  $\sim 100$  km east of Shetland, and the opening of a marine corridor or significant embayment between Pobie Bank and Viking Bank, to (shortly) before 18.0 ka. Coincident with this, our geomorphological and onshore dating evidence indicate that the Shetland Ice Cap (SIC) underwent a major size reduction between  $\sim 19$  and  $\sim 17$  ka BP. New TCN exposure ages from Dalsetter in southernmost Shetland place the ice margin on land here by  $\sim 18.0$ – $18.5$  ka BP and perhaps slightly earlier in NE Unst (although the latter ages probably suffer from a degree of nuclide inheritance). We suggest that marine-margin retreat of partially floating glacier fronts, as evidenced by well-developed subaqueous (de Geer) moraines in the Fair Isle Channel (Fig. 6) (Bradwell *et al.*, 2008), accentuated recession along both the Atlantic and the North Sea margins, driving the SIC rapidly back towards the present-day Shetland landmass and areas of shallow seabed. Eustatic sea levels rose abruptly at this time as the Northern Hemisphere continental ice sheets waned, with a distinct global meltwater pulse at  $\sim 19$  ka BP (Clark *et al.*, 2004b). The 'ice bridge' connection between grounded ice centred on Orkney and Shetland would have been lost at this time. During this dynamic phase the SIC experienced massive sustained losses along its substantial marine margins, reducing in size from ca. 45 000 to 15 000 km<sup>2</sup> in perhaps only a few centuries ( $\sim 19$ – $18$  ka BP). This almost certainly represents the most rapid ice-mass loss in this sector over the whole glacial cycle (30–15 ka BP) – akin to instability-driven ice-sector collapse currently ongoing at the marine margins of the West Antarctic Ice Sheet (e.g. Joughin *et al.*, 2014; Rignot *et al.*, 2014). SIC collapse continued, probably losing  $>50\%$  of its remaining area between  $\sim 18$  and 17 ka BP. Clusters of TCN-exposure ages on Out Skerries, Papa Stour, Muckle Roe, North Roe and one from SW Unst show that the SIC had retreated to the Shetland landmass by  $\sim 16.5$ – $17.0$  ka BP, and by this time probably covered only ca. 2000 km<sup>2</sup>, with large tidewater glaciers discharging into the main voes and sounds between the islands.

### **Final deglaciation: $16.5 \pm 0.3 - 14.9 \pm 2.0$ ka [BL6–9]**

After  $\sim 16.5$  ka BP the SIC continued to reduce in size, although probably at a much reduced rate, now centred wholly on the Shetland landmass, although possibly with subsidiary ice centres on one or more large, subaerially exposed, continental shelf banks (see below). We expect ice-mass losses to have been focused on the remaining tidewater glacier termini within the first part of this time period. This  $\sim 2000$ -year time interval was characterized by a general climate deterioration (GS-2a) in the Northern Hemisphere lasting until the abrupt warming at the onset of GI-1 (14.7 ka; Lowe *et al.*, 2008). We infer that tidewater glacier margins in Shetland were probably back beyond the marine limit by  $\sim 16.0$  ka BP – supported by TCN ages from North Roe and radiocarbon ages in St Magnus Bay – and that small terrestrial glaciers may have existed in Shetland until close to the onset of GI-1.

Two TCN ages from boulders on moraines in central Mainland Shetland are difficult to interpret. Based on all the marine and terrestrial geological and geomorphological evidence, we can see no parsimonious pattern of ice-mass retreat that would result in deglaciation of Skella Dale (central Shetland) at 18–19 ka BP before the islands of Muckle Roe and

Papa Stour to the west. Although we accept that such an ice-mass configuration is possible, it would require the SIC to have separated into several, much smaller, independent ice centres before  $\sim 18$ – $19$  ka BP. We have no geomorphological evidence to support this, and thus we prefer to attribute the age conflict to a degree of cosmogenic nuclide inheritance in the two samples from Skella Dale, probably resulting from pre-glacial exposure and/or supraglacial transportation, making their apparent age older than their true exposure age.

Our youngest meaningful TCN ages are from the NW Shetland mainland, indicating active ice-cap recession on land at  $\sim 16.4$  ka BP. Beyond that, it is difficult to draw any firm conclusions regarding the shape, size and location of the ice-cap core after 16.5 ka BP based on the very limited moraine evidence in eastern Shetland and the absence of firmly dated deglacial sites (Birnie *et al.*, 1993; Gordon and Sutherland, 1993). We note that one of our OSL age assessments from late-stage moraines in central Shetland is consistent with active ice-front recession at  $\sim 16.4$  ka BP, albeit accompanied by a relatively large uncertainty term ( $\pm 1.8$  ka). It is likely that the final ice-cap remnants on Shetland were a number of small thin ice-fields along the spine of highest ground, much like the situation in present-day NW Iceland (ca. 66°N). However, we have no evidence to suggest persistence of ice masses beyond the marked GI-1e warming event ( $\sim 14.7$  ka BP). The disappearance of glaciers at the end of GS-2 is supported by a small number of biostratigraphical sites in central and southern Shetland (e.g. Burn of Aith, Clettnadal) indicating ice-free, relatively mild, conditions with organic productivity by  $\sim 14.5$  ka BP (Birnie *et al.*, 1993; Whittington *et al.*, 2003). Unfortunately, the absence of any dated high-level Lateglacial sites ( $>200$  m asl), the precise context of some dated low-level sites, and the uncertainties surrounding radiocarbon measurements in these settings leaves the timing of final deglaciation on Shetland imprecisely constrained. This is reflected in the elevated uncertainties in the youngest part of our Bayesian model chronosequence (Table 8; Fig. 16).

### **Pobie Bank ice centre?**

A question mark still remains regarding the final pattern and timing of deglaciation on the continental shelf east of Shetland. What was the fate of the portion of the SIC centred on or east of Pobie Bank, at ca. 0°E? Alas, we can shed little light on this, other than speculate why two cores (088VC and 089VC) with no apparent breaks and good stratigraphic context (i.e. deglacial sediment on morainic/subglacial diamicts) have yielded consistently young deglacial ages  $\sim 16$  ka BP. To address this, we must include the possibility that during the latter stages of (probably rapid) recession, the SIC separated into at least two subsidiary centres – one on Shetland and one located on, or near, Pobie Bank (Figs. 1 and 17). Our new dating evidence would place final ice-mass demise on Pobie Bank shortly before  $\sim 16$  ka BP, although our Bayesian modelling uses a simple radial configuration and so cannot resolve a complex multi-centred deglaciation pattern (Fig. 17). It is worth noting that we have found no previously published evidence to refute this glaciologically plausible scenario, which requires further work to substantiate.

## **Summary and conclusions**

The main purpose of this work was to add much-needed chronology to the deglaciation of the northernmost sector of the last BIIS – including Shetland and the northern North Sea Basin (referred to in this study as Britice-Chrono 'Transect 1').

In addition, this work also presents important new geomorphological (pattern) and geological (stratigraphic) information from onshore and offshore regarding former ice-margin positions and ice-sheet fluctuations during the last glacial cycle. Although building on the original, terrestrially focused, Britice Version 1 glacial map and database (Clark *et al.*, 2004a) and ice-sheet-wide, Britice Version 2 compilations (Clark *et al.*, 2018), much of the new pattern information presented here supersedes or refines the data presented in previous overview works and in several other more geographically focused studies (e.g. Bradwell *et al.*, 2008; Sejrup *et al.*, 2015; Hall, 2014; Bradwell and Stoker, 2015; Merritt *et al.*, 2017).

We have generated a valuable new chronological database of 71 absolute-age assessments from Shetland and the adjacent continental shelf to the east and west of the islands. This greatly exceeds the existing number of published deglacial ages (according to Hughes *et al.*, 2016 and Small *et al.*, 2017) for this important coalescent sector of the BIIS and FIIS (Figs. 1, 6 and 18). The age assessments break down as follows: 32 TCN exposure ages and four OSL ages from 11 terrestrial deglacial sites in Shetland; and 35 AMS radiocarbon dates from 23 marine cores recording deglaciation offshore, with 23 finite and 11 non-finite ages (Tables 2–6). Collectively, these age assessments span the interval from ~35 to ~11 ka cal BP (excluding non-finite radiocarbon ages), with many showing good statistical agreement and spatial coherence. We have used these to derive a new absolute chronology of ice-sheet/ice-cap deglaciation, via probabilistic Bayesian modelling, and generate a sector-wide reconstruction of the BIIS north of 59°N (Figs. 17 and 18).

In summary, this palaeoglaciological sector reconstruction clearly shows widespread and significant variations in ice sheet, latterly ice cap, extent, shape and, by inference, flow configuration over time, between ~30 and ~15 ka BP. During the last glacial cycle, a substantial ice dome centred on the Orkney–Shetland Platform, at times coalescent with the FIS to the east, underwent an overall size reduction from ca. 85 000 km<sup>2</sup> at its maximum extent ~26–25 ka BP, to <50 000 km<sup>2</sup> by ~23 ka BP. Soon after this time, connection between the BIIS and FIS was lost. This was accompanied by a period of major instability ca. 21–20 ka BP, possibly triggering surge-type behaviour, as the rejuvenated independent SIC adjusted and equilibrated to new boundary conditions. Collectively, our data suggest that this period of ice-mass areal increase was followed by a rapid reduction, or collapse, in ice cap area (and volume), from around 45 000 to 15 000 km<sup>2</sup> ca. 19–18 ka BP – probably via sustained marine margin losses, perhaps in as little as a few centuries. Rapid retreat of the SIC continued, possibly accentuated by rising sea levels, with little interruption until the ice cap margins eventually stabilized near the present-day Shetland coastline at ~17.0–16.5 ka BP – with a glacierized area of ca. 2000 km<sup>2</sup>. Final demise of the terrestrial ice cap was probably relatively slow, occurring between 16.5 and 15 ka BP, although robust spatial and temporal constraints on final deglaciation are still lacking. Furthermore, we cannot preclude the existence of a late-stage subsidiary ice centre on the continental shelf (Pobie Bank) to the east of Shetland until ~17–16 ka BP.

We suggest that the unusually dynamic behaviour of the ice sheet/ice cap (>59.5°N), between 21 and 18 ka BP, characterized by numerous extensive lobe readvances and flow redistributions followed by sustained mass losses, was driven by significant changes in ice-mass geometry and ice-divide location resulting from high calving fluxes in this strongly marine-influenced sector. It is highly likely that the unusual dynamism within the northernmost sector of the BIIS was forced largely by internal (i.e. glaciological)

factors specific to the Shetland Ice Cap with its extensive marine margins, and to a lesser degree by external factors (i.e. climate and ocean warming) common to the BIIS complex as a whole.

Finally, perhaps one of the most striking conclusions of this work is that a large, independent ice sheet/ice cap fluctuated in shape and size, from >50 000 to <2000 km<sup>2</sup> in area, over a considerable period (from ~21 to 17 ka BP) without a physical connection to the larger FIS to the east and, it would appear, with little or no glaciological connection to the ice sheet centred over mainland Scotland. This fact addresses the original ‘invasive ice sheet’ vs ‘local ice cap’ hypothesis head on. However, in the light of these new findings, we suggest that the wider palaeoclimatic, palaeo-oceanographic, glacio-isostatic and geotechnical implications of a large, highly dynamic, Late Weichselian ice mass centred on the northern North Sea Shelf (58.5°N–61.5°N) should become a priority for further study.

**Acknowledgements.** This work was supported by the UK Natural Environment Research Council consortium grant Britice-Chrono NE/J009768/1; NERC Cosmogenic Isotope Analysis Facility, and NERC Radiocarbon Facility. We thank staff at the SUERC AMS Laboratory, East Kilbride, for carbon and beryllium isotope measurements. We thank the BGS Marine Operations team (vibrocoring) and NOC/NMEP team (piston corer) for their help during JC123. We also thank the master and crew of the *RRS James Cook* (JC123). James Shreeve and Briony Shreeve (Geotek) are thanked for assistance with XCT data acquisition. Figure 14 contains Maritime and Coastguard Agency MBES data (Crown Copyright), collected as part of the UKHO Civil Hydrography Programme, which is gratefully acknowledged. D.D. publishes with the permission of the Executive Director, BGS. Martyn Stoker is thanked for his advice, assistance and inspiration during the early stages of this project. We thank two anonymous reviewers for their helpful comments on an earlier draft of the manuscript. All relevant data will be made available in the forthcoming Britice-Chrono online data repository, or upon reasonable request from the lead author.

**Abbreviations.** AMS, accelerator mass spectrometer; BGS, British Geological Survey; BIIS, British–Irish Ice Sheet; DSM, digital surface model; FIS, Fennoscandian Ice Sheet; gESD, generalized extreme Studentized deviate; GI, Greenland Interstadial; GIS, geographical information system; GMRM, Greenwich Meridian Readvance Moraine; GRPR, Glen Roy production rate; ICP-MS, inductively coupled plasma mass spectrometry; MBES, multibeam echo sounder; MCMC, Markov chain Monte Carlo; MIS, Marine Isotope Stage; NESNMC, NE Shetland nested moraine complex; OD, overdispersion; OSL, optically stimulated luminescence; PC, piston core; SUERC, Scottish Universities Environmental Research Centre; TCN, terrestrial cosmogenic nuclide; TWTT, two-way travel time; UWM, uncertainty-weighted mean; VC, vibrocoring.

## Supporting information

Additional supporting information may be found in the online version of this article at the publisher’s web-site.

**Fig. S1.** Small multi-grain aliquots De distributions for the two samples from Gon Firth and the two samples from Sel Ayre. The components identified when applying FMM are indicated as dashed lines and the corresponding values and probabilities are indicated on the plots.

**Fig. S2.** Recovered doses from 98 aliquots bleached and irradiated of sample Shfd14140. 35 of those were accepted based on the same criteria applied to natural samples. On the plot, the dark line indicates the given dose value (36 Gy); red dashed line indicates the threshold limit of “low-age component” 15 Gy.

**Fig. S3.** IR depletion ratio as a function of the measured dose for all accepted aliquots of samples Shfd14140 and

Shfd14141. The acceptance interval (20% of unity including errors) is indicated by the shaded area. Red dashed line indicates the threshold of 15 Gy established to identify “low-age doses”.

**Fig. S4.** Thermal quenching ratio (blue OSL at 200 °C/blue OSL at 125 °C) as a function of the measured dose for sample Shfd14140 (blue squares), calibration quartz (green circles) and calibration feldspar (orange circles). The “low age dose” threshold (15 Gy) is indicated (red dashed line).

## REFERENCES

- Applegate PJ, Urban NM, Keller K, *et al.* 2012. Improved moraine age interpretations through explicit matching of geomorphic process models to cosmogenic nuclide measurements from single landforms. *Quaternary Research* **77**: 293–304, <https://doi.org/10.1016/j.yqres.2011.12.002>
- Arosio R, Dove D, Ó Cofaigh C, *et al.* 2018. Submarine deglacial sediment and geomorphological record of southwestern Scotland after the Last Glacial Maximum. *Marine Geology* **403**: 62–79, <https://doi.org/10.1016/j.margeo.2018.04.012>
- Balco G, Briner J, Finkel RC, *et al.* 2009. Regional beryllium-10 production rate calibration for late-glacial northeastern North America. *Quaternary Geochronology* **4**: 93–107, <https://doi.org/10.1016/j.quageo.2008.09.001>
- Balco G, Stone JO, Lifton NA, *et al.* 2008. A complete and easily accessible means of calculating surface exposure ages or erosion rates from <sup>10</sup>Be and <sup>26</sup>Al measurements. *Quaternary Geochronology* **3**: 174–195, <https://doi.org/10.1016/j.quageo.2007.12.001>
- Ballantyne CK. 2010. Extent and deglacial chronology of the last British–Irish Ice Sheet: implications of exposure dating using cosmogenic isotopes. *Journal of Quaternary Science* **25**: 515–534, <https://doi.org/10.1002/jqs.1310>
- Ballantyne CK, Fabel D, Gheorghiu D, *et al.* 2017. Late Quaternary glaciation in the Hebrides sector of the continental shelf: cosmogenic nuclide dating of glacial events on the St Kilda archipelago. *Boreas* **46**: 605–621, <https://doi.org/10.1111/bor.12242>
- Ballantyne CK, McCarroll D, Nesje A, *et al.* 1998. High-resolution reconstruction of the last ice sheet in NW Scotland. *Terra Nova* **10**: 63–67, <https://doi.org/10.1046/j.1365-3121.1998.00168.x>
- Ballantyne CK, Schnabel C, Xu S. 2009. Readvance of the last British–Irish ice sheet during Greenland interstade 1 (GI-1): the Wester Ross readvance, NW Scotland. *Quaternary Science Reviews* **28**: 783–789, <https://doi.org/10.1016/j.quascirev.2009.01.011>
- Bateman MD, Evans DJA, Roberts DH, *et al.* 2018. The timing and consequences of the blockage of the Humber Gap by the last British–Irish Ice Sheet. *Boreas* **47**: 41–61, <https://doi.org/10.1111/bor.12256>
- Becker LWM, Sejrup HP, Hjelstuen BO, *et al.* 2018. Ocean–ice sheet interaction along the SE Nordic Seas margin from 35 to 15 ka BP. *Marine Geology* **402**: 99–117, <https://doi.org/10.1016/j.margeo.2017.09.003>
- Bentley MJ, Ó Cofaigh C, Anderson JB, *et al.* 2014. A community-based geological reconstruction of Antarctic Ice Sheet deglaciation since the Last Glacial Maximum. *Quaternary Science Reviews* **100**: 1–9, <https://doi.org/10.1016/j.quascirev.2014.06.025>
- Berger A, Loutre MF. 1991. Insolation values for the climate of the last 10 million years. *Quaternary Science Reviews* **10**: 297–317, [https://doi.org/10.1016/0277-3791\(91\)90033-Q](https://doi.org/10.1016/0277-3791(91)90033-Q)
- BGS (Institute of Geological Sciences). 1971. *Western Shetland. Drift Edition. Sheet 127 & parts of Sheets 125, 126 & 128. One inch series.* British Geological Survey: Keyworth.
- BGS (Institute of Geological Sciences). 1978. *Southern Shetland. Drift Edition. Sheet 126 & parts of Sheets 123 & 124. One inch series.* British Geological Survey: Keyworth.
- BGS (Institute of Geological Sciences). 1982. *Central Shetland. Drift Edition. Sheet 128. One Inch Series.* British Geological Survey: Keyworth.
- BGS. 2002. *Unst and Fetlar. Solid and drift. Sheet 131. 1:50,000* Geology series. British Geological Survey: Keyworth.
- BGS. 2018. Geology of Britain viewer. A digital [Online] *Spatial Database of UK Geology*. British Geological Survey: Keyworth. Accessed at: [mapapps.bgs.ac.uk/geologyofbritain/home.html](http://mapapps.bgs.ac.uk/geologyofbritain/home.html).
- Birnie J, Harkness DD. 1993. Radiocarbon dates on Late-glacial sediments at Aith Voe, Cunningsburgh, and adjustments for rock-flour effects. In *The Quaternary of Shetland*, Birnie J, Gordon JE, Bennett K (eds). Quaternary Research Association: Cambridge.
- Birnie JF, Gordon KJ, Bennett KJ, *et al.* 1993. *The Quaternary of Shetland*. Quaternary Research Association: Cambridge.
- Blomdin R, Stroeven AP, Harbor JM, *et al.* 2016. Evaluating the timing of former glacier expansions in the Tian Shan: a key step towards robust spatial correlations. *Quaternary Science Reviews* **153**: 78–96, <https://doi.org/10.1016/j.quascirev.2016.07.029>
- Borchers B, Marrero S, Balco G, *et al.* 2016. Geological calibration of spallation production rates in the CRONUS-Earth project. *Quaternary Geochronology* **31**: 188–198, <https://doi.org/10.1016/j.quageo.2015.01.009>
- Boulton GS, Peacock JD, Sutherland DG. 1991. Quaternary. In *The Geology of Scotland*, Craig GY (ed). The Geological Society: London; 503–542. Third Edition.
- Boulton GS, Hagdorn M. 2006. Glaciology of the British Isles Ice Sheet during the last glacial cycle: form, flow, steams and lobes. *Quaternary Science Reviews* **25**: 3359–3390.
- Bradwell T. 2013. Identifying palaeo-ice-stream tributaries on hard beds: mapping glacial bedforms and erosion zones in NW Scotland. *Geomorphology* **201**: 397–414, <https://doi.org/10.1016/j.geomorph.2013.07.014>
- Bradwell T, Stoker M, Larter R. 2007. Geomorphological signature and flow dynamics of The Minch palaeo-ice stream, northwest Scotland. *Journal of Quaternary Science* **22**: 609–617, <https://doi.org/10.1002/jqs.1080>
- Bradwell T, Stoker MS. 2015. Asymmetric ice-sheet retreat pattern around Northern Scotland revealed by marine geophysical surveys. *Earth and Environmental Science Transactions of the Royal Society of Edinburgh* **105**: 297–322, <https://doi.org/10.1017/S1755691015000109>
- Bradwell T, Stoker MS, Gолledge NR, *et al.* 2008. The northern sector of the last British Ice Sheet: maximum extent and demise. *Earth-Science Reviews* **88**: 207–226, <https://doi.org/10.1016/j.earscirev.2008.01.008>
- Bronk Ramsey C. 2009a. Dealing with outliers and offsets in radiocarbon dating. *Radiocarbon* **51**: 1023–1045, <https://doi.org/10.1017/S0033822200034093>
- Bronk Ramsey C. 2009b. Bayesian analysis of radiocarbon dates. *Radiocarbon* **51**: 337–360, <https://doi.org/10.1017/S0033822200033865>
- Bronk Ramsey C. 2013. *OxCal 4.3. Manual [Online]*. Available at: [https://c14.arch.ox.ac.uk/oxcalhelp/hlp\\_contents.html](https://c14.arch.ox.ac.uk/oxcalhelp/hlp_contents.html)
- Callard SL, Ó Cofaigh C, Benetti S, *et al.* 2018. Extent and retreat history of the Barra Fan Ice Stream offshore western Scotland and Northern Ireland during the last glaciation. *Quaternary Science Reviews* **201**: 280–302, <https://doi.org/10.1016/j.quascirev.2018.10.002>
- Carr SJ, Hiemstra JF. 2013. Sedimentary evidence against a local ice-cap on the Shetland Isles at the Last Glacial Maximum. *Proceedings of the Geologists' Association* **124**: 484–502, <https://doi.org/10.1016/j.pgeola.2012.10.006>
- Carr SJ, Holmes R, van der Meer JJM, *et al.* 2006. The Last Glacial Maximum in the North Sea Basin: micromorphological evidence of extensive glaciation. *Journal of Quaternary Science* **21**: 131–153, <https://doi.org/10.1002/jqs.950>
- Child D, Elliott G, Mifsud C, *et al.* 2000. Sample processing for earth science studies at ANTARES. *Nuclear Instruments and Methods in Physics Research Section B* **172**: 856–860, [https://doi.org/10.1016/S0168-583X\(00\)00198-1](https://doi.org/10.1016/S0168-583X(00)00198-1)
- Clark CD, Ely J, Hughes A, *et al.* 2018. BRITICE Glacial Map, version 2: a map and GIS database of glacial landforms of the last British–Irish ice sheet. *Boreas*. <https://doi.org/10.1111/bor.12773>
- Clark CD, Evans DJA, Khatwa A, *et al.* 2004a. Map and GIS database of glacial landforms and features related to the last British Ice Sheet. *Boreas* **33**: 359–375, <https://doi.org/10.1080/03009480410001983>
- Clark CD, Hughes ALC, Greenwood SL, *et al.* 2012. Pattern and timing of retreat of the last British–Irish Ice Sheet. *Quaternary Science Reviews* **44**: 112–146, <https://doi.org/10.1016/j.quascirev.2010.07.019>
- Clark CD, Meehan RT. 2001. Subglacial bedform geomorphology of the Irish Ice Sheet reveals major configuration changes during

- growth and decay. *Journal of Quaternary Science* **16**: 483–496, <https://doi.org/10.1002/jqs.627>
- Clark PU, McCabe AM, Mix AC, *et al.* 2004b. Rapid rise of sea level 19,000 years ago and its global implications. *Science* **304**: 1141–1144, <https://doi.org/10.1126/science.1094449>
- Croll J. 1870. The boulder clay of Caithness: a product of land ice. *Geological Magazine* **7**: 209–214, <https://doi.org/10.1017/S0016756800467439>
- Darvill CM, Bentley MJ, Stokes CR. 2015. Geomorphology and weathering characteristics of erratic boulder trains on Tierra del Fuego, southernmost South America: implications for dating of glacial deposits. *Geomorphology* **228**: 382–397, <https://doi.org/10.1016/j.geomorph.2014.09.017>
- Davison S. 2005. Reconstructing the last Pleistocene (Late Devensian) glaciation on the continental margin of Northwest Britain. PhD Thesis, University of Edinburgh.
- Dove D, Arosio R, Finlayson AG, *et al.* 2015. Submarine glacial landforms record Late Pleistocene ice-sheet dynamics, Inner Hebrides, Scotland. *Quaternary Science Reviews* **123**: 76–90, <https://doi.org/10.1016/j.quascirev.2015.06.012>
- Dowdeswell JA, Canals M, Jakobsson M, *et al.* 2016. The variety and distribution of submarine glacial landforms and implications for ice-sheet reconstruction. *Geological Society, London, Memoirs* **46**: 519–552, <https://doi.org/10.1144/M46.183>
- Duller GAT, Wintle AG, Hall AM. 1995. Luminescence dating and its application to key pre-late Devensian sites in Scotland. *Quaternary Science Reviews* **14**: 495–519, [https://doi.org/10.1016/0277-3791\(95\)00017-J](https://doi.org/10.1016/0277-3791(95)00017-J)
- Evans DJA, Rea BR. 2005. Surging glacier landsystem. In *Glacial Landforms*, DJA Evans (ed). Hodder Arnold: London; 259–289.
- Fabel D, Ballantyne CK, Xu S. 2012. Trilines, blockfields, mountain-top erratics and the vertical dimensions of the last British–Irish Ice Sheet in NW Scotland. *Quaternary Science Reviews* **55**: 91–102, <https://doi.org/10.1016/j.quascirev.2012.09.002>
- Finlay TM. 1932. A tönsgbergite boulder from the boulder-clay of Shetland. *Transactions of the Edinburgh Geological Society* **12**: 180.
- Flinn D. 1967. Ice front in the North Sea. *Nature* **215**: 1151–1154, <https://doi.org/10.1038/2151151a0>
- Flinn D. 1970. The glacial till of Fair Isle, Shetland. *Geological Magazine* **107**: 273–276, <https://doi.org/10.1017/S0016756800055746>
- Flinn D. 1973. The topography of the seafloor around Orkney and Shetland and in the northern North Sea. *Journal of the Geological Society* **129**: 39–59, <https://doi.org/10.1144/gsjgs.129.1.0039>
- Flinn D. 1978. The most recent glaciation of the Orkney–Shetland Channel and adjacent areas. *Scottish Journal of Geology* **14**: 109–123, <https://doi.org/10.1144/sjg14020109>
- Flinn D. 1992. A note on the Dalsetter Erratic, Dunrossness, Shetland. *Shetland Naturalist* **1**: 49–50.
- Flinn D. 1994. The geology of Yell and some neighbouring islands in Shetland, *Memoir of the British*. Geological Survey, HMSO: London.
- Flinn D. 2014. Geology of Unst and Fetlar in Shetland: Memoir for 1: 50 000 Geological sheet 131 (Scotland) Unst and Fetlar. British Geological Survey: Nottingham.
- Galbraith RF, Green PF. 1990. Estimating the component ages in a finite mixture. *International Journal of Radiation Applications and Instrumentation. Part D. Nuclear Tracks and Radiation Measurements* **17**: 197–206, [https://doi.org/10.1016/1359-0189\(90\)90035-V](https://doi.org/10.1016/1359-0189(90)90035-V)
- Golledge NR, Finlayson A, Bradwell T, *et al.* 2008. The last glaciation of Shetland, North Atlantic. *Geografiska Annaler: Series A, Physical Geography* **90**: 37–53, <https://doi.org/10.1111/j.1468-0459.2008.00332.x>
- Gordon JE, Sutherland DG. 1993. *Quaternary of Scotland*. Chapman & Hall: London.
- Graham AGC, Lonergan L, Stoker MS. 2007. Evidence for Late Pleistocene ice stream activity in the Witch Ground Basin, central North Sea, from 3D seismic reflection data. *Quaternary Science Reviews* **26**: 627–643, <https://doi.org/10.1016/j.quascirev.2006.11.004>
- Graham AGC, Lonergan L, Stoker MS. 2009. Seafloor glacial features reveal the extent and decay of the last British Ice Sheet, east of Scotland. *Journal of Quaternary Science* **24**: 117–138, <https://doi.org/10.1002/jqs.1218>
- Graham AGC, Stoker MS, Lonergan L, *et al.* 2011. The Pleistocene glaciations of the North Sea Basin. *Developments in Quaternary Sciences* **15**: 261–278, <https://doi.org/10.1016/B978-0-444-53447-7.00021-0>
- Hall AM. 2014. The last glaciation of Shetland: local ice cap or invasive ice sheet? *Norwegian Journal of Geology* **93**: 229–242.
- Hall AM, Gordon JE, Whittington G, *et al.* 2002. Sedimentology, palaeoecology and geochronology of Marine Isotope Stage 5 deposits on the Shetland Islands, Scotland. *Journal of Quaternary Science* **17**: 51–67, <https://doi.org/10.1002/jqs.644>
- Hall AM, Gordon JG, Whittington G. 1993. Early Devensian Interstadial peat at Sel Ayre. In *The Quaternary of Shetland*, Birnie J, Gordon JE, Bennett K, Hall AM (eds). Quaternary Research Association: Cambridge.
- Heyman J, Applegate PJ, Blomdin R, *et al.* 2016. Boulder height – exposure age relationships from a global glacial <sup>10</sup>Be compilation. *Quaternary Geochronology* **34**: 1–11, <https://doi.org/10.1016/j.quageo.2016.03.002>
- Hjelstuen BO, Sejrup HP, Valvik E, *et al.* 2018. Evidence of an ice-dammed lake outburst in the North Sea during the last deglaciation. *Marine Geology* **402**: 118–130, <https://doi.org/10.1016/j.margeo.2017.11.021>
- Home DM. 1881. On the glaciation of Shetland. *Geological Magazine* **8**: 1–7.
- Hoppe G. 1974. The glacial history of the Shetland Islands. *Transactions of the Institute of British Geographers, Special Publication* **7**: 197–201.
- Hughes ALC, Greenwood SL, Clark CD. 2011. Dating constraints on the last British–Irish Ice Sheet: a map and database. *Journal of Maps* **7**: 156–184, <https://doi.org/10.4113/jom.2011.1145>
- Hughes ALC, Gyllencreutz R, Lohne ØS, *et al.* 2016. The last Eurasian ice sheets - a chronological database and time-slice reconstruction, DATED-1. *Boreas* **45**: 1–45, <https://doi.org/10.1111/bor.12142>
- Hulme PD, Shirriffs J. 1994. The Late-glacial and Holocene vegetation of the Lang Lochs Mire area, Gulberwick, Shetland: a pollen and macrofossil investigation. *New Phytologist* **128**: 793–806, <https://doi.org/10.1111/j.1469-8137.1994.tb04040.x>
- Johnson H, Richards PC, Long D, *et al.* 1993. United Kingdom Offshore Regional Report: the Geology of the Northern North Sea. HMSO for the British Geological Survey: London.
- Jones RS, Small D, Cahill N, *et al.* 2019. iceTEA: tools for plotting and analysing cosmogenic-nuclide surface-exposure data from former ice margins. *Quaternary Geochronology* **51**: 72–86, <https://doi.org/10.1016/j.quageo.2019.01.001>
- Joughin I, Smith BE, Medley B. 2014. Marine ice sheet collapse potentially underway for the Thwaites Glacier Basin, West Antarctica. *Science* **344**: 735–738, <https://doi.org/10.1126/science.1249055>
- Kaplan MR, Strelin JA, Schaefer JM, *et al.* 2011. In-situ cosmogenic <sup>10</sup>Be production rate at Lago Argentino, Patagonia: implications for late-glacial climate chronology. *Earth and Planetary Science Letters* **309**: 21–32, <https://doi.org/10.1016/j.epsl.2011.06.018>
- Kohl CP, Nishiizumi K. 1992. Chemical isolation of quartz for measurement of *in situ*-produced cosmogenic nuclides. *Geochimica et Cosmochimica Acta* **56**: 3583–3587, [https://doi.org/10.1016/0016-7037\(92\)90401-4](https://doi.org/10.1016/0016-7037(92)90401-4)
- Le Bas MJ. 1992. The petrography of the Shetland tönsgbergite. *Shetland Naturalist* **1**: 51–56.
- Lowe JJ, Rasmussen SO, Björck S, *et al.* 2008. Synchronisation of palaeoenvironmental events in the North Atlantic region during the Last Termination: a revised protocol recommended by the INTIMATE group. *Quaternary Science Reviews* **27**: 6–17, <https://doi.org/10.1016/j.quascirev.2007.09.016>
- Marrero SM, Phillips FM, Borchers B, *et al.* 2016. Cosmogenic nuclide systematics and the CRONUScalc program. *Quaternary Geochronology* **31**: 160–187, <https://doi.org/10.1016/j.quageo.2015.09.005>
- Merritt JW, Connell ER, Hall AM. 2017. Middle to Late Devensian glaciation of north-east Scotland: implications for the north-eastern quadrant of the last British–Irish Ice Sheet. *Journal of Quaternary Science* **32**: 276–294, <https://doi.org/10.1002/jqs.2878>
- Mykura W. 1976. *British Regional Geology: Orkney and Shetland*. HMSO: Edinburgh.
- Ó Cofaigh C, Evans DJA. 2007. Radiocarbon constraints on the age of the maximum advance of the British–Irish Ice Sheet in the Celtic Sea.

- Quaternary Science Reviews* **26**: 1197–1203, <https://doi.org/10.1016/j.quascirev.2007.03.008>
- Ottesen D, Dowdeswell JA, Bellec VK, *et al.* 2017. The geomorphic imprint of glacier surges into open-marine-waters: examples from eastern Svalbard. *Marine Geology* **392**: 1–29, <https://doi.org/10.1016/j.margeo.2017.08.007>
- Patton H, Hubbard A, Andreassen K, *et al.* 2016. The build-up, configuration, and dynamical sensitivity of the Eurasian ice-sheet complex to Late Weichselian climatic and oceanic forcing. *Quaternary Science Reviews* **153**: 97–121, <https://doi.org/10.1016/j.quascirev.2016.10.009>
- Peach BN, Horne J. 1879. The glaciation of the Shetland Isles. *Quarterly Journal of the Geological Society* **35**: 778–811, <https://doi.org/10.1144/GSL.JGS.1879.035.01-04.57>
- Peacock JD. 1995. Late Devensian to Early Holocene palaeoenvironmental changes in the Viking Bank area, northern North Sea. *Quaternary Science Reviews* **14**: 1029–1042, [https://doi.org/10.1016/0277-3791\(95\)00041-0](https://doi.org/10.1016/0277-3791(95)00041-0)
- Peck VL, Hall IR, Zahn R, *et al.* 2007. The relationship of Heinrich events and their European precursors over the past 60 ka BP: a multi-proxy ice-rafted debris provenance study in the North East Atlantic. *Quaternary Science Reviews* **26**: 862–875, <https://doi.org/10.1016/j.quascirev.2006.12.002>
- Peters JL, Benetti S, Dunlop P, *et al.* 2015. Maximum extent and dynamic behaviour of the last British–Irish Ice Sheet west of Ireland. *Quaternary Science Reviews* **128**: 48–68, <https://doi.org/10.1016/j.quascirev.2015.09.015>
- Phillips FM, Argento DC, Balco G, *et al.* 2016. The CRONUS-Earth project: a synthesis. *Quaternary Geochronology* **31**: 119–154, <https://doi.org/10.1016/j.quageo.2015.09.006>
- Phillips WM, Hall AM, Ballantyne CK, *et al.* 2008. Extent of the last ice sheet in northern Scotland tested with cosmogenic  $^{10}\text{Be}$  exposure ages. *Journal of Quaternary Science* **23**: 101–107, <https://doi.org/10.1002/jqs.1161>
- Putkonen J, Swanson T. 2003. Accuracy of cosmogenic ages for moraines. *Quaternary Research* **59**: 255–261, [https://doi.org/10.1016/S0033-5894\(03\)00006-1](https://doi.org/10.1016/S0033-5894(03)00006-1)
- Putnam AE, Schaefer JM, Barrell DJA, *et al.* 2010. In situ cosmogenic  $^{10}\text{Be}$  production-rate calibration from the Southern Alps, New Zealand. *Quaternary Geochronology* **5**: 392–409, <https://doi.org/10.1016/j.quageo.2009.12.001>
- Rasmussen SO, Andersen KK, Svensson AM, *et al.* 2006. A new Greenland ice core chronology for the last glacial termination. *Journal of Geophysical Research* **111**: D6, <https://doi.org/10.1029/2005JD006079>
- Reimer PJ, Bard E, Bayliss A, *et al.* 2013. IntCal13 and Marine13 radiocarbon age calibration curves 0–50,000 years cal BP. *Radiocarbon* **55**: 1869–1887.
- Rignot E, Mouginot J, Morlighem M, *et al.* 2014. Widespread, rapid grounding line retreat of Pine Island, Thwaites, Smith, and Kohler glaciers, West Antarctica, from 1992 to 2011. *Geophysical Research Letters* **41**: 3502–3509, <https://doi.org/10.1002/2014GL060140>
- Rise L, Rokoengen K. 1984. Surficial sediments in the Norwegian sector of the North Sea between 60°30' and 62°N. *Marine Geology* **58**: 287–317, [https://doi.org/10.1016/0025-3227\(84\)90206-8](https://doi.org/10.1016/0025-3227(84)90206-8)
- Ritchie JD, Ziska H, Johnson H, *et al.* 2011. United Kingdom Offshore Regional Report: the Geology of the Faroe-Shetland Basin and Adjacent Areas. HMSO for the British Geological Survey: London.
- Ross HM. 1996. The last glaciation of Shetland. PhD Thesis, University of St. Andrews.
- Scourse JD, Haapaniemi AI, Colmenero-Hidalgo E, *et al.* 2009. Growth, dynamics and deglaciation of the last British–Irish ice sheet: the deep-sea ice-rafted detritus record. *Quaternary Science Reviews* **28**: 3066–3084, <https://doi.org/10.1016/j.quascirev.2009.08.009>
- Sejrup HP, Clark CD, Hjelstuen BO. 2016. Rapid ice sheet retreat triggered by ice stream debuttressing: evidence from the North Sea. *Geology* **44**: 355–358, <https://doi.org/10.1130/G37652.1>
- Sejrup HP, Hjelstuen BO, Nygård A, *et al.* 2015. Late Devensian ice-marginal features in the central North Sea – processes and chronology. *Boreas* **44**: 1–13, <https://doi.org/10.1111/bor.12090>
- Sejrup HP, Hjelstuen BO, Torbjørn Dahlgren KI, *et al.* 2005. Pleistocene glacial history of the NW European continental margin. *Marine and Petroleum Geology* **22**: 1111–1129, <https://doi.org/10.1016/j.marpetgeo.2004.09.007>
- Sejrup HP, Nygård A, Hall AM, *et al.* 2009. Middle and Late Weichselian (Devensian) glaciation history of south-western Norway, North Sea and eastern UK. *Quaternary Science Reviews* **28**: 370–380, <https://doi.org/10.1016/j.quascirev.2008.10.019>
- Sejrup HP, Hafliðason H, Aarseth I, *et al.* 1994. Late Weichselian glaciation history of the northern North Sea. *Boreas* **23**: 1–13, <https://doi.org/10.1111/j.1502-3885.1994.tb00581.x>
- Small D, Austin W, Rinterknecht V. 2013. Freshwater influx, hydrographic reorganization and the dispersal of ice-rafted detritus in the sub-polar North Atlantic Ocean during the last deglaciation. *Journal of Quaternary Science* **28**: 527–535, <https://doi.org/10.1002/jqs.2644>
- Small D, Clark CD, Chiverrell RC, *et al.* 2017. Devising quality assurance procedures for assessment of legacy geochronological data relating to deglaciation of the last British–Irish Ice Sheet. *Earth-Science Reviews* **164**: 232–250, <https://doi.org/10.1016/j.earscirev.2016.11.007>
- Small D, Fabel D. 2015. A Lateglacial  $^{10}\text{Be}$  production rate from glacial lake shorelines in Scotland. *Journal of Quaternary Science* **30**: 509–513, <https://doi.org/10.1002/jqs.2804>
- Small D, Fabel D. 2016. Response to Bromley *et al.* “Comment on ‘Was Scotland deglaciated during the Younger Dryas?’”. *Quaternary Science Reviews* **152**: 206–208, <https://doi.org/10.1016/j.quascirev.2016.09.021>
- Smith MJ, Rose J, Booth S. 2006. Geomorphological mapping of glacial landforms from remotely sensed data: an evaluation of the principal data sources and an assessment of their quality. *Geomorphology* **76**: 148–165, <https://doi.org/10.1016/j.geomorph.2005.11.001>
- Stern JV, Lisiecki LE. 2013. North Atlantic circulation and reservoir age changes over the past 41,000 years. *Geophysical Research Letters* **40**: 3693–3697, <https://doi.org/10.1002/grl.50679>
- Stoker MS, Balsom PS, Long D. 2011. An overview of the lithostratigraphical framework for the Quaternary deposits on the United Kingdom continental shelf. British Geological Survey Research Report RR/11/03.
- Stoker MS, Hitchen K, Graham CG. 1993. United Kingdom Offshore Regional Report: the Geology of the Hebrides and West Shetland Shelves, and Adjacent Deep-Water Areas. HMSO for the British Geological Survey: London.
- Stoker MS, Holmes R. 1991. Submarine end-moraines as indicators of Pleistocene ice-limits off northwest Britain. *Journal of the Geological Society* **148**: 431–434, <https://doi.org/10.1144/gsjgs.148.3.0431>
- Stroeven AP, Hättestrand C, Kleman J, *et al.* 2016. Deglaciation of Fennoscandia. *Quaternary Science Reviews* **147**: 91–121, <https://doi.org/10.1016/j.quascirev.2015.09.016>
- Sutherland DG. 1984. The Quaternary deposits and landforms of Scotland and the neighbouring shelves: a review. *Quaternary Science Reviews* **3**: 157–254, [https://doi.org/10.1016/0277-3791\(84\)90017-9](https://doi.org/10.1016/0277-3791(84)90017-9)
- Svendsen JJ, Briner JP, Mangerud J, *et al.* 2015. Early break-up of the Norwegian Channel ice stream during the Last Glacial Maximum. *Quaternary Science Reviews* **107**: 231–242, <https://doi.org/10.1016/j.quascirev.2014.11.001>
- Todd BJ. 2016. Recessional moraines on the southern Scotian Shelf of Atlantic Canada. *Geological Society, London, Memoirs* **46**: 257–258, <https://doi.org/10.1144/M46.112>
- Whittington G, Buckland P, Edwards KJ, *et al.* 2003. Multiproxy Devensian Late-glacial and Holocene environmental records at an Atlantic coastal site in Shetland. *Journal of Quaternary Science* **18**: 151–168, <https://doi.org/10.1002/jqs.746>
- Xu S, Dougans AB, Freeman SPHT, *et al.* 2010. Improved  $^{10}\text{Be}$  and  $^{26}\text{Al}$ -AMS with a 5MV spectrometer. *Nuclear Instruments and Methods in Physics Research Section B* **268**: 736–738, <https://doi.org/10.1016/j.nimb.2009.10.018>
- Young NE, Schaefer JM, Briner JP, *et al.* 2013. A  $^{10}\text{Be}$  production-rate calibration for the Arctic. *Journal of Quaternary Science* **28**: 515–526, <https://doi.org/10.1002/jqs.2642>